DEVELOPMENT OF ALUMINIUM-COPPER DIE-ATTACH ALLOY FOR HIGH OPERATIONAL TEMPERATURE APPLICATION

SIAH MENG ZHE

DEPARTMENT OF MECHANICAL ENGINEERING
FACULTY OF ENGINEERING
UNIVERSITY OF MALAYA
KUALA LUMPUR

2019

DEVELOPMENT OF ALUMINIUM-COPPER DIE-ATTACH ALLOY FOR HIGH OPERATIONAL TEMPERATURE APPLICATION

SIAH MENG ZHE

DISSERTATION SUBMITTED IN FULFILLMENT OF THE
REQUIREMENTS FOR THE DEGREE OF MASTER OF
ENGINEERING SCIENCE

DEPARTMENT OF MECHANICAL ENGINEERING
FACULTY OF ENGINEERING
UNIVERSITY OF MALAYA
KUALA LUMPUR

2019

UNIVERSITY OF MALAYA
ORIGINAL LITERARY WORK DECLARATION

Name of Candidate: SIAH MENG ZHE

Matric No: KGA170002

Name of Degree: MASTER OF ENGINEERING SCIENCE

Title of Project Paper/Research Report/Dissertation/Thesis (“this Work”): DEVELOPMENT OF ALUMINIUM-COPPER DIE-ATTACH ALLOY FOR HIGH OPERATIONAL TEMPERATURE APPLICATION

Field of Study: ELECTRONIC PACKAGING (MECHANICAL ENGINEERING)

I do solemnly and sincerely declare that:

(1) I am the sole author/writer of this Work;
(2) This Work is original;
(3) Any use of any work in which copyright exists was done by way of fair dealing and for permitted purposes and any excerpt or extract from, or reference to or reproduction of any copyright work has been disclosed expressly and sufficiently and the title of the Work and its authorship have been acknowledged in this Work;
(4) I do not have any actual knowledge nor do I ought reasonably to know that the making of this work constitutes an infringement of any copyright work;
(5) I hereby assign all and every rights in the copyright to this Work to the University of Malaya (“UM”), who henceforth shall be owner of the copyright in this Work and that any reproduction or use in any form or by any means whatsoever is prohibited without the written consent of UM having been first had and obtained;
(6) I am fully aware that if in the course of making this Work I have infringed any copyright whether intentionally or otherwise, I may be subject to legal action or any other action as may be determined by UM.

Candidate’s Signature Date:

Subscribed and solemnly declared before,

Witness’s Signature Date:

Name:

Designation:

DEVELOPMENT OF ALUMINIUM-COPPER DIE-ATTACH ALLOY FOR HIGH OPERATIONAL TEMPERATURE APPLICATION

ABSTRACT

Die attach material plays an important role in electronic packaging as it serves as an interconnection between SiC device and substrate, provides physical and mechanical support and serves as a heat dissipating path. An aluminum-copper (Al-Cu) nanopaste formulated by mixing Al and Cu nanoparticles with organic additives (i.e., resin binder, terpineol and ethylene glycol) which is meant for high-temperature die-attach applications has been developed. Various weight percent of V006A (4%,5%,6% and 7%) and the Al loading (10%, 20%, 30% and 40%) have been loaded into the Al-Cu nanopaste, followed by sintering in open air at temperature of 380°C for 30 min without the need of applied external pressure. The physical and electrical properties were investigated. X-ray diffraction results showed that Al_2Cu and CuO phases were formed in sintered Al-Cu nanopaste. Overall, Al-Cu nanopaste with 5% V006A has exhibited the best electrical conductivity [21μΩ.cm], lowest oxygen element [15.36%] and smallest crystallite size [8.15nm], which is suitable for high temperature electronic applications. Also, $Al_{0.5}$-$Cu_{4.5}$ demonstrated the lowest electrical resistivity at 21.70 μΩ.cm, which is acceptable for a high temperature die-attach material.

PEMBANGUNAN ALUMINUM-KUPRUM SEBAGAI BAHAN KEPILAN DALAM PEMBUNGKUSAN ELEKTRONIK UNTUK APLIKASI SUHU TINGGI

ABSTRAK

Bahan lampir-dai memainkan peranan penting dalam pembungkusan elektronik kerana ia berfungsi sebagai sambungan antara peranti dan substrat SiC, menyediakan sokongan fizikal dan mekanik dan berfungsi sebagai jalan pelesapan haba. Satu nano-pes aluminum-kuprum (Al-Cu) yang dirumuskan dengan mencampurkan nanopartikel Al dan Cu dengan penambah organik (pelekat resin, terpineol dan ethylene glycol) telah dihasilkan bagi diaplikasikan sebagai bahan lampir-dai suhu tinggi. Pelbagai berat pelekat resin (4%, 5%, 6% dan 7%) telah ditambahkan ke dalam nano-pes Al-Cu, diikuti oleh pensinteran di udara terbuka pada suhu 380°C selama 30 min tanpa bantuan tekanan luar, untuk mengkaji kesan terhadap sifat-sifat fizikal, elektrikal, dan terma. Keputusan belauan sinar-X menunjukkan fasa Al_2Cu dan CuO terbentuk dalam nano-pes Al-Cu tersinter. Nano-pes Al-Cu tersinter dengan 5% pelakat resin menunjukkan terbaik bagi keberaliran elektrik [21μΩ/cm], peratus oksigen yang terendah [15.36%] dan saiz kryastille yang terkecil [8.15nm]. Nano-pes Al-Cu mempamerkan kesesuaian untuk aplikasi suhu tinggi. $Al_{0.5}$-$Cu_{4.5}$ menunjukkan terbaik bagi kebaliran electrik [21.70 μΩ/cm], ia juga diterima untuk aplikasi suhu tinggi.

ACKNOWLEGDEMENTS

I would like to express my deepest gratitude to my supervisor, Ir. Dr. Wong Yew Hoong for his guidance and supports throughout my master studies. He is a great mentor who gave me lots of freedom to work on the study in my way and fully committed whenever I need his guidance on my paper and experimental works. I appreciate your positive problem solving skills, clear minded and open minded to achieve my greatest goal in my research. I also like to convey my appreciation to my co-supervisor Dr. Nazatul Liana Sukiman for her advice and supervision.

To all my colleagues, Dennis, Alex, Zhen Ce, Tahsin, Moktar, Aainaa, Henry, and Nurul, thank you for your help and encouragement. Thank you to all the lab assistants, Puan Hartini and Puan Suraya for their supportive assistance and making sure the lab is always in perfect working conditions.

Last but not least to my beloved parents for their kind support and always pray for my success. To my brother, sister and friends, thank you for their never ending words of encouragement. With their unfailing love and support, I could be able to go through all the hardships throughout my master candidature.

Thank you all.

TABLE OF CONTENTS

CHAPTER 1

CHAPTER 2

CHAPTER 3

CHAPTER 4

CHAPTER 5

LIST OF FIGURES

LIST OF TABLES

LIST OF SYMBOLS AND ABBREVIATIONS

Symbols/Abbreviations	**Meanings**
Si	Silicon
SiC	Silicon Carbide
GaN	Gallium Nitride
Al	Aluminum
Cu	Copper
Ag	Silver
Sn	Tin
Pb	Lead
Bi	Bismuth
In	Indium
Au	Gold
Ni	Nickel
MEMS	Micro-electro-mechanical Systems
MEA	More Electric Aircraft
WBG	Wide Band-Gap
ECA	Electrical Conductive Adhesives
ICA	Isotropic Conductive Adhesives
ACA	Anisotropic Conductive Adhesives
NCA	Non-Conductive Adhesives
ROS	reactive oxygen species
PCB	printed circuit board
BGA	ball grid arrays

QFN	quad flat no-leads packages
CSP	chip-scale packages
PWE	pulse wired evaporation
N_2	Nitrogen
CuO	copper oxide
Al_2O_3	alumina
DOE	Design of Experiments
CTE	Coefficient of Thermal Expansion
ICDD	International Centre for Diffraction Database
M	Performance Index
K	Thermal Conductivity
α	Coefficient of Thermal Expansion
D	diameter
T_o	operating temperature
T_m	melting temperature
T_h	homologue temperature
EG	Ethyl Glycol
V006A	6% viscosity resin binder
R	Resistance
V	Voltage
A	Current
ρ	resistivity
L	Length of stencil printed area
A	cross section of stencil printed area
D	Crystallite Size
β	peak width with half maximum intensity

λ	wavelength
θ	peak position
K	shape factor
Cu2 + 1O	Cuprite

CHAPTER 1

INTRODUCTION

1.1 Background

The trend of electronic packaging is moving toward to design the electronic devices and sensors which are suitable for high temperature applications in recent years. For instance, brake and exhaust systems in automotive (300-1000^{o}C), geothermal and hydrocarbon sensors in down-hole oil and gas industry (~600 ^{o}C), electronic devices for space exploration (>500 ^{o}C) and turbine and gas sensors for avionics (~600 ^{o}C) (K. S. Tan, Wong, & Cheong, 2015). For such demanding applications, silicon (Si) based cannot fulfill the demand from the market of high temperature electronic devices because of its critical limitations, which could not being operated at temperature beyond 250°C. Therefore, scientists were trying hard to search for suitable wide band-gap semiconductors. Consequently, Silicon Carbide (SiC) has emerged to replace Si-based devices attributed to its wide band-gap semiconductor properties (3.26eV) and high electronic breakdown field strength (3.2 MV/cm) (Callanan, 2011; Choi, 2017; Watson & Castro, 2015). These distinct properties allow SiC-based devices to be operated beyond 250°C, which is capable to address the limitations of Si-based devices without any current leakage. Nevertheless, a proper design and development of electronic packaging for high temperature applications is required in order to full utilize the advantages of SiC-based devices. The main aspects of development to be focused include die-attach material, substrate material, wire bonding material and encapsulation material. Die-attach material is the one particular concern among these because it is an interconnection that provides sufficient properties between the substrate and the SiC die.

1.2 Problem Statements

In recent years, many industries are calling for electronic devices that can be operated in high temperature and hostile environment. Generally, cooling technique must be applied when designing devices for high temperature applications (Watson & Castro, 2012, 2015). However, cooling technique is not possible in some applications. Thus, a new design and development of electronic packaging for high temperature applications is necessary to fulfill the demand of industries. Silicon Carbide (SiC) for example, has been documented its success to operate at a temperature beyond 500°C. Still, there is a need for a comprehensive design of high temperature electronic packaging; one of the critical parts is the interconnection between SiC device and substrate, or called die-attach material. Die-attach material plays an important role as it provides physical and mechanical support and serves as a heat dissipating path. In order to design a die-attach material which is in line with high temperature SiC devices, the selection of materials for die-attach uses must primarily withstand high temperature.

In general, die-attach materials can be classified into five categories, which are conductive adhesive, solder alloy, conductive glass, metal film, and metal paste (Manikam & Cheong, 2011). It is commonly accepted that both conductive adhesive and tin-based solder alloys (Sn-Pb and Sn-Ag-Cu) are widely used for die-attach material, this is because their ease of processing at temperature below 300^{o}C. Nevertheless, for high temperature applications (>350 ^{o}C) in automotive, well logging in oil and gas industry, avionics, radars, nuclear power plant and space exploration (K. S. Tan et al., 2015); these die-attach material failed to meet their stringent requirement, and one of the significant disadvantages is their low melting and operating temperature.

A few of high temperature die-attach material have been reported. Silver (Ag) for example is a very promising candidates due to it exhibits high melting temperature (960 ^oC), high thermal and electrical conductivity, and better reliability. Other potential die attach material such as are off-eutectic gold(Au)-based alloy, liquid-based, bismuth-based, and silver-indium-based die attach materials also been reported.

The off-eutectic gold-tin (Au-Sn) alloy shows excellent performance at high temperature: high thermal and electrical conductivity, superior corrosion resistance and a fluxless soldering process. However, Au-Sn solder is limited to an operating temperature of 280 ^oC. The melting temperature of Au-Sn solder can be shifted to 700 ^oC by increasing the Au content, however, this type of alloy requires a high processing temperature. Hence, the investment in the soldering is expected to be higher. Another Au based solder alloy, Au-nickel (Ni) exhibits high melting point of 980^oC that meet the operating temperature requirement. However, soldering of Au-Ni solder alloy requires very high temperature, which is a major drawback for this solder. Bismuth (Bi) based solder alloys are the next proposed alternative solutions. Of these, Bi based solder alloys display poor thermal conductivity [7-11 W/m-K], low electrically conductivity [0.02-0.12 x10^5 (Ω-cm)$^{-1}$] and moderate melting point [262-361°C], which are not possible to be considered as alternative solutions. Therefore, the next alternative solution, namely inter-diffusion bonding has been introduced to overcome the weakness of Au-Ni solders: high soldering temperature. For instance, Au-indium (In) and silver (Ag)-In re particular die-attach materials that utilized inter-diffusion bonding technique to form a joint between metal films at temperature of 206 to 210°C with pressure of 40 to 80 psi. Nevertheless, the application of pressure may lead to cracking issue for both the die and the substrate because it can complicate the process of manufacturing..

In recent years, a new novel of die-attachment has been introduced, which it is named as nanopaste. The reduction of particle size from nano to micro aims to increase the chemical driving force of metal particles and thus to eliminates the application of external pressure during sintering. Ag nanopaste and Cu nanopaste are the representatives for this strategy, where they could be sintered at low temperature (280-400°C) and pressureless environment. Furthermore, the positive results of both Ag and Cu Nanopaste have been reported: (i) high melting point of 960-1083°C has met the operating temperature requirement of a SiC device. (ii) high thermal conductivity [200-240 W/m-K] and electrical conductivity [2.50-2.60 x10^5 $(\Omega\text{-cm})^{-1}$]. (iii) high bonding strength [2-54 MPa] could be attained with atomic inter-diffusion between the nanopaste and the metallization layer on a die or substrate. (iv) sintered nanopaste have a lower Young's modulus than its bulk materials and solder alloys, it can help to reduce the build-up of thermal stress when the device is being operated. (v) no existent of die-shifting issue as the nanopaste does not undergo liquid-state transformation during sintering. However, both Ag and Cu nanopaste have their own limitations: Ag nanopaste has low electrochemical migration resistance and high cost, while Cu nanopaste has the oxidation concern, which need annealing to remove oxides.

In this research, Al-Cu nanopaste has been introduced for high temperature die-attachment. Both Al and Cu have high melting point (Al: 660°C, Cu: 1085°C), Cu also has a higher thermal conductivities among other metals. Moreover, Al-Cu die-attach systems would able to solve the cost restraint in electronic packaging. However, the electrical and thermal conductivity of Al is fairly lower than Cu. Therefore in this research, the content of Cu with be more than Al content. The Al-Cu nanopaste is formulated by mixing Al and Cu nanoparticles with organic additives. This nanopaste can be sintered at 380°C in open air without the need of applying external pressure. The study covered the detailed investigation of the physical, electrical and thermal properties of Al-Cu nanopaste with various Cu loadings, as these properties are crucial for die-attach applications.

1.3 Objectives

In this research, the primary objective is to employ Al and Cu nanoparticle to form a die-attach nanopaste system which is appropriate for high temperature applications. The die-attach system should demonstrate acceptable characteristic at high temperature. The following objectives derived from main objective are listed as below:

1. To develop a Al-Cu die-attach material system by using metallic nanoparticles and organic additives.
2. To design an effective sintering profile which can promote the coalescence of Al and Cu nanoparticle and organic additives burn off to form an Al-Cu die-attach nanopaste system.
3. To investigate the physical, thermal and electrical attributes of Al-Cu nanopaste: (i) varying by (i) the loading of metallic nanoparticle (Al:Cu) (ii) the loading of organic additives.

1.4 Scope of Study

In this research, Al and Cu nanoparticle were used to mix with organic additives in order to formulate the Al-Cu die-attach nanopaste. The weight of Al nanoparticle loading and organic additives was varied to achieve the optimum electrical and physical properties of the sintered Al-Cu die-attach nanopaste. A sintering profile was designed by studying the organic additives burn off during sintering process. A Semiconductor Parameter Analyzer (SPA) system was employed to measure the electrical properties. Scanning electron microscope (SEM) analysis was used to observe the surface morphology of sintered Al-Cu die-attach nanopaste.

1.5 Outline of Thesis

This thesis is divided into 5 chapters: Chapter 1 discussed an overview of high temperature die-attach material for SiC power device, the problem statements for current die-attach material research and development, research objective as well as scope of the research project. Chapter 2 provided a literature review for the high temperature die-attach material, findings and problems encountered. Chapter 3 demonstrated the materials, equipment used as well as the research methodology carried out in this research project. Chapter 4 presented the results and findings of this research work. Chapter 5 delivered conclusion and future recommendation to this work.

CHAPTER 2

LITERATURE REVIEW

2.1 Introduction

The demand of electronic devices for high temperature application is increasing in recent years. For instance combustion systems for automotive (500-1000^{o}C), well logging application in oil and gas industry (~600 ^{o}C), turbine and gas sensors for avionics (~600 ^{o}C), electronic devices for space exploration (>500 ^{o}C), detectors and reactors for nuclear power plant (700-1000^{o}C) (Dreike, Fleetwood, King, Sprauer, & Zipperian, 1994; Kwak & Hubing, 2007; Manikam & Cheong, 2011; Watson & Castro, 2015). Conventional Silicon (Si) based electronic device with its low operating temperature is no longer meet the high temperature requirement. Therefore, a series of wide band-gap (WBG) semiconductors such as silicon carbide (SiC), gallium nitride (GaN) and diamond has emerged as the solution for high temperature electronic applications. This technology addresses the limitations associated with silicon (Si) based devices, for instance power density, switching speed, junction temperatures (Dreike et al., 1994; Manikam & Cheong, 2011). SiC, for example, has demonstrated the ability to function under extreme conditions and enable significant improvements to a wide range of applications and systems. The research of high temperature electronic devices is thereby targeting to develop die-attach materials that is in line with the SiC-based electronic devices. The die-attach materials designed for SiC technology should be able to withstand high temperature and not show any deterioration of its mechanical and electrical properties. This chapter reviews the recent research works for high temperature die-attach materials on wide band-gap materials, their concerns, success and the possibilities for high temperature applications. Subsequently, the fundamental of nanomaterials and fabrication approaches will be discussed.

2.2 High Temperature Applications

2.2.1 Automotive

In automotive industry, microelectromechanical systems (MEMS) are the leading technology for modern vehicles such as hybrid electric vehicles and fuel cell vehicles. By applying MEMS, a vehicle is improved in overall safety, fuel efficiency and reduce the emission (Kiencke & Nielsen, 2000). However, a MEMS-based vehicle needs to be installed up to 1000 electronic sensors for monitoring brake and exhaust system, angular position and speed, power steering, engine's condition and so on (Fleming, 2008).

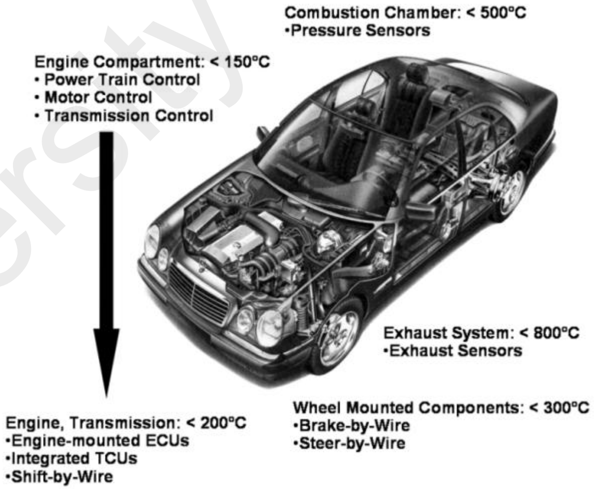

Figure 2.1: Automotive temperatures and related systems

The operating temperature of sensors varies at different installed locations. Although the automotive industry set the high temperature as electronic sensors is operated above 125^{o}C, the operating temperature of the sensors is dependent on the installed location, thermal design and the ability of the electronics to dissipate heat energy. **Table 2.1** demonstrates the operating temperature in every related system: pressure sensors used in combustive chamber and exhaust sensor used in exhaust system, the operating temperature for these 2 locations can be up to more than 500°C.

An automotive exhaust system consists of an exhaust manifold, a flexible, centre, front and tail pipe, catalytic converter and a main muffler (as illustrated in **Figure 2.3**). In some model, the catalytic converters and/or a sub-muffler is/are more than one. The operating temperature of particular components exhaust system for an automotive can reach to 1000°C as shown in **Table 2.1**. In order to enhance the entire system of an automotive, these installed sensors are required to withstand high temperature without failure.

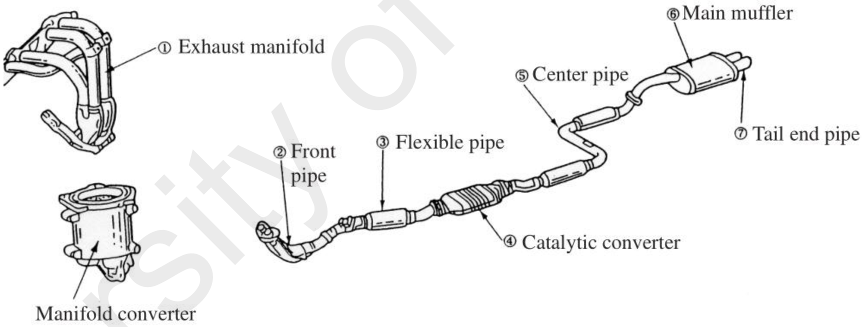

Figure 2.2: Components for Automotive Exhaust System

The function of exhaust manifold is to collect exhaust gas from each of the engine cylinders and direct it to front pipe, the service temperature of this component is as high as 900°C. Therefore, the properties required for those installed sensors and devices are high melting temperature, oxidation resistance and thermal fatigue properties. Catalytic converter is another crucial component in exhaust system, because it purifies the air pollutants caused by exhaust gas. The converter consists of a catalyst, a co-catalyst, washcoat and catalyst carrier. Since the catalytic convert is mounted immediately below the exhaust manifold, the installed sensors and devices must firstly workable under high temperature and severe service conditions such as vibration and so forth.

Table 2.1: Exhaust system components and respective service temperature

Component	**Service temperature** (°C)	**Required properties**	**Reference**
Exhaust manifold	750-950	i) High temperature strength ii) Thermal fatigue life iii) Oxidation resistance iv) Workability	(Inoue & Kikuchi, 2003)
Front pipe & flexible pipe	600-800		
Catalytic converter	1000-1200	i) Oxidation resistance ii) Thermal shock resistance	
Center pipe	400-600	i) Salt damage resistance	
Main muffler & tail end pipe	100-400	i) Corrosion resistance at inner surface (condensate) ii) Corrosion resistance at outer surface (salt damage)	

2.2.2 Well Logging

Oil & gas industry is the oldest and currently largest users for high temperature electronic devices. In well logging application, sophisticated sensors and data acquisition electronic systems are installed in vicinity to the drilling head in oil, gas and geothermal wells to monitor parameters such as temperature, pressure, flow rate, density and chemical composition (Baird et al., 1993; Kirschman, 1999; Parmentier, Vermesan, & Beneteau, 2003; Traeger & Lysne, 1988; Turner, Fuierer, Newnham, & Shrout, 1994). In this application, the operating temperature is dependent on the depth of the well. In past decades, the operating temperature was ranging between 150°C to 175°C. However, deeper drilling is motivated due to the shortage resources on surface and subsurface coupled with the advancement in technology. The applications for high-temperature electronics in the downhole industry can be quite complex. During a drilling operation, the functions of electronics and sensors are to steer drilling equipment and monitor the health of drilling head by measuring the drilling depth as a function of temperature: the temperature of existing well is typically maxed to 250°C, it also can be ranging up to 600°C for the deepest drilling depth which can be attained by current drilling technology. While drilling, the electronics and sensors are used to acquire data and information through the process, such as surrounding geologic formation and hydrocarbon saturation, this information allows determining the adequate amounts of hydrocarbon that can be extracted from the well. Finally, during the hydrocarbon extraction stage, sensors and electronics are used to monitor temperature, pressure, vibration and multiphase flow of hydrocarbon; this is to ensure the productivity from the well is optimized, and also to prevent any catastrophes that could be occurred.

2.2.3 Avionics

The revolution of aviation technologies is moving toward a “more electric aircraft” (MEA). The MEA initiative is to utilize electrical power for all non-propulsive systems. These non-propulsive systems in a conventional aircraft are driven by centralized control system embodied with a combination of hydraulic, mechanical, pneumatic and electrical power (AbdElhafez & Forsyth, 2009; Naayagi, 2013; Sarlioglu & Morris, 2015). This system requires a large amount of wiring, piping and connector interfaces to transmit the signal and power generated from the central electronic controller to the respective systems. In line with the target of MEA, a distributed control system is being introduced where the electronic controller are placed near to the engines. In a MEA aircraft, the complex wiring interconnections, large amount of piping system is effectively reduced, thereby saving the weight of aircraft and reduces the maintenance complexity. Consequently, it provides a better control reliability, survivability and fuel efficiency than a conventional aircraft. However, these electronic controllers need to be operated at high temperature environment. For instance, the controller installed to monitor rotation speed of turbine disk in aircraft engine has to withstand at an elevated a high temperature of 600°C; controllers and sensors for combustion emission monitoring need to operate at temperature ranging up to 800°C.

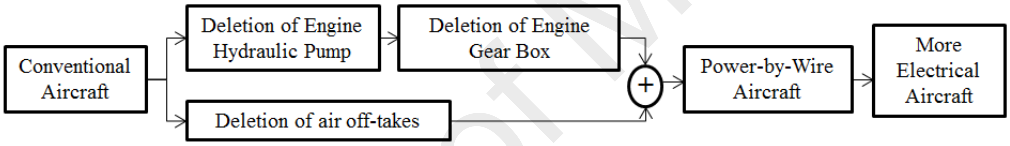

Figure 2.3: Current trend towards a more electric aircrafts

2.2.4 Space Exploration

Space missions have unique requirements for the payloads of electronic devices and other components. Venus was the first target of interplanetary flyby and lander missions since past decades, despite of the most hostile surface environment: the surface temperature of Venus is ranging between 460°C-480°C, with a 92 bars of carbon dioxide-nitrogen atmosphere, and sulfuric acid cloud coverage at a distance of 50km from the surface (Von Zahn, Kumar, Niemann, & Prinn, 1983). The electronic devices and sensors are fabricated for Venus exploration must be able to sustain under harsh and hostile conditions in order to execute the missions on this planet.

2.3 Wide Band-gap Semiconductor

In recent year, the demand of electronic device that possesses higher switching speeds, high power density and lower switching losses is increasing. Silicon semiconductor has reached its saturation point, therefore, sourcing efforts for wide band-gap (WBG) semiconductors such as silicon carbide (SiC), Gallium Nitride (GaN) and diamond (Casady & Johnson, 1996; Glass, Messier, & Fujimori, 1990). Wide band-gap material generally possesses some superior properties: (i) WBG material such as SiC (3.26 eV) allow the device to be operated at high temperature, SiC-based integrated circuit is capable to work under 300-500°C which will be extensively applied in many sectors such as automotive, avionics, nuclear plant and etc. (ii) WBG materials demonstrate higher electrical breakdown field, which allow device to be operated at high voltage. For instance, Si schottky barrier diode (Si-SBD) has a blocking voltage of 100V, however SiC schottky barrier diode (SiC-SBD) have reached the maximum blocking voltage of 1700V. Thus, SiC material is much easier to implement the high voltage applications such as manufacturing of PIN diode and IGBT. (iii) The thermal conductivity of SiC material is 4.9W/cm°C, which is approximately 3 times higher than Si material.The implementation of SiC integrated circuit can reduce or even eliminate the cooling system, which effectively reduces the weight and volume of an system and greatly improves its integration. In addition, SiC devices can enhance the reliability and stability in high temperature and harsh environment. (iv) SiC material has large maximum electron saturation velocity, which indicates that SiC material has faster switching speed and higher current density, more appropriate for high power and high frequency applications (Casady & Johnson, 1996; She, Huang, Lucia, & Ozpineci, 2017).

Table 2.2: Material properties of SiC and GaN in comparison with those of silicon and diamond

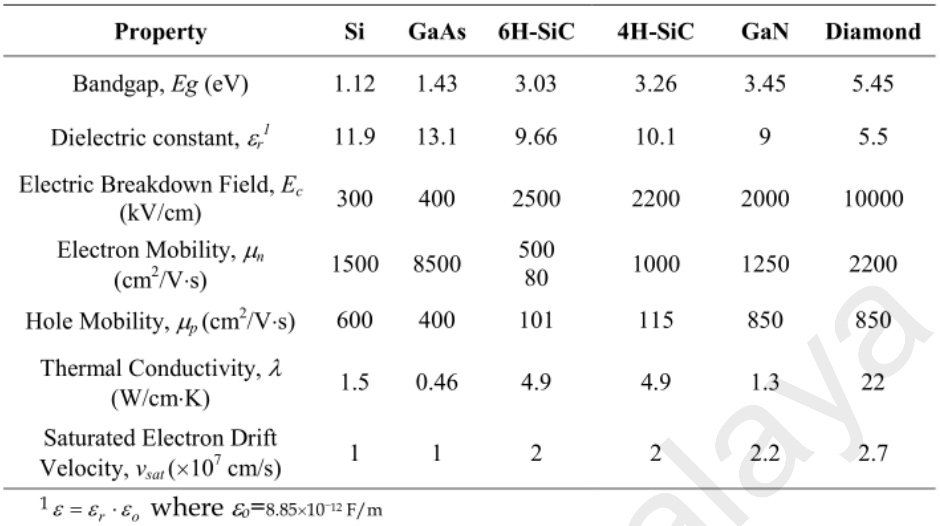

Property	Si	GaAs	6H-SiC	4H-SiC	GaN	Diamond
Bandgap, E_g (eV)	1.12	1.43	3.03	3.26	3.45	5.45
Dielectric constant, ε_r^1	11.9	13.1	9.66	10.1	9	5.5
Electric Breakdown Field, E_c (kV/cm)	300	400	2500	2200	2000	10000
Electron Mobility, μ_n (cm^2/V·s)	1500	8500	500 80	1000	1250	2200
Hole Mobility, μ_p (cm^2/V·s)	600	400	101	115	850	850
Thermal Conductivity, λ (W/cm·K)	1.5	0.46	4.9	4.9	1.3	22
Saturated Electron Drift Velocity, v_{sat} ($\times 10^7$ cm/s)	1	1	2	2	2.2	2.7

$^1\ \varepsilon = \varepsilon_r \cdot \varepsilon_o$ where ε_0=8.85×10^{-12} F/m

2.3.1 Characteristics of SiC power electronic devices

The first commercial SiC-SBD products were introduced by Infineon in 2001. After 2001, more commercial SiC devices have been gradually being introduced. Figure 2.4 shows the development process of the commercialization of SiC power electronic devices.

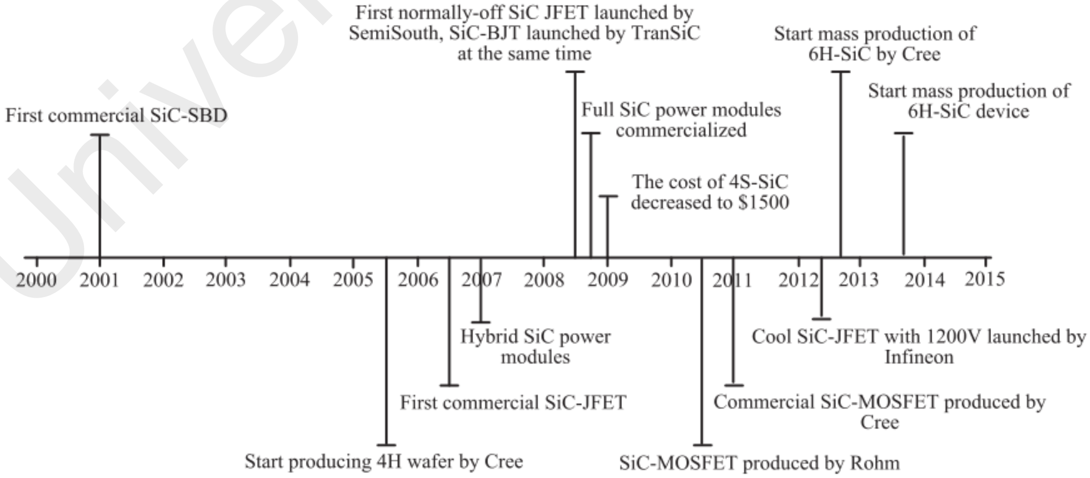

Figure 2.4: The development process of SiC semiconductor devices

Table 2.3: The main manufacturer's device and the highest level of SiC-SBD

Manufacturers	Type	V_{RRM} /V	I_{f} /A	V_{fT} /V @ 25 °C	I_R /uA @ 25 °C
Cree	C3D25170H	1700	26.3	1.8	100
Infineon	IDH15S120	1200	15	1.8	360
Microsemi	APT30SCD120B	1200	30	1.8	600
ST	STPSC6H12	1200	6	1.9	400
Rohm	SCS240KE2	1200	40	1.4	400

2.3.1.1 SiC-SBD

In comparison, the SiC-SBD is much better than conventional Si diode. The significant advantages of SiC-SBD are improved blocking voltage, and almost no reverse recovery process and better thermal stability. Currently, Cree, ST and other manufacturers are available to provide the following commercial SiC-SBD products: 600 V (1–20 A), 50 V (1–50 A), 1200 V (1–50 A), 1700 V (1–50 A). Figure 2.5 shows the comparison of the reverse recovery process between SiC-SBD and Si fast recovery diode (Si-FRD). It can be seen that there are almost no reverse recovery time for SiC-SBD, and it is not affected by temperature variation (She et al., 2017).

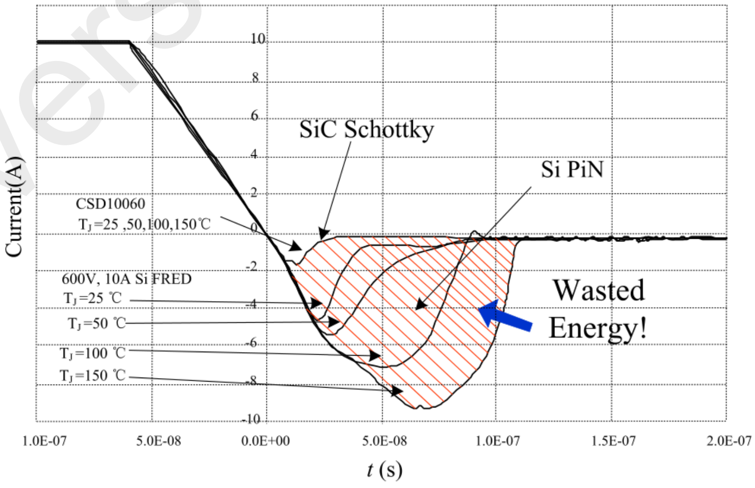

Figure 2.5: Reverse recovery contrast comparison of SiC-SBD with Si-FRD

2.3.1.2 SiC JFET

SiC-JFET is a kind of controllable devices with low on-resistance, high switching speed, high temperature resistance and high thermal stability. SiC-JFET has two types, i.e., normally-on and normally-off. Generally, the normally-on SiC-JFET is in on-state when there is no drive signal, this will easily cause the short circuit of the bridge arm and reduce the reliability of bridge arm circuit. Although there is no such problem for normally-off SiC-JFET, the threshold voltage is low, only about 1 V, this makes the bridge arm circuit very susceptible to be misenergized caused by crosstalk of bridge arm. Currently, Infineon has commercialized SiC-JFET discrete devices with the characteristics of 1200 V/25 A and 1200 V/35 A, and SemiSouth has commercialized SiC-JFET discrete device of 1700V normally-on type (She et al., 2017).

2.3.1.3 SiC-MOSFET

SiC-MOSFET has high withstanding voltage level. Currently, Cree, Rohm and other companies have launched 1200 V SiC-MOSFET devices, with single-discrete package and multiple-module package. Cree also has produced 1700 V single discrete SiC-MOSFET device, and has commercialized 1200 V/300 A bridge arm module. The junction temperature of the commercialized SiC-MOSFET from the two companies almost reaches to 175 °C. The on-state resistance of 1200 V/40 A discrete SiC-MOSFET made by Rohm is only 80 mΩ (She et al., 2017).

2.3.1.4 SiC-BJT

SiC-BJT is one of the most attractive SiC power electronic devices that having features of low resistivity, small temperature dependence and fast switching speed. SiC-BJT also has excellent short-circuit capability without secondary breakdown, which makes SiC devices work more reliable. Currently, GeneSiC has launched the 1700 V/100 A SiC-BJT. Overall, the commercialized SiC power electronic devices have the advantages of lower on-state resistance, smaller interelectrode capacitance and faster switching speeds (She et al., 2017).

2.4 Die-attach Materials

2.4.1 Electrical Conductive Adhesives

Electrical conductive adhesives (ECAs) are another die-attach alternatives for solder connection technology. Compared to solders, ECAs require lower curing temperature and fewer processing steps. Therefore, the role of ECAs is increasingly important in the electronic package applications. The advantages of ECAs are: (i) minimal toxicity and adversely environmental impacts. (ii) Lower curing temperature reduces the stress cracking and joint fatigue issues. (iii) The smaller filler particle size enables to facilitate finer line resolution. (iv) The higher flexibility and the closer match in coefficient of thermal expansion enable a more compliant connection and minimize failures. However, ECAs still have its own limitations: (i) High humidity, high temperature, and high current densities have been shown to increase contact resistance that could lead to circuit failure. (ii) the weaker bond strengths in ECAs, rework is not as convenient, and ECAs tend not to be as reliable as metallurgical or separable interconnects because of the vast number of particle-particle interfaces that occur (Li & Wong, 2006).

Table 2.4: Characteristics of ECAs and Pb-Sn solders (Li & Wong, 2006)

Characteristics	ECAs	Pb-Sn solders
Thermal conductivity (W/mK)	3.5	30
Electrical resistivity (Ω cm)	0.00035	0.000015
Minimum processing temperature (^{o}C)	150-170	215
Shear strength (psi)	2000	2200
Thermal fatigue	Minimal	Yes
Environmental impact	Very minor	Negative

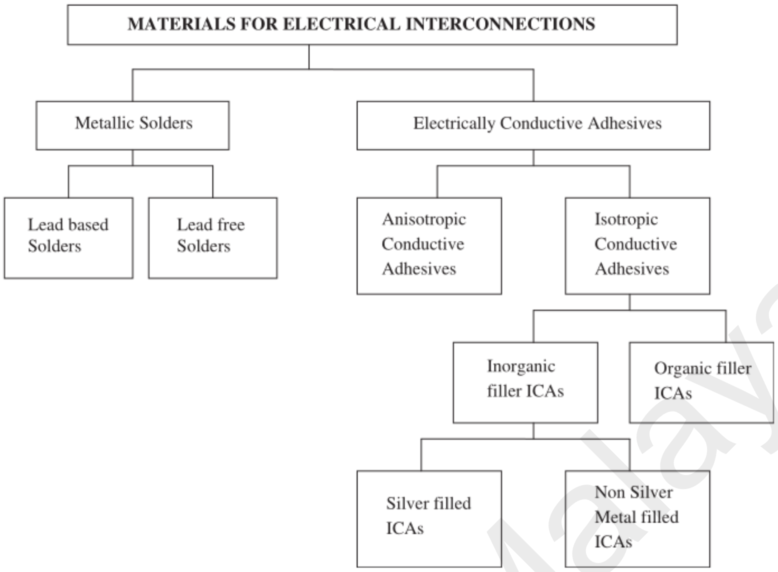

Figure 2.6: Different materials used in electrical interconnections

Electrical conductive adhesives (ECAs) mainly consist of a polymeric resin and metal filler. Polymeric resin refers to non-electrical conductive material such as an epoxy, a silicone or polyimide, which presents to provides physical and mechanical strength of ECAs, a metal filler (such as silver, gold, nickel or copper) exists to conduct electricity. Depends on the filler's structure, ECAs can be further categorized into isotropically conductive adhesives (ICAs), anisotropically conductive adhesives (ACAs) and nonconductive adhesives (NCAs) as illustrated in Figure 2.7. ICAs have a 1-10µm sized of metal filler that enable to conduct electricity in all *x*,*y* and *z* directions. ACAs however, the metal filler is typically sized between 3-5µm, which is only able to provide electrical conductivity in both *x* and *y* directions (Li & Wong, 2006).

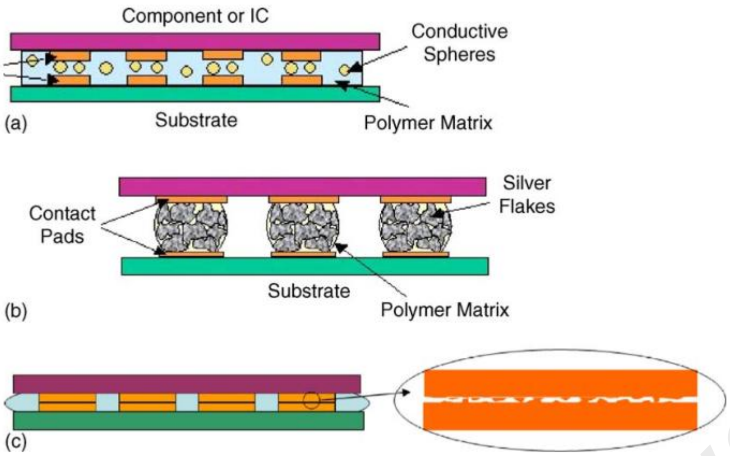

Figure 2.7: Schematic illustrations of (a) ACA, (b) ICA and (c) NCA in flip–chip bonding.

2.4.1.1 Anisotropic Conductive Adhesives

Anisotropic conductive adhesives (ACAs) allow only one-axis' electrical conductivity; this property can be achieved by using the conductive filler's concentration below the percolation threshold, therefore the concentration of conductive filler is limited to allow the *z*-axis' electricity, and not *x*-*y* plane. ACAs are available in form of film or paste, which they are attached between the substrate surface and a die to form the die-attachment; heat and pressure are applied concurrently to this assembly until the particles bridges the two adherents. ACAs also can be used for non-conductive adhesives (NCAs), which are used to provide structural supports on devices. The applications of ACAs include flip-chip technology and smart cards where soldering are not applicable because of the thermal sensitivity of the substrate (Li & Wong, 2006).

2.4.1.2 Isotrophic conductive adhesives

Isotropic conductive adhesives (also known as "polymer solder") mainly consist of metal filler and polymer resin. The materials used for polymer resin are thermoplastic (phenolic epoxy, maleimide acrylic preimidized polyimide, etc.) or thermosetting (epoxy, cyanate ester, silicone, polyurethane, etc.). Epoxies are currently used for many commercial ICAs due to its unique properties: sufficient adhesive strength, low cost and acceptable chemical and corrosion resistance. However, thermoplastic are usually used for softening and rework under moderate heat. The metal filler can be silver (Ag), nickel (Ni), gold (Au) or copper (Cu) in various shapes and sizes. Especially silver flakes, which are the most commonly used for conductive fillers for current ICAs, this is because Ag exhibits high thermal and electrical conductivity among all metal fillers. Besides, Ag requires no curing process to remove oxides which can simplify the manufacturing process. Other metal fillers such as Cu and Ni are easily oxidized which leads to degradation of ICAs' properties. Therefore Ni and Cu based ICAs do not have good resistance stability. Even with antioxidants, Cu based ICAs shows an increase in bulk resistivity after aging, particularly under high humidity and high temperature environment (Li & Wong, 2006; Mir & Kumar, 2008).

Ye, Lai, Liu, and Tholen (1999) studied the effects of Ag particle size on electrical conductivity of ICAs: the weight percentage of Ag flakes is kept at 70% for all the samples. Results showed that the more nano-sized Ag particle is introduced to micro-sized particles, the higher electrical resistivity can be obtained. This is due to the introduction of nanoparticle reduces the chances of direct contact between micro-sized Ag particles. Also, the contact area for nano-Ag and micro-Ag is smaller than micro-Ag and micro-Ag particles. The different of particle sizes and contact area between particles, which are crucial factor for an ICAs.

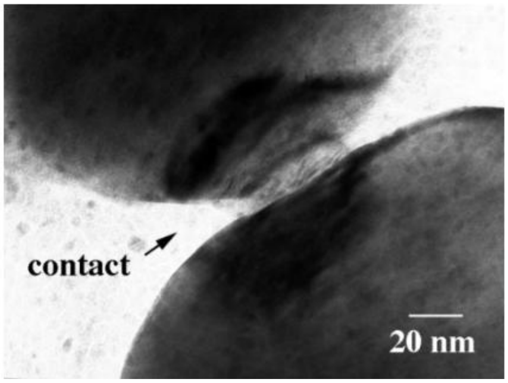

Figure 2.8: Direct contact between two micro-sized particle (TEM image)

Table 2.5: Different size of Ag and their respective electrical resistivity

	Ag flake	**Micro Ag particle**	**50% micro-50% nano Ag particle**	**80% micro-20% nano Ag particle**	**Nano Ag particle**
Electrical Resistivity (Ωcm)	4.23×10^{-3}	7.21×10^{-3}	5.88	0.36	Non-conductive

H.-H. Lee, Chou, and Shih (2005) also investigated the effect of nano-sized Ag particle on the electrical resistivity on ICAs: the minor addition of nano-sized Ag would lower the electrical resistivity of ICAs if the micro-sized Ag flake and ICAs is near the percolation threshold. However, where the micro-sized Ag flake is exceed the percolation threshold, additions of nano-sized Ag would reduce the chance of direct contact between Ag flake, which would exhibit a negative effect of electrical conductivity of ICAs.

2.4.2.3 Reliability of ECAs

The existence of conductive adhesives is a promising lead-free alternative for die-attachment. However, the replacement of solder by this technology has not been widely adopted by the electronics industry owing to several drawbacks which are mainly seen in the reliability aspect of the adhesive joining.

(i) Impact strength

Impact strength is one of the crucial properties for ECAs to replace solders. Hence, a drop test has been devised by National Centre for Manufacturing Science (NCMS) to evaluate the impact strength of ICAs. In this test, a mounted chip carrier and circuit board assemblies are dropped from 1.5m height onto hard surface. A conductive adhesive must pass six drops for application as a replacement of solder (Zwolinski et al., 1996). Falling wedge technique is another impact resistance test for conductive adhesives. This test is capable to differentiate the impact performance of ECAs for bonding purpose, as well as providing useful information for ECA development (S. Xu & Dillard, 2003). Unlike drop test, it can only quantitatively distinguish the impact performance of ECAs.

Macarthy suggested improving the impact strength by decreasing the loading of conductive filler, this effort could lead to decrease in electrical properties of ECAs (Macarthy, 1995). Vons, Tong, Kuder, and Shenfield (1998) developed the ECAs using low modulus resins which can absorb impact energy developed during the drop. Similarly, a conformal coating of surface mount was used to improve mechanical properties of ECAs, and it is proven that conformal coating could improve the impact strength of an ECA. Lu and Wong (1999) incorporated high toughness and good adhesion polyurethane materials to increase the impact strength of ECAs. This class of ECAs demonstrates good damping properties and impact strength and substantial stable contact resistance with non-noble metal surfaces such as Sn/Pb, Sn and Cu.

(ii) Adhesion strength

The adhesion strength of an ECA is provided by its nonconductive polymeric matrix. However, the incorporation of conductive fillers can decrease the adhesion property, which limits its use in many applications. Inada and Wong (1998) studied the effect of silver flake's orientations on epoxy matrix and adhesive strength of ECAs, randomized orientation of silver flakes was found to be effective in improving the adhesive strength of ECAs. Matienzo, Egitto, and Logan (2003) used organo-silane as coupling agent in epoxy based ECAs. It was found that the organo-silane not only enables to improve the adhesion properties, but also can acts as corrosion inhibitors on aluminum surfaces to stabilize the electrical performance. Similarly, F. Tan, Qiao, Chen, and Wang (2006) reported the use of two different coupling agent: titanate and silane to improve an epoxy based ECAs . Liong, Wong, and Burgoyne (2005), reported the use of polyarylene ether to improve the adhesion properties of a thermoplastic ECA. The adhesion properties can be improved by two methods: coupling agents and blending thermoplastic ECA with epoxy, both method were investigated its successful in improving adhesion strength of ECAs.

(iii) Contact resistance

Contact resistance between an conductive adhesive and non-conductive finished components is the main cause of electrical reliability issues. NCMS set criteria for solder replacement ECA: the contact resistance is stable if shift is less than 20% after 50h at 85^{o}C/85% relative humidity aging (Zwolinski et al., 1996). The unstable electrical conductivity is because of the growth of oxide layer between conductive filler in the adhesive from its substrate (Tong, Vona, Kuder, & Shenfield, 1998). The increase of contact resistance can be interpreted by two mechanisms: simple oxidation and corrosion of the non-noble metal surface. In literature, simple oxidation was the main reason for the increase of contact resistance, while some literature reported that corrosion as the possible mechanism for resistance shift. Galvanic corrosion between dissimilar metals at the contact surface is indicated by some authors for the main mechanism of resistance shift of the ICAs (D. Lu, Q. K. Tong, & C. Wong, 1999a; D. Lu, Q. K. Tong, & C. P. Wong, 1999b). At anode side, the non-noble metal is reduced by losing electrons, and turns into metal ions (M^{n+}). At cathode side, the formation of OH^- takes place. Overall, the M^{n+} combine with OH^- to form metal hydroxide ($M(OH^-)$) and then metal oxide (MO).

Anode $\mathrm{M} - \mathrm{n}e^- \rightarrow \mathrm{M}^{\mathrm{n}+}$

Cathode $2\mathrm{H_2O} + \mathrm{O_2} + 4e^- \rightarrow 4\mathrm{OH}^-$

Overall $\mathrm{M}^{\mathrm{n}+} + \mathrm{OH}^- \rightarrow \mathrm{M(OH)_n} \rightarrow \mathrm{MO}$

A layer of MO is formed at the interface of conductive filler in the adhesive of its substrate. This layer is insulating the movement of electrons, results in the increase of contact resistance, which could negatively affect the electrical performance of ECAs. Galvanic corrosion is induced in wet conditions, so ECAs with low moisture adsorption can minimize the galvanic corrosion at the interface of ECAs. Besides, impurities of the polymer binder lead to galvanic corrosion at interface as well (Lu et al., 1999a).

Lu and Wong (2000) studied the effect of purity of the resins and moisture absorption on contact resistance. Additives such as corrosion inhibitors and oxygen scavengers have been used for the study of contact resistance stability under elevated temperature and humidity ageing. ECA with higher purity and low moisture adsorption demonstrates more stable contact resistance. In comparison, corrosion inhibitors are more effective than oxygen scavengers in stabilizing contact resistance.

(iv) Environmental reliability

During ECAs' service life, they might be exposed to various environmental conditions. The presence of moisture in service environment is one of the important factors to determine the reliability of an ECA. The moisture adsorbed in nonconductive polymer matrix can lead to both reversible and irreversible effects, e.g. plasticization (the intermolecular interactions is being weaken), de-bonding at the filler-matrix interface, leaching of un-reacted functional group, structural damage (micro-cavities, crazes), further cross-linking and chemical degradation by hydrolysis and oxidation during long-term exposure to water. Moisture adsorption in polymer could significantly affect the thermal properties, mechanical properties (young modulus, bonding strength) and fracture toughness (Mir & Kumar, 2008).

S. Xu and Dillard (2003) studied the failure mechanisms of ECA joints, they studied Ag-filler epoxy based adhesive systems in conjunction with printed circuit board substrates with metallization of Au/Ni/Cu and Cu. The failure mechanisms were divided into three phases: displacement of adhesive from the substrate, formation of metal oxides at the interface and weakening of metal oxides. In terms of environmental friendliness, ECAs are generally better than solders according to numerous studies. Thus, ECAs will be a very promising solder replacement in electronic packaging.

2.4.2 Eutectic Die-attach Solder

Eutectic die attach solders are typical alloys fabricated at their respective eutectic temperature. Generally, the eutectic temperature of the alloy will determine the maximum operating temperature of the device. The complex heating and cooling mechanisms are employed to achieve a high reliability eutectic solder.

Pb-Sn eutectic solder has been used for die-attach material for a period because of its good soldering properties, low price, manufacturability and reliability. Both 63Sn-37Pb and 60Sn-40Pb are primarily used for in board level packaging. The Sn-Pb binary system allows the soldering conditions at 183^{o}C, which are compatible with most of the substrate materials and devices. The uses of Pb has gained some technical advantages, which include the following to Sn-Pb solders: (i) the addition of Pb helps to reduce the surface tension of pure Sn (550mN/m at 232^{o}C), and also reduce the surface tension of 63Sn-37Pb solder (470mN/m at 280 ^{o}C) which facilitates the wetting process. (ii) Pb enables other joint constituents such as Cu and Sn, forming intermetallic bonds rapidly by diffusing in the liquid state. Nevertheless, the uses of Pb as alloying element had been restricted by legislation on end-of-life disposal because Pb is toxic to human. As a result, the Pb-Sn solder is eliminated from consumer electronics sold in markets and stimulated the research and development to discover the alternatives for Pb-Sn solders (Abtew & Selvaduray, 2000).

The adoption of lead free solders must fulfill some requirements: the primary requirement for the alloy candidates to replace Pb must be non-toxic, low melting and other properties that equivalent to Pb. The alloy candidates that are commonly considered include Indium (In), Bismuth (Bi), Cadmium(Cd), Antimony (Sb), Germanium (Ge), Silver (Ag), Gold (Au), Copper (Cu), Manganese (Mn), Nickel (Ni), Cobalt (Co), Iron (Fe), Titanium (Ti), Platinum (Pt), rare earth elements and nanoparticles. Cd and Sb are listed as hazardous substances because of their toxicity concerns in human and animals.

Table 2.6: List of lead-free solders, their melting temperature and characteristics (Cheng, Huang, & Pecht, 2017)

Element	**Melting point (°C)**	**Characteristic**
Indium (In)	156.6	- Lower melting point - Very scarce and expensive - high indium contents cause extreme soft and poor of mechanical strength in alloy - prone to corrosion - prone to oxidation during melting
Tin (Sn)	232	- Base alloy element - Lower melting point - readily available - Formation of tin whiskers and tin pest can be problematic
Bismuth (Bi)	271.5	- Lower melting point - Higher tensile strength - Increase brittleness in alloy and prone to thermal fatigue - Expands on solidifications - Becomes more brittle when contaminated with Pb - Some toxicity concerns in animals
Cadmium (Cd)	321.1	- Cadmium and its compounds are listed as hazardous substances. - Not suitable to be used in alternative lead-free solder joints.
Antimony (Sb)	630.5	- Enhance mechanical properties - slightly reduces electrical and thermal conductivity - Considered toxic and not to be used in alternative lead-free solder joints.
Germanium (Ge)	937.4	- Antioxidant
Silver (Ag)	962	- Absorbs Cu, intermetallic growth with Cu - Expensive
Gold (Au)	1063	- Higher melting point - Gold brittlement issues when increasing its content - Very expensive
Copper (Cu)	1084	- Economical and affected the least by lead impurities - prone to oxidation, removal of oxide layer can be difficult
Manganese (Mn)	1245	
Nickel (Ni)	1453	- Inhibits Cu dissolution
Cobalt (Co)	1495	- A bluish-white, lustrous, hard, brittle metal - Ferromagnetic properties - Active chemically and forms many compounds
Iron (Fe)	1535	
Titanium (Ti)	1660	
Platinum (Pt)	1772	- Can dissolve to Cu sublattice of Cu_6Sn_5
Chromium (Cr)	1857	- Can improve the share ductility of SAC solders - Can suppress void formation and coalescence at the Cu/Cu_3Sn interface

2.4.2.1 Considerations for Development of Solders

The development of lead-free solders must consider solder property, mechanical and reliability property of solder joint, regulations and costs.

Solder melting temperature is one of the crucial factors when developing a lead-free solder. The melting temperature affects complexity of the soldering process, performance of electronic devices and also the reliability of the electronic components. Generally, the soldering temperature is higher than the solder melting temperature. E.g. the melting temperature of SAC305 solder paste is 217°C, the soldering temperature could be 25°C higher than its melting temperature. The electronic components can be damaged if the solder processing temperature is too high, e.g. melting of the internal solders connections, or decomposes the material. Higher reflow temperature might evaporate the entrapped moisture in the board, eventually resulting in crack formation. In contrast, low solder processing temperature could result in non-proper soldered components as well. When the melting temperature alternative solder is different with SAC305 solder, the alteration of equipment and process may be needed, which eventually can increase the cost. Therefore, the alternative solder adopted for replacement should work at a similar process temperature to SAC305, demonstrate similar performance of SAC305, or cost less. Except for some high temperature applications, the solders must have high melting temperature to warrant it does not melt during field use (Cheng et al., 2017; Frazier, Warrington, & Friedrich, 1995; Guarnieri, Di Noto, & Moro, 2010).

Solder Wettability is a property of molten solder to cover the surface of metal in the solder joint. Solder wettability is influenced by both wettability level and wettability speed. Wettability level sets how far the melted solder is spread on surface, whereas wettability speed is the speed of melting and spreading. Typically, the wetting for lead-free solders is significantly different from Sn-Pb solder: Lead-free solder has longer wetting period than Sn-Pb solder. When the soldering temperature increases, the wetting period decreases, this is because the surface tension and viscosity of lead-free solder is higher when the temperature increases. Figure 2.9 shows the wettability of both Sn-Pb solders and lead-free solder, Sn-Pn solder can achieve its good wettability at low temperature compared to lead-free solders. Therefore, in order to increase the wettability of lead-free solders, two options which are (i) increase the flux activity and (ii) reducing the O_2 concentration can be considered, rather than increasing soldering temperature (Dušek, Szendiuch, Bulva, & Zelinka; X. Xu, Gurav, Lessner, & Randall, 2011).

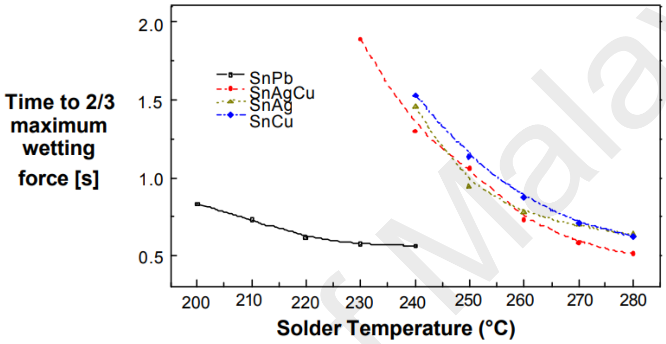

Figure 2.9: Wettability of Sn-Pb and lead-free solder alloys in air (Dušek et al.)

Solder drossing is another consideration that should be taken account in the lead-free alternatives, The oxides formed and displaced to the surface of the wave during the wave soldering in air. Drossing issue incurs high operation costs and causes imbalance of solder’s composition in the pot. The drossing issue in soldering process is caused by the Ag in SAC alloys. Cu dissolution is another factor to account for, portion of the Cu dissolve into the molten alloy when contact from the PCB pads and component terminations. The dissolution of Cu results in decreasing the properties of the PCB pad and terminations. Cu dissolution is a known problem with many lead-free alloys, e.g. causing hole-fill defects, generates more Cu intermatellic compound suspensions. Therefore, the lead-free alternative are expected to have low drossing and low Cu dissolution, which will help to reduce the operating cost for wave soldering (solder pot maintenance) and the use of "additive" bars to regulate the Cu content in the solder pot (Cheng et al., 2017).

In addition, an alternative solder should be non-toxic to human and the environment, Some elements in lead-free solders are considered toxic. E.g. Cd, Cr and Ni promotes the generation of reactive oxygen species (ROS), which can greatly damage DNA structure and contribute to the pathology of various disease (Ni, Huang, Wang, Zhang, & Wu, 2014). Bi has its toxicity concerns because of the risk of long-term toxicity to kidneys (Dorso et al., 2016). Besides, the alternative solder should be available in several forms. For instance, solder paste, wire, bars and spheres, for PCB assembly, component packaging and any required repair process. In addition, the quality of the lead-free solder should not be degraded throughout its storage life. Besides, an alternative solder should not degrades when contaminate with Pb. For instance, SnAgBi alloys have good mechanical properties, however the mechanical properties degrade when mixing with Pb. Trace amounts of Pb could turn SnBi alloy into powder during thermal cycling. This poses serious concerns for the applicability of SnBi solders, since Pb-based solders are still actively used in high-reliability applications and could cause contamination. This was one reason that SnBi solders were not chosen for widespread replacement as a lead-free solder alternative.

Lastly, a lead-free alternative should achieve a certain performance level which can suit to the targeted application. To determine the performance level, reliability tests includes vibration, thermal cycling, shock and drop tests need to be carried out to qualify an lead-free alternative. Data must be available for reliability tests on multiple electronic packages, ranging from lead frame leaded devices, ball grid arrays (BGAs, multiple ball alloys), quad flat no-leads packages (QFNs), and chip-scale packages (CSPs). The common reliability tests for solders are as follows (Cheng et al., 2017).

Table 2.7: Properties of solder alloys relevant to manufacturing, performance and reliability (Abtew & Selvaduray, 2000)

Properties relevant to manufacturing	Melting/liquidus temperature, Wettability (of copper), Cost, Environmental friendliness, Availability and number of suppliers, Manufacturability using current processes, Ability to be made into balls, Copper pick-up rate, Recyclability, Ability to be made into paste.
Properties relevant to reliability and performance	Electrical conductivity, Thermal conductivity, Coefficient of thermal expansion, Shear properties, Tensile properties, Creep resistance, Fatigue properties, Corrosion and oxidation resistance, Intermetallic compound formation.

2.4.3 Lead-free solders

2.4.3.1 Bismuth-based solders

Bi is one of the promising alternatives for lead free solder joints, the lower surface tension of Bi offer some advantages when it presents in minor amount to some lead-free solder alloy composition. For instance, it improves the wettability and solders spread, reduce melting temperature and surface tension of the alloys. Bi also used together with Ni in solder composition to reduce dissolution of Cu. (Lalena, Dean, & Weiser, 2002; Smith & Fickett, 1995; Song, Chuang, & Wen, 2007; Song, Chuang, & Wu, 2006, 2007).

Huang and Wang (2005) investigated the effect minor addition of Bi on microstructure and tensile properties of Sn-Ag based solders, the Bi addition decreases the solidus temperature of bulk solder, and inhibit the formation of large Ag_3Sn intermetallic in the bulk solder. In addition, minor amount of Bi presents in bulk solder increase the tensile strength while decrease the ductility of bulk solder. Y. Liu, Sun, and Liu (2010) investigated the effect of Bi in Sn0.3-Ag0.7-Cu-X-Bi solder with different ratio). Results were observed and compared to Sn0.3-Ag0.7-Cu solders by conducting different tests to determine wettability, strength, melting point and thermal aging. With proper adding of Bi element (X was 3.0), a positive effect on decreasing the melting point and improving wettability of Sn0.3-Ag0.7-Cu solder. However, excessive Bi addition into Sn0.3-Ag0.7-Cu solders broadened the range of melting temperature between liquidus and solidus, which may increase the brittleness of solder, leading to further solidification crack or even brittle failure in solder materials. With the adding of Bi, the growth of intermetallic compounds was prolonged during thermal aging. The shear test results after thermal aging proved that Bi addition prevented the degradation of the solder's mechanical property.

In recent research, Ahmed, Basit, Suhling, and Lall (2016) researched om the aging effects toward the mechanical behavior for SAC-Bi solder material. Mechanical stress-strain test had performed and some of the reflow samples were aged at a temperature of 100°C and stored for 3 months. It was discovered that SAC-Bi solder have improved in its mechanical attributes and also enhance its anti-aging resistant.

2.4.3.2 Zinc-based solders

Zinc (Zn)-based solders have gained the attention of researchers, this is because Zn is much cheaper and more abundantly available than other metals such as Au and Ag. Therefore, Zn is more suitable for mass manufacturing scenario. For instance, Zn-Sn solders exhibit a good die shear strength of 30-34Mpa, good thermal and electrical conductivity (1-1.06W/cm.K), Zn-Sn solders resist to oxidation in high temperature and humidity environment (Manikam & Cheong, 2011).

J.-E. Lee, Kim, Suganuma, Takenaka, and Hagio (2005) studied the effect of Sn element to the interfacial reaction of Zn-Sn solder on AIN ceramic substrates. Si die was coated with Au/TiN thin layers, no reaction with the solder alloy was observed. However, three layers of intermetallic compounds namely Cu, $CuZn_5$, Cu_5Zn_8 were formed. This research also reported that Zn-Sn solder exhibits its good characteristics. However, Kim,

Kim, Kim, and Suganuma (2009) pointed out clearly about an Au/Tin barrier was required for Zn-Sn solders that composite more than 30% of Sn loading to prevent the growth of intermetallic Zn-Cu, while performing the bonding of copper-solder-copper substrates. This is because the formation of Cu-Zn creates poor jointing strength in interfaces of copper-solder-copper substrate. In a similar literature work by J.-E. Lee, Kim, Suganuma, Inoue, and Izuta (2007), both Zn-Sn30 and Zn-In30 were studied; the Zn-In30 solder rusted seriously but no rusting observed on the Zn-Sn30 solder during thermal and humidity exposure for 1000h at 85°C and 85% relative humidity.

Jiang, Wang, and Hsiao (2006) doped different element with minor amount and investigated their effects on Zn-Sn solders. They found that Zn doping was effectively retarding the growth of intermetallic compounds Cu_3Sn and Cu_6Sn_5, whereas Ni doping could only inhibit the growth of intermetallic Cu_3Sn. Other elements doping has no effect on the intermetallic growth on Ni/Au surface. Beside, El-Daly, El-Hosainy, Elmosalami, and Desoky (2015) also doped Zn element into SAC 207 solder to study the doping effects on morphology and tensile properties, found that proper amount of Zn addition could refine the Ag_3Sn and Cu_6Sn_5 intermetallic compounds and promote γ-$(Cu,Ag)_5Zn_8$.These phases attributed to a dispersion strengthening effect to Sn-Ag-Cu 207 solder with minor of Zn element.

2.4.3.3 Gold-based solders

Gold (Au) possesses excellent thermal and electrical properties which has been widely accepted for most of the electronic applications.. For instance, Au-Sn solder is the one of the particular Au-Sn die attach solder which is used for laser diodes, microwave devices, RF power amplifiers and other high thermal applications (Hartnett & Buerki, 2009). Au-Sn solder exhibits excellent thermal and electrical conductivity, good creeping behavior and corrosion resistance, allow processing temperature at 320°C. However, the intermetallic compounds caused by the Au-Sn inter-diffusion degrade the mechanical properties of Au-Sn solders (Ivey, 1998).

Ivey (1998) pointed out clearly that Au-Sn solder is more brittle than pure Au, and harder than Sn. Therefore, Au-Sn as a hard solder typical used for optoelectronic applications. When Au-Sn solder parts are subjected to high temperature, the intermetallic Au-Sn will lead to delamination or brittle fracture. C. C. Lee, Wang, and Matijasevic (1993) pointed out clearly that Au-Sn solder is more brittle than pure Au, and harder than Sn. Therefore, Au-Sn as a hard solder typical used for optoelectronic applications. When Au-Sn solder parts are subjected to high temperature, the intermetallic Au-Sn will lead to delamination or brittle fracture. Another work, Datian, Zhifa, Huabo, and Jinwen (2008) prepared and characterized a novel type of Au-19.25Ag-12.80Ge solder using a vacuum medium-frequency induction furnace. Figure 2.10 shows the solder had a melting temperature range between 446.76 and 494.40 ºC, and the temperature interval between the solidus and liquidus is approximately 47.64ºC. The solder showed good wettability with Ni whose main composition was Au element. However, the reliability test for this solder is required with wide band-gaps or power device as a die-attach solder.

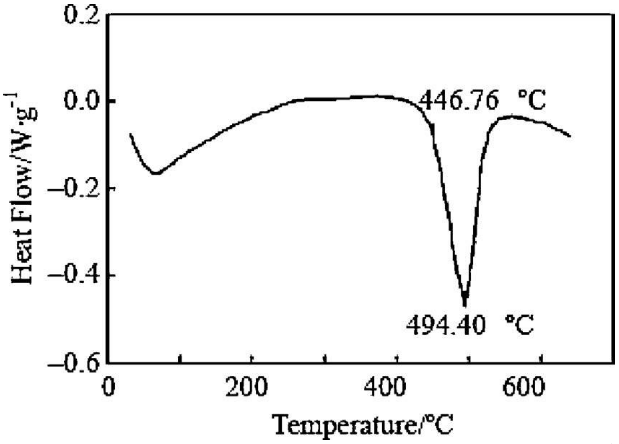

Figure 2.10: DTA curve of the Au-19.25Ag-12.80Ge alloy showcasing the melting range

Naidich, Zhuravlev, and Krasovskaya (1998) studied the wettability od Au-Si solder on SiC devices at 1500°C, where it was discovered that the addition of Si to Au increased the interaction of Au-Si solder, meanwhile decreasing its interfacial tension and contact angle. A point was noted that further addition of Au to Si improved wettability of the solders because of the bonding of Au with Si of the SiC. Although there has a lot of Au-based solders have emerged; most of the Au-based solders are not being used doe lead-free alternative. Au-Sn system still remains as the primary Au-based solders.

2.4.3.4 Silver-based solders

Silver (Ag)-based solders have always been an promising solution over Au, because Ag is much cheaper than Au, meanwhile Ag demonstrates the best electrical conductivity and second best thermal conductivity in the world. Ag also has a high melting point of 961°C and has excellent mechanical properties.

Chuang and Lee (2002) produced silver-indium (Ag-In20) joints for high temperature uses at low temperature. In their work, they created Ag-In20 joints by using two-step fluxless bonding at 206°C. Subsequently, the joint were annealed continuously for 26h at 145°C, the Ag-In20 joints' melting temperature was reached up to 765-780°C. Results showed that a nearly void-free, uniformly joint with thickness ranging from 7.2 to 7.8µm was created. The layers of intermetallic compounds (Ag_2In and $AgIn_2$) were formed in Ag-In alloy matrix. Figure 2.11 depicts the SAM images on samples for thermal tests at 500°C for (a) 10, (b) 100 and (c)1000 h did not show any cracks, voids or joints failure.

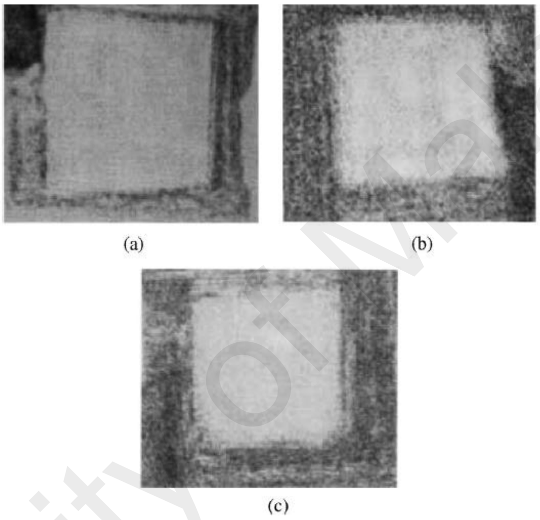

Figure 2.11: SAM images after thermal tests at 500 °C for (a) 10 h, (b) 100 h, and (c) 1000 h

2.4.4 Silver Glass Systems

Silver glass system as die attach material provide sufficient adhesive strength and high electrical and thermal conductivity (Coppola, Huff, Wang, Burgos, & Boroyevich, 2007; Kisiel & Szczepański, 2009; Nguyen, 1990). However, the firing temperature for formulating a die-attach silver glass is much higher (>600°C), pressure may needed to achieve sufficient adhesive and bonding strength (Nguyen, 1990). Figure 2.12 depicts a typical firing profile for silver-filled glass die attach material: at 50-200°C, the solvent is evaporated; the polymer resin is evaporated at 300°C. The silver-glass sintering accelerates at 340°C, and the reaction is completed when the temperature reaches to 410–430 °C for approximately 10 min (Nguyen, 1990).

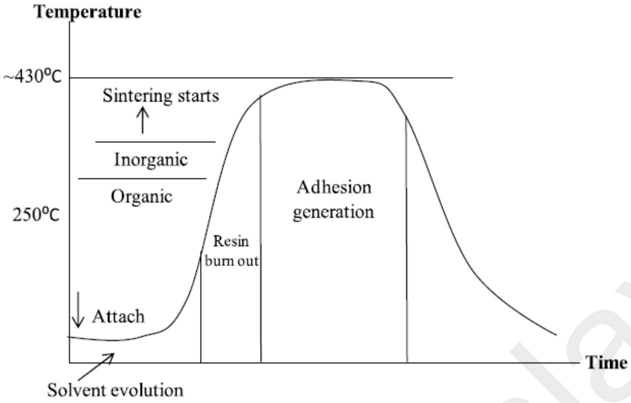

Figure 2.12: Firing Profile for Die-attach Silver Glass

FO-3 and FO-13 are the two commercially available sliver-glass die attach that from ITME Poland, both products and allow for working temperatures at 300 °C (Kisiel & Szczepański, 2009). Besides, F0-13 has a volume resistivity of 7µ·cm. Another silver-glass die attach system named QMI 3555R form Loctite has high resistance to degradation during temperature cycling from -65°C to +150 °C (Coppola et al., 2007).

Table 2.8: Major properties of several silver-glass systems

Silver-glass die attach system	Maximum temperature (°C)	Thermal conductivity (W/mK)	CTE (10^{-6} °C^{-1})	Reference
F0-3,F0-13	300	~60	25	(Coppola et al., 2007)
QMI-3555R	300	80	16	(Kisiel & Szczepański, 2009)

Silver glass die attach system is seemly promising solution for high temperature application, the preparation steps are lengthy and high temperature is required. For mass manufacturing purposes, such lengthily processing techniques are not acceptable.

2.4.5 Nanopaste systems

Nanomaterials are of the scientific interest due to their distinct properties which are obtainable at nanoscale compared to their bulk counterpart. Bulk silver exhibits high electrical and thermal conductivity, and nanoscale silver can reduce the processing length and sintering temperature. Thus, the application of nano-metallic particles creates an alternatives die-attach solutions for high temperature application. The nanoparticles are synthesized through various means, generally are classified into two major groups: "top-down" and "bottom-up" methods. "Top-down" methods refer to various lithography methods to slice or successive cut a bulk material for patterning 2-dimensional nanoscale feature. There are two leading methods for conventional lithography: photolithography and electron-beam lithography, other top down methods are viable such as soft lithography, nano-imprint lithography, scanning probe lithography and block copolymer lithography, etc. In most of the lithography method, the preparation of a protecting mask is needed to cover required material, and the exposed material is etched either by chemical (acids) or mechanical (X-ray, electron beam, ultraviolet) means that determine the feature resolutions of final product. Bottom up methods are related to the build of nano-structural materials and devices by the self-assembly of molecules or atoms: atomic layer deposition, chemical reduction, thermal decomposition, electrochemical synthesis, radiolysis, sonochemical synthesis, biosynthesis and ion implantation, etc. are belonged to bottom-up nanofabrication (Biswas et al., 2012; Colson, Henrist, & Cloots, 2013). This methodology is able to generate multifunctional devices by manipulated assembly molecules or atoms, without creating waste or contaminated parts of final products. Some major challenges such as surface preparation, conditioning for atomic deposition, controlling of impurities and site uniformity, amount of the reactants, etc. still remain to be solved .

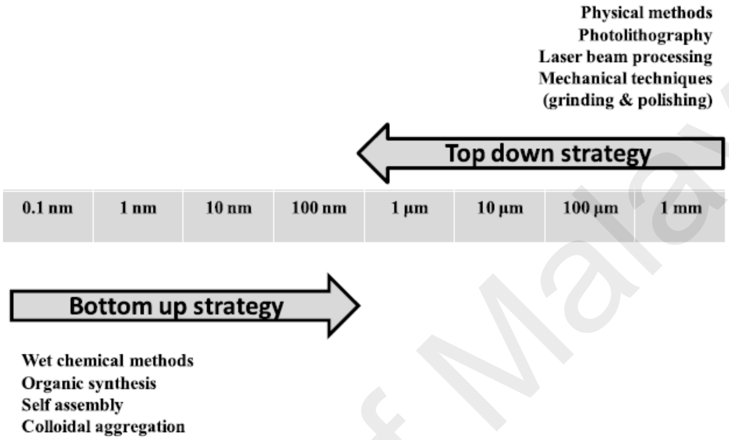

Figure 2.13: Strategies for manufacturing nanoparticles (Manikam, Cheong, & Razak, 2011)

Table 2.9: Conventional methods for synthesizing nanoparticles and nanoalloys (Manikam et al., 2011)

Method	Description of method	Practicability(s)	Limitation(s)
Chemical reduction	Using precursor salts, reducing agents, surfactants/stabilizers to synthesize nanoparticles.	- Simple, convenient, significant and this technique is quite standard - Can produce bulk quantities of nanoparticles/ nanoalloy easily. - The process is more inexpensive compared to other synthesis techniques - This synthesis enables to produce nanoparticles close to 1nm and can be readily control.	- The chemicals used can be toxic and expensive. - Poor reducing ability and may introduce other impurities to the process. - Process is time consuming and need to control many parameters.
Molecular beam	Creating clusters of metallic nanoparticles/nanoalloy by directing beam to the specific metal targets using laser vaporization, pulsed arc, magnetic sputtering, etc.	- Enables to synthesis any nanoparticles/nanoalloy from metallic/alloy target. - Process is quick and not lengthy	- process is expensive, in most cases the setup of equipment is required
Electrochemical	Using two electrodes (metallic element) and an electrolysis cell. The synthesis of nanoalloys is viable in solution. This method creates core-shell structure.	- A wide variety of nanoalloy combinations can be synthesized. - The setup of cell is easy and does not need any extensive equipment. - Simple and inexpensive due to no reducing agent and expensive equipments required.	- Use of chemicals as electrolytes which may yield hazardous gases as by-products.
Thermal decomposition	High temperature solvents or mediums used to synthesize nanoalloy/nanoparticles	- Synthesis is possible at low temperature. - can produce large scale of nanoalloy/nanoparticles	- Uses of chemicals can be hazardous to environment
Sonochemical synthesis	Irradiation of metal salt solutions using ultrasound to create nanoparticles and nanoalloys	- Sonic wave irradiation is able to create narrow particle sizes.	
Biosynthesis	Synthesize nanoparticles/ nanoalloy using biological means: microorganisms, plants, etc. Biosynthesis can create a more bio-compatible nanoparticles.	- Does not require extensive equipment. - Inexpensive and uses sources from natural environment.	- process is slow and time consuming

2.4.5.1 Silver Nanopaste

John G Bai, Zhang, Calata, and Lu (2006) reported the successful of the nanoscale Ag paste fabrication: the nanoscale Ag paste was prepared by mixing an average size of 30-50nm Ag nanoparticle and organic system that containing dispersant, thinner and binder. The sintered nanoscale Ag paste was compared with bulk Ag as shown in Table 2.10. The density specific heat, thermal diffusivity and thermal conductivity of sintered Ag is lower than bulk Ag, the thermal conductivity of sintered Ag still higher than most of the die-attach materials.

Table 2.10: Comparison of thermal properties between sintered and bulk Ag

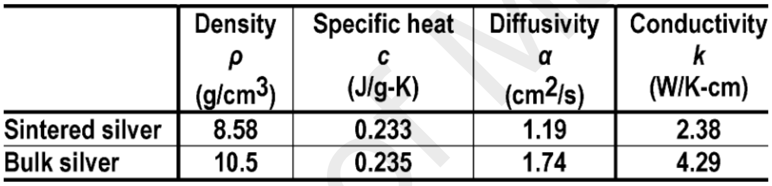

	Density ρ (g/cm^3)	Specific heat c (J/g-K)	Diffusivity α (cm^2/s)	Conductivity k (W/K-cm)
Sintered silver	8.58	0.233	1.19	2.38
Bulk silver	10.5	0.235	1.74	4.29

In addition, the electrical resistivity and tensile strength test were also conducted in this research: the electrical resistivity of sintered Ag increases at elevated temperature. However, the resistivity of sintered Ag is still lower than other commercial solder-alloy. The elastic modulus and ultimate tensile strength of sintered Ag paste is 9GPa and 43MPa， respectively, which is comparable to those of the common solder alloys.

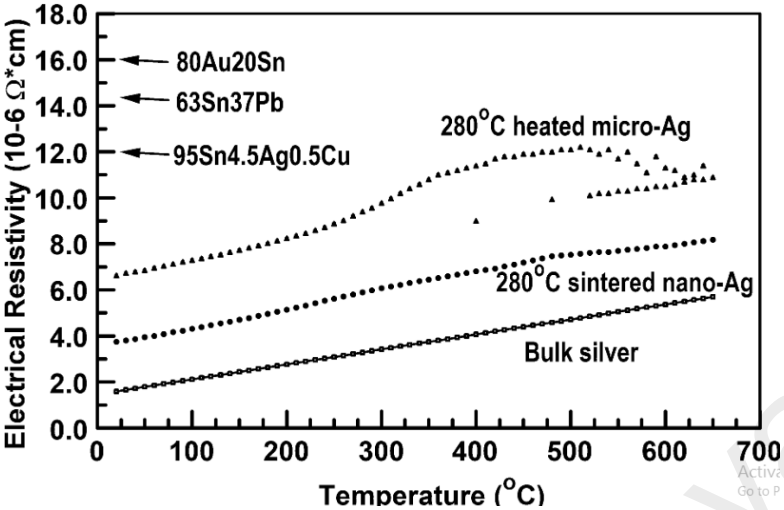

Figure 2.14: The electrical resistivity of different die-attach systems at elevated temperature

Subsequently, John Guofeng Bai, Yin, Zhang, Lu, and van Wyk (2007) pasted the sintered silver on SiC devices to test its overall performance. The strong bonding and silver metallization can be clearly seen in SEM images as per Figure 2.15. Furthermore, EDS results also showed that purity of the sintered silver can be achieved to more than 99%, rest of the composition is carbon and no oxygen component was detected. The density of sintered silver is 80% of the bulk silver.

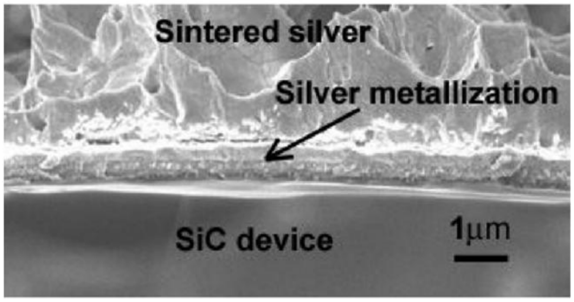

Figure 2.15: Silver metallization of between sintered silver and SiC device

Forward and reverse I-V measurements were also conducted to determine the electrical performance of packaged SiC devices at high temperature. The attempts were failed for testing the device at temperatures above 300^{o}C because of the degradation of the dielectric coating on the tested devices. However, the results showed that the SiC devices with sintered Ag die-attachment can be well-operated at high temperature up the the limitation of the Schottky devices themselves.

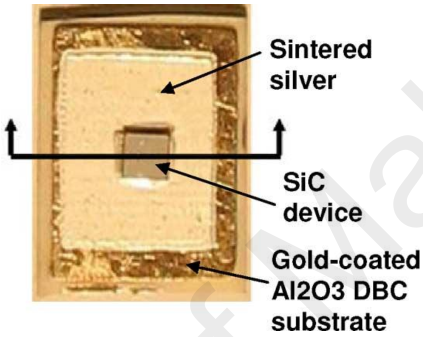

Figure 2.16: Low-temperature sintered silver die-attachment

Authors concluded that this sintering experiment for nano-Ag paste could achieve 80% of bulk Ag density at a low temperature of 300 ^{o}C, 40MPa of die-shear strength which is close to Pb-Sn solders. Scanning acoustic microscopy also showed no large and comparable voids in the sintered-Ag layer. SEM images also depicted a uniform distributed of micropores. The combination of these results showed that sintered-Ag nanopaste has a very high suitability as a die-attachment for high operating temperature applications, such as SiC power device, SiC switching power supplies and etc.

2.4.5.2 Copper Nanopaste

Copper (Cu) exhibits high melting temperature and acceptable thermal and electrical conductivity, therefore it has the potential to become an alternative lead-free die-attach material for high temperature applications. However, Cu nanoparticles require pretreatment to remove oxides, which can greatly affect the properties of Cu afterward.

Krishnan, Haseeb, and Johan (2012) synthesized Cu nanoparticle for high power applications. The synthesis of Cu nanoparticles was economical, it was produced by a pulse wired evaporation (PWE) system. In this system, Cu wire was used as the source of Cu nanoparticle, and de-ionized (DI) water was used as exploding medium. The Cu nanoparticle in the size range of 30-50 nm was produced with mixing any precursors or organic binders. Subsequently, the Cu nanoparticles were sintered in N_2 environment at 400°C.

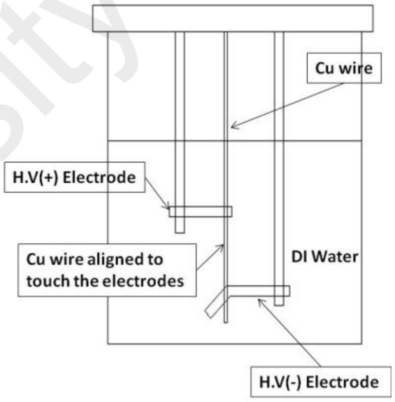

Figure 2.17: Schematic diagram of the PWE system

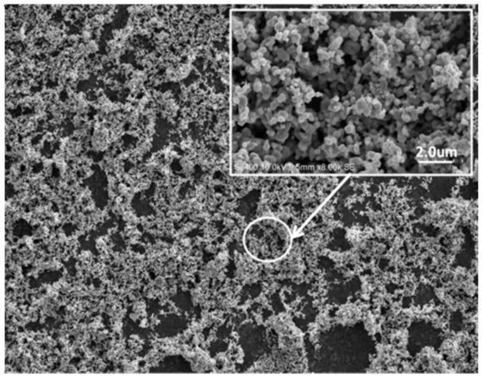

Figure 2.18: Cu nanoparticles after screen printing and vacuum dry on leadframe surface. SEM image of the screen printed Cu nanoparticles (inset).

However, the characteristics of Cu nanopaste such as thermal and electrical properties were not investigated in this research. Author suggests that Cu nanopaste should maintain certain level of pores to absorb thermal stress during the reliability cycling. Furthermore, some common findings were suggested e.g. the increase in temperature/ application of external pressure helps to improve the bonding strength of Cu nanopaste. As Cu has a very high melting point (1083 °C), it is expected to be the candidate for high temperature die-attach material. Especially the oxide-free Cu interface is also expected to exhibit electrical and thermal conductivity that is superior to existing solders.

2.4.5.3 Bimetallic Nanopaste

(i) Ag-Cu nanopaste

K. S. Tan and Cheong (2013) used both Ag and Cu nanoparticles to form a novel Ag-Cu nanopaste for high temperature die-attachment purpose. The formulation of Ag-Cu nanopaste is relatively simple by mixing Ag and Cu nanoparticles (average size of 50nm) with organic additives. The Ag-Cu nanopaste was then sintered at low temperature to achieve solid-state fusion of nanoparticles. K. S. Tan and Cheong (2013) studied the effect of sintering temperature on Ag-Cu nanopaste's die-attach quality, the testing temperature was ranging from 150°C to 450°C. Results demonstrated that when the Ag-Cu nanopaste sintered at high temperature, a higher electrical conductivity can be achieved: this is because high sintering temperature enables the densification of Ag-Cu nanopaste. Furthermore, XRD analysis also detected the phase $Ag_{97}Cu_3$ and Ag_1Cu_{99} within samples. Subsequently, K. S. Tan et al. (2015) investigated the thermal characteristics of Ag-Cu die-attach nanopaste by differing the weight percentage (wt%) of Ag, this study showed the sample with 80 wt% of Ag demonstrated the best thermal performance, these results was better and more suitable than most of the die-attach materials for high temperature applications.

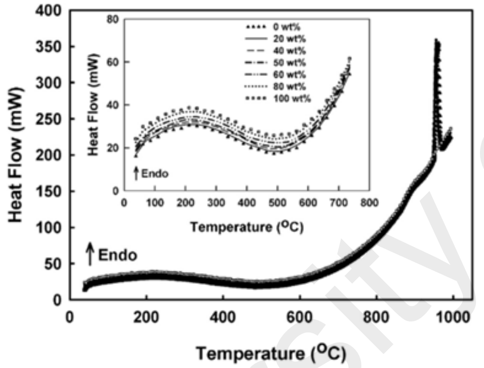

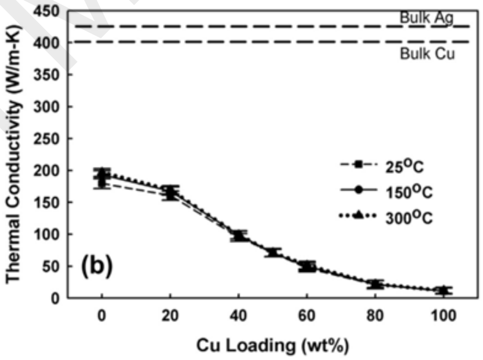

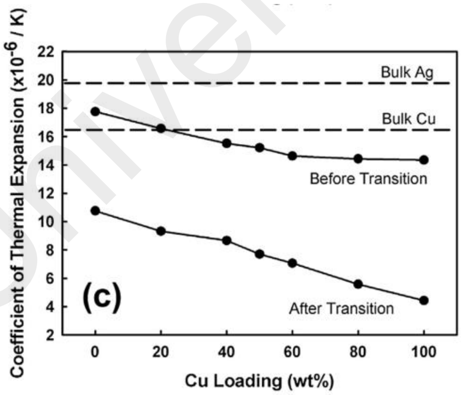

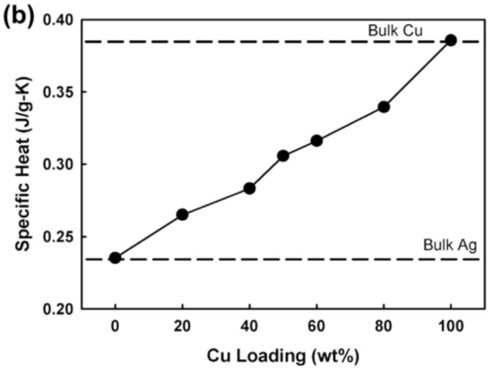

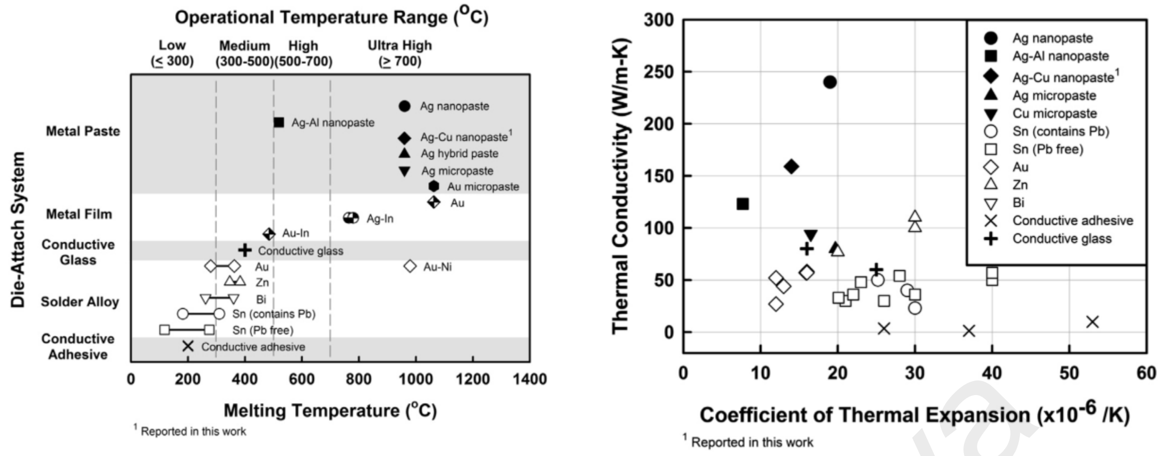

Figure 2.19: (a),(b),(c),(d) shows the DSC curve, thermal conductivity, CTE and specific heat for sintered pure Ag nanopaste (0 wt% Cu), sintered pure Cu nanopaste (100 wt% Cu) and sintered Ag-Cu nanopaste with increasing of Cu loading (20-80 wt% Cu), (e) Melting temperature of various die-attach systems and their operational temperature range, (f) thermal conductivity plotted against CTE for various die-attach systems.

In same research, K. S. Tan and Cheong (2014b) studied the effects of Cu loading on physical and electrical characteristic of Ag-Cu die-attach nanopaste: In XRD analysis, three phases namely $Ag_{97}Cu_3$, Ag_1Cu_{99}, and CuO compounds were formed in sintered nanopaste. The formation of $Ag_{97}Cu_3$ and Ag_1Cu_{99} phases indicates the solid-state fusion between Ag and Cu can effectively take place. Higher Cu loading demonstrated lesser in density, increase of porosity, lower surface roughness, smaller grain size and degrade in electrical conductivity.

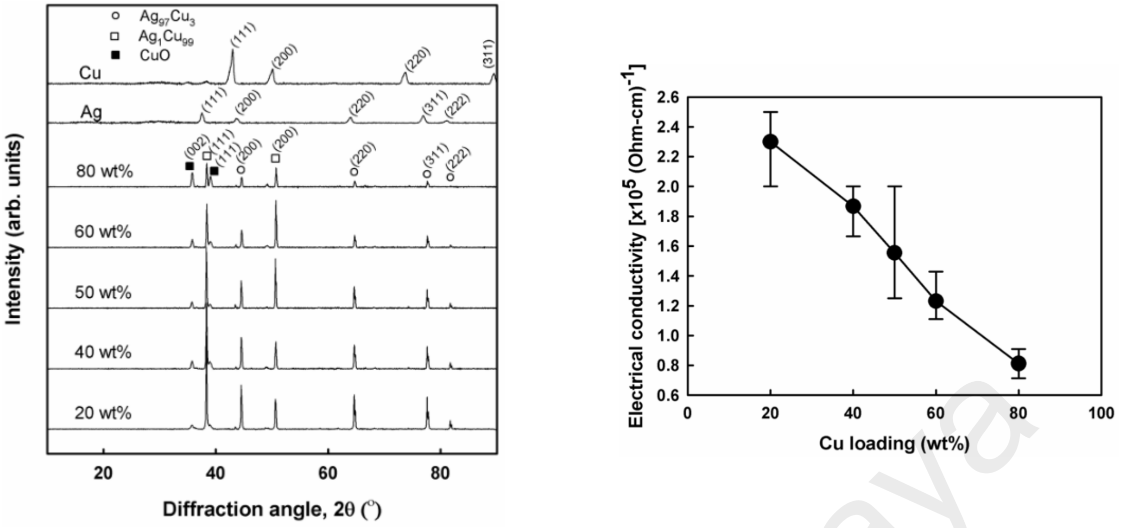

Figure 2.20: XRD pattern and Electrical conductivity of Ag-Cu nanopaste with increasing Cu weight percent content

Furthermore, the effects of nanoparticle loadings toward mechanical attributes of Ag-Cu nanopaste were investigated (K. S. Tan & Cheong, 2014a). Nanoindentation test were performed to measure the hardness, stiffness and Young’s modulus of samples, the loading and unloading rates were set at 1mN/s, respectively. Lap shear test was also carried out to measure the bonding strength of samples. The hardness, stiffness and Young’s modulus of Ag-Cu nanopaste increase with an increment of Cu loading. This is because Cu exhibits a higher Young’s modulus, stiffness and hardness than Ag, therefore, alloying Cu into Ag-Cu nanopaste improves the overall mechanical attributes of Ag-Cu nanopaste. However, the bonding strength of Ag-Cu nanopaste decline with an increasing of Cu loading. The low bonding strength can be associated with the plastic deformation of Cu occurs within the sintered nanopaste. In a conclusion, Ag_{80}-Cu_{20} sintered nanopaste demonstrates the best thermal, physical, mechanical and electrical properties.

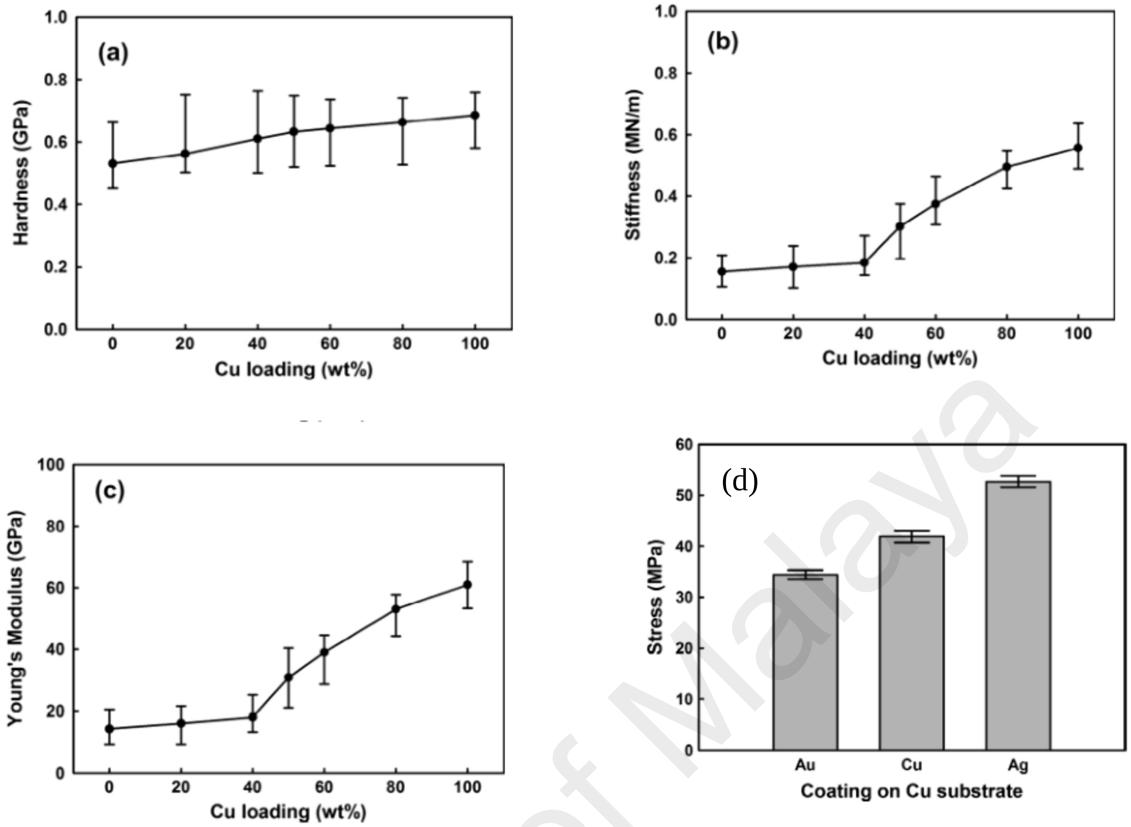

Figure 2.21: (a) Hardness, (b) Stiffness and (c) Young's Modulus of Ag-Cu nanopaste with increasing Cu weight percent content, (d) Bonding strength of Au,Cu and Ag

(ii) Ag-Al nanopaste

The method to formulate of Ag-Al nanopaste is similar to Ag-Cu nanopaste, where the Ag and Al nanoparticles were mixed with organic constituent (binder and surfactant/dispersant), the Ag-Al nanopaste was sintered at 380^{o}C for 30 min. Figure 2.22 shows the function of organic constituent and sintering profile of Ag-Al nanopaste: (a) the organic constituent help to form a coating where surround the nanoparticle to avoid the agglomeration, (b) the sintering profile was designed based on TGA results, where 380 ^{o}C promotes the organic burn-off and the coalescence of Ag and Al nanoparticles (Manikam, Razak, & Cheong, 2012b).

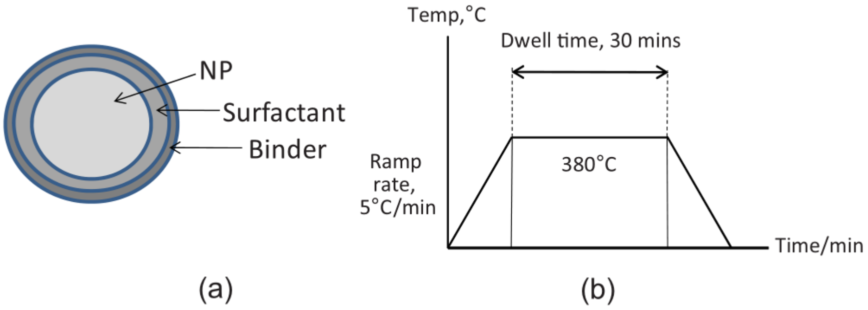

Figure 2.22: (a) Schematic of nanoparticles with surfactant and binder coating (b) Nanopaste sintering profile

In designing the sintering profile, authors perform the statistical analysis and design of experiment (DOE). Dwell time and ramp rate were considered as design factor. Study found that the sintering dwell time has effects on the physical properties of the Ag_{80}-Al_{20} sintered nanopaste. From DOE result, sintered samples under 30 min dwell time gave no uncured or cracking issues (Manikam, Razak, & Cheong, 2012a).

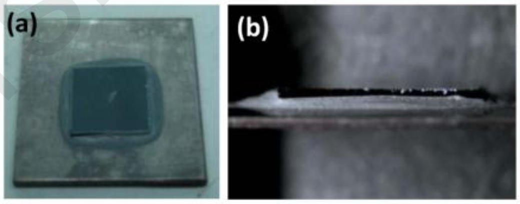

Figure 2.23: SiC die attached to post-sintered Agso-Al_{20} nanopaste; (a) Top view, (b) Side view

The coalescence of Ag and Al nanoparticles can be revealed by XRD and FESEM analysis. In XRD analysis, both Ag_3Al and Ag_2Al were detected in XRD diffractogram, it is proven that fusion of the Ag and Al nanoparticles can occur under the designed sintering conditions. FESEM images in Figure 2.24 (b) the micropores formation can be observed in the Ag-Al layer. The formation of micropores helps to reduce the the thermal stress between the die and the substrate (Manikam et al., 2012b).

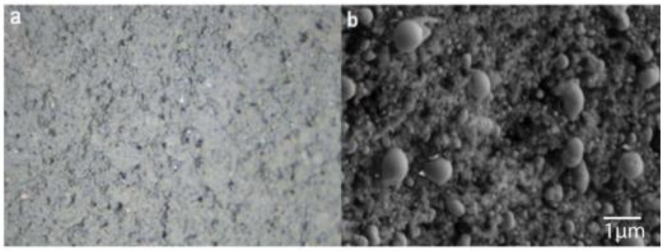

Figure 2.24: Micropores on post-sintered Ag-Al nanopaste. (a) Optical scope image at 10 × magnification. (b) SEM image at 10 000 × magnification

For thermal analysis, thermal conductivity and expansion had been performed to characterize sintered Ag-Al nanopaste. From the Figure 2.25, a decline trend of thermal conductivity was spotted with the increase of Al content.

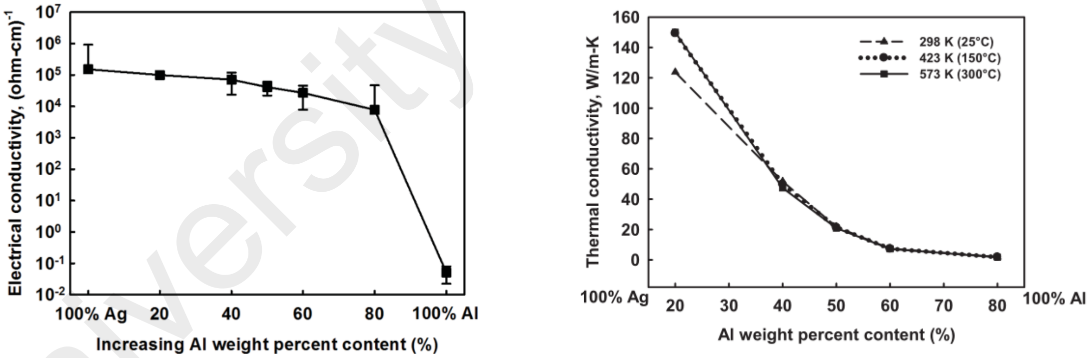

Figure 2.25: Electrical and thermal conductivity plot for Ag–Al nanopastes with increasing Al weight percent content

The effects of organic additive content were also studied in this research, the weight content of nanoparticles increased from 84.7 to 87.0 %. Study shows that the Ag_{80}-Al_{20} die-attach material with lower organic content demonstrated the most desirable electrical and physical properties for high temperature applications. For instance, lower organic content of Ag_{80}-Al_{20} die-attach nanopaste resulted in lower surface roughness, the reduction of surface roughness helps to improve the particle coalescence and grain growth, which can actually improve the physical and electrical properties of Ag_{80}-Al_{20} die-attach nanopaste. The excessive organic additives hinder the solid-state fusion of Ag and Al nanoparticles, which will form pores in the Ag-Al layer. In addition, the authors concluded that for both smaller and thinner die attach samples, they exhibit better surface morphology and electrical conductivity. (Manikam, Razak, & Cheong, 2013b).

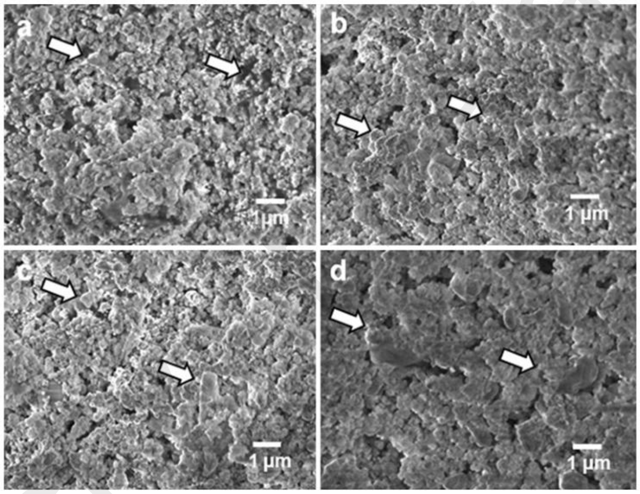

Figure 2.26: SEM images at 10,000x magnification of Ag 80 –Al 20 die attach material with different nanoparticle weight percent loading after sintering at 380^{o}C: (a) 84.7 %, (b) 85.5 %, (c) 86.2 % and (d) 87.0 %

In same research, Manikam, Razak, and Cheong (2013c) investigated the reliability of Ag_{80}-Al_{20} die-attach nanopaste. The reliability test of Ag-Al nanopaste was carried out with SiC die and Au-Ni substrate. Al has peeling problem which could be revealed on SEM cross section images, this is because Al was oxidized during the sintering process, which causing it to become brittle and detach from the SiC die’s surface. In addition, the mechanical properties (Young modulus, hardness and stiffness) of Ag_{80}-Al_{20} die attach nanopaste is much lower than other solder alloys and bulk metals, this can be attributed to the formation of pores in the Ag_{80}-Al_{20} die attach nanopaste, which leads to degradation in mechanical properties. Furthermore, the electrical conductivity of Ag_{80}-Al_{20} degraded during thermal aging repetitions but it is insignificant.

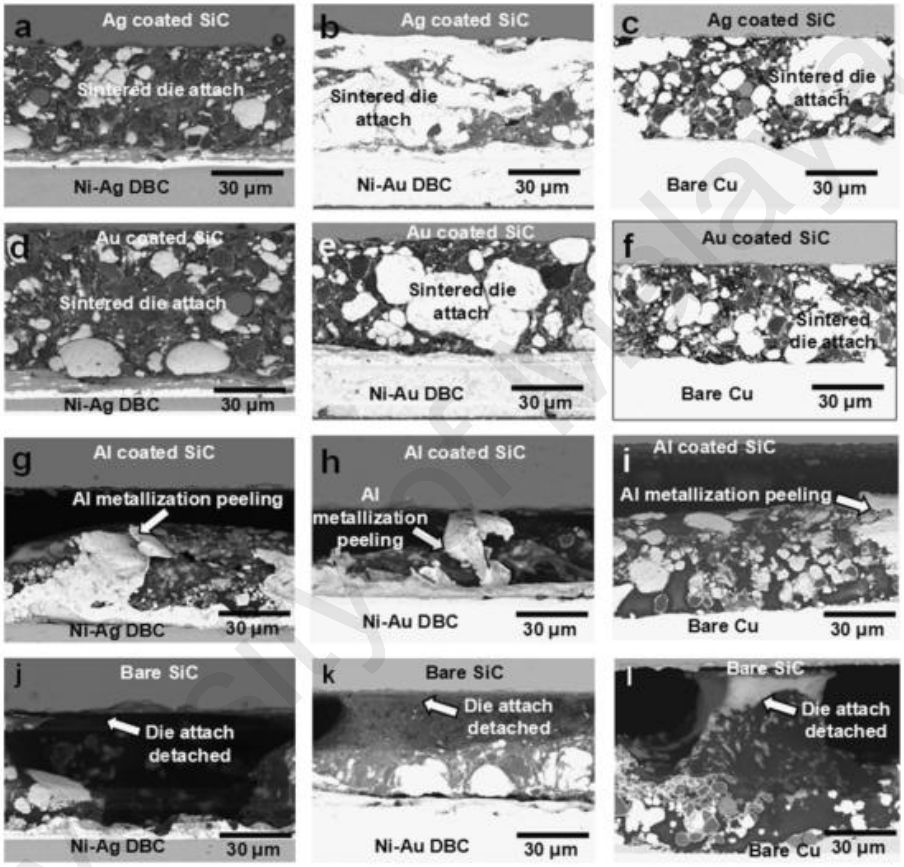

Figure 2.27: SEM cross section images for SiC–Ag 80 –Al 20 die attach material-substrate structures after thermal aging tests.

2.4.6 Summary

Nanoparticle-based die attach systems have proven that they have higher suitability for high temperature applications than other sorts of die attach systems. For instance, pure Ag nanopaste, Ag-Al nanopaste and Ag-Cu nanopaste have a melting temperature more than 500°C, which is much higher than conductive glass, conductive adhesive and most of the solder alloys (shown in Figure 2.28). Higher melting temperature allows them to be operated at high temperature environments which has discussed in section above. Besides melting temperature, nanoparticle-based die attach system also demonstrate higher thermal conductivity (159-240W/m.K), higher electrical conductivity (>10 μΩ/cm) than conductive adhesives and solder alloys. Performance index (*M*) is used to measure the suitability of die-attach systems for high temperature applications. The *M* is defined in Equation 2.1:

$$M = K/\alpha \tag{2.1}$$

According to Table 2.11, Ag nanopaste, Ag-Al nanopaste and Ag-Cu nanopaste have yielded a performance index more than 10.0, larger value of *M* indicates the die attach material has the ability to conduct thermal energy for the die to the substrate rather than absorbing and storing thermal energy in the atoms of die-attach material. Die-attach material with higher *M* also causes less displacement of their inter-atomic distance, resulting less deformation of the die attach systems.

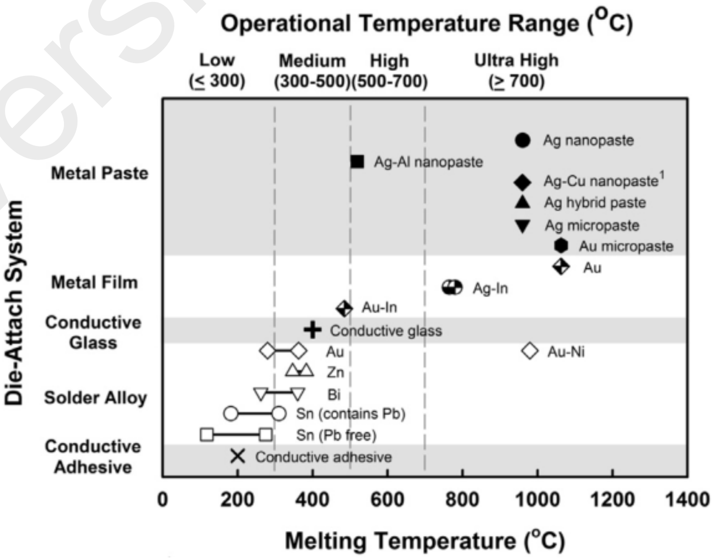

Figure 2.28: Melting temperature of various die-attach systems and their operational temperature range

Table 2.11: The CTE difference, thermal and electrical conductivity between typical high-temperature die-attach systems and electronic packaging component

Electronic Packaging Component	Thermal Conductivity (W/m-K)	Electrical Conductivity (μΩ/cm)	CTE, α (μ/K)	Performance index (*M*)
Die				
SiC			2.8-5.1	
GaN			5.4-7.2	
Substrate				
AIN			4.5	
Al_2O_3			6.5-7.3	
BeO			6.1-8.0	
AlSiC			7.0	
Die attach System				
Ag nanopaste	240	25-26	19-20	10.0-12.6
Ag-Al nanopaste	123	10.1	8	15.4
Ag-Cu nanopaste	159		13	12.2
Conductive glass	60-80	7-8	16-25	2.4-5.0
Pb-Sn solder alloys	35-43	5-9	19-30	1.2-1.8
Au-based solder alloys	27-59	2-4	NA	NA
Sb-Sn solder alloys	20-48	NA	NA	NA
Bi-Ag solder alloys	9	0.5-1	NA	NA
Polyme Ag-filled adhesives	1.29-9.96	NA	26-53	0.1-0.5

2.5 Sintering

Sintering is a thermal induced treatment to bond particle, which intent to improve the strength and lower system energy. Coolidge (1913) used “sinter together” to describe the heating process of forming tungsten lamp filament; White and Shremp (1939) described the bonding of ceramic particle as “sintering” with reference to properties of beryllia heated under different conditions. Nowadays, “sintering” was generally used to describe the thermal-induced particle bonding; bonds grow at particle contact during heating.

Table 2.12: History of Sintering

Year	Description of Sintering and Its Application Field
1780	i. Bonding of mineral particle. ii. Formation of crusted stone in Iceland.
1854-1860	i. Thermal bonding of coal particle. ii. Thermal hardening of iron ore (induration).
1865	i. First used term in U.S. patent literature, used to describe the thermal cycle of calcinations. ii. Agglomeration of iron ore in sinter plants.
1880	i. Platinum bonding and platinum jewelry's fabrication. ii. Silver and gold purification. iii. Consolidation of iron powder.
1913	i. Coolidge used "sinter" to refer the process of heating to form tungsten lamp filaments. ii. Agglomeration of refractory, abrasive, or insulator powders in ceramics.
1939	i. White and Shremp used "sintering" to describe the bonding of ceramic particle
1943 onward	i. The term "Sintering" commonly means thermally induced particle bonding.

Since sintering is a heat-induced process, the emerge of sintering theory is trying to explain the changes induced by heat, these theories include a series of mathematical calculation of key parameters. The key parameters can be divided into two major portions: material and process. Material parameters include atomic size, crystal structure, surface energy of material and activation energy for diffusion; Process parameters consist of heating rate, particle size, hold temperature and hold time. Therefore, a comprehensive sintering model is constructed by much background knowledge as a foundation.

Sintering techniques are categorized into 2 main groups: pressure-assisted sintering and pressureless sintering. Figure 2.29 organizes the sintering techniques into general categorizations. Most industrial sintering is performed pressureless sintering techniques. For pressureless sintering, it is branched to solid-state and liquid phase processes. There are few options for solid-state pressureless sintering: (i) Single phase, solid-state sintering: much simpler form of sintering technique: (ii) Mixed phase, solid-state sintering such as composites, activated and homogenization. Mixed phase sintering are used to form composite and alloys.

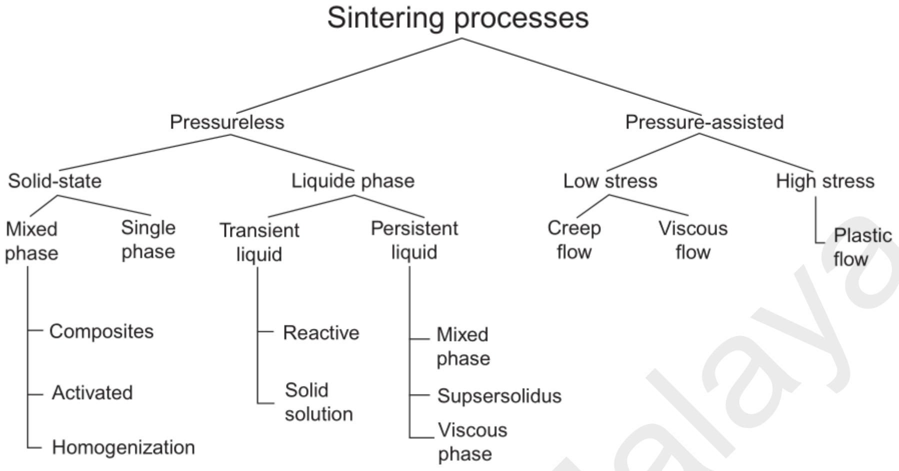

Figure 2.29: Classification of Sintering Process

Table 2.13: Three Types of Mixed-phase sintering

Mixed phase sintering	**Description**
Homogenization	Alloy produced when sintering mixed powder are soluble in each other.
Activated	Accelerate sintering by the segregation of small quantities, insoluble species to the grain boundaries.
Composites	One phase is dispersed in a matrix phase.

Liquid-phase sintering is branched to transient liquid and persistent liquid. Liquid phase sintering are employed in most of industries, 90% of all sintered products are formed using liquid phase sintering. Transient, liquid-phase sintering produces a liquid during heating, the liquid subsequently dissolves into the solid. Whereas in persistent, liquid-phases sintering, high temperature portion of the sintering cycle exists and can be formed using pre-alloyed powder (also known as super-solidus liquid phase sintering).

2.5.1 *Qualitative Sintering Theory*

In the early 1900s, qualitative descriptions of sintering provide several conceptualizations: (i) Sintering has an onset temperature, it does not occur below this temperature. (ii) At sintering process, surface energy of material increases during heating. (iii) For brittle solids, sintering increase in its plasticity. (iv) Plastic material exhibit sintering. (v) Surface contamination films of particles delay sintering. (vi) Only metals such as Co and Fe undergo polymorphic-phase transition sintering. (vii) Only mixed powders with a chemical affinity can be sintered. (viii) Sintering occurs below melting temperature when only external pressure is applied or particles with high surface curvature. (ix) Sintering provides re-crystallization of compacted particles. Stirred vacuum chamber is the one of the earlier technique to determine the sintering temperature. When the stirred chamber was unable to continue rotating, the sintering temperature was detected. However, this technique is inaccurate because iron powder in vacuum sintered at 750°C, which is much different when iron was sintered in air (150 °C) due to the oxidation effect. Such report confused the understanding of sintering (R. M. German, 1996).

Qualitative sintering concepts arose as observations of sintering accumulated. Therefore, Lenel outlined the key elements sintering as listed below (R. German, 2014): (i) Neck material has the same characteristics as the parent material. (ii) Application of pressure increases the bonding between particles and dislodges interfering film between particles. (iii) The neck expand laterally under surface energy promotes initial neck growth. (iv) Gas trapped in pores and gas evolution lead to swelling. (v) Typical aspects of sintering often initiate at contact points between particle, such as re-crystallization, grain growth and recovery. (vi) Changes in properties of material reflects the structural changes during sintering, and do not have any unique aspects attributed to sintering. (vii) Late stage sintering involves the deposition of atoms into pores, causing pore closure, especially for small spherical pores near the compact surface which fill earlier in sintering.

These observations were followed by similar ideas from Lenel about liquid phase sintering. He noted the two variants were a persistent (WC-Co, W-Ni-Cu) and transient (Cu-Sn) liquid. About 20 different compositions were studied to show that the events during liquid phase sintering commonly involve several steps, starting with compaction, establishing a protective atmosphere, and heating the compact to a temperature where a melt forms. Most systems exhibit solubility of the solid in the liquid, so small grains dissolve and large grains grow by a solution-reprecipitation process. During grain growth, the grains reshape to allow liquid to fill voids, giving rapid densification. On cooling, the liquid freezes to provide a matrix phase between the solid grains. In transient liquid phase sintering, the liquid dissolves into the solid over time and the rapid densification process comes to a halt, so obviously diffusion in the liquid is an important event in sintering (R. M. German, 1996).

Frenkel explained the theory in term of surface energy and viscous flow in his sintering model: Surface energy leads the coalescence of two viscous, spherical particles in point contact to form a larger sphere, as depicted in Figure 2.30. The diameter (D) of the sintered sphere is 1.26 times the D of the initial sphere. In Frenkel's model, sintering is tracked by neck growth; surface energy is the main driving force to pull two spheres together, which leads to neck growth and coalescence of two spheres. As the bond grows, surface energy and surface area decline, mass conservation dictates that the sphere centers move together to give shrinkage. In Frenkel's sintering model, particles are assumed to be spherical and no inter-particle grain boundary or dihedral angle. Thus, Frenkel's model works for explaining sintering of amorphous materials, but this model is not applicable to crystalline materials (Pokluda, Bellehumeur, & Vlachopoulos, 1997).

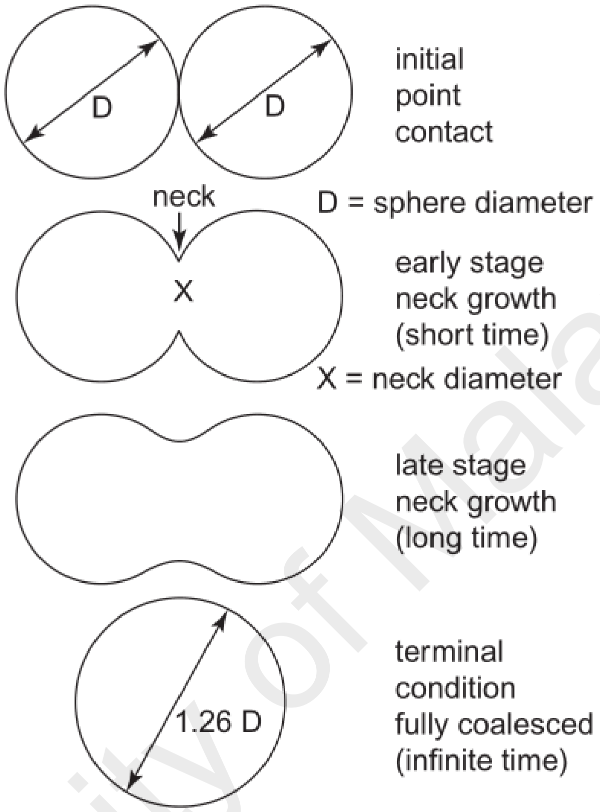

Figure 2.30: Frenkel-surface energy and viscous flow sintering model

The sintering process can be described in 3 main stages: Initial stage is shrinkage of material, the rearrangement of particles by sliding or rotation across each other, the necking is thus formed between particles; at the intermediate stage, densification of particles occurs and the formation of stable pores shapes as dictated by high surface energies. The pores will become unstable and eventually break away from each other; the final stage are the elimination of isolated pores and grain growth within the particles, thereby smaller particles will be consumed by much larger particles (R. M. German, 1996; Kang, 2004).

2.6 Factors to consider for Al-Cu die attach material

2.6.1 Selection of metallic nanoparticle for nanopaste

Nanomaterials are of the scientific interest due to their distinct properties which are obtainable at nanoscale compared to their bulk counterpart. The selection of proper nanoparticles for die-attach nanoalloy is very important, because the attributes of the selected nanoparticles have effects on preparation, storage, fate of transport and also the performance of the die-attach system . Therefore, the understanding of the nature of metallic nanoparticles is important (Biswas et al., 2012).

Copper (Cu) for an example, has been selected in various application due to its good thermal and electrical characteristics, higher melting point, inexpensive compare to Gold (Au) and Silver (Ag), and abundant on earth's crust. However, the major drawback of Cu nanoparticles is it is prone to oxidation under atmospheric conditions. Therefore, the preparation and storage of Cu and its respective alloy is recommended at inert atmosphere by many works. In order to prevent Cu nanoparticle from oxidation, a capping agent is commonly used during the preparation of Cu nanoparticles, this capping agent is able to form a protecting coat that covering the surface of Cu nanoparticle. Aluminum (Al) as another candidate for nanopaste has an acceptable electrical and fourth best thermal conductivity amongst all metals in periodic table. Besides, it also has good ductility and corrosion resistance. Both Al and Cu are more inexpensive materials than Ag and Au, thus considering Al-Cu nanopaste could replace the uses of Ag and its alloy as die attach solutions. However, the reliability of Al-Cu still need to be determined by the outcome of the tests conducted throughout this research work (Fedlheim & Foss, 2001; McLean, 1962).

Table 2.14: Comparison of attributes of common die attach metals (Fedlheim & Foss, 2001)

Attributes	Au	Ag	Cu	Al
Density (g/cm^3)	19.30	10.49	8.94	2.70
Electrical conductivity, (x10$^5\Omega^{-1}$cm^{-1})	4.52	6.25	5.96	3.77
Thermal conductivity, W/mK	318	428	401	237
CTE (ppm/^{o}C)	14	19.7	17	23
Melting point (^{o}C)	1064	961	1085	660
Young's modulus of elasticity (E)	79	74	128	70

2.6.2 Al-Cu systems

Al-based alloys have been widely used in avionics and automotive sector. The system Al-Cu has been investigated during the last decades. The major assessment of Al-Cu system was done by Murray in 1985. The equilibrium phases include 5 intermetallic compounds stable at ambient temperature and 7 additional compounds stable at elevated temperature (Murray, 1985). Riani et al. (2004) and X. Liu, Ohnuma, Kainuma, and Ishida (1998) give a more recent Al-Cu phase diagram that combining the assessment of Murray.

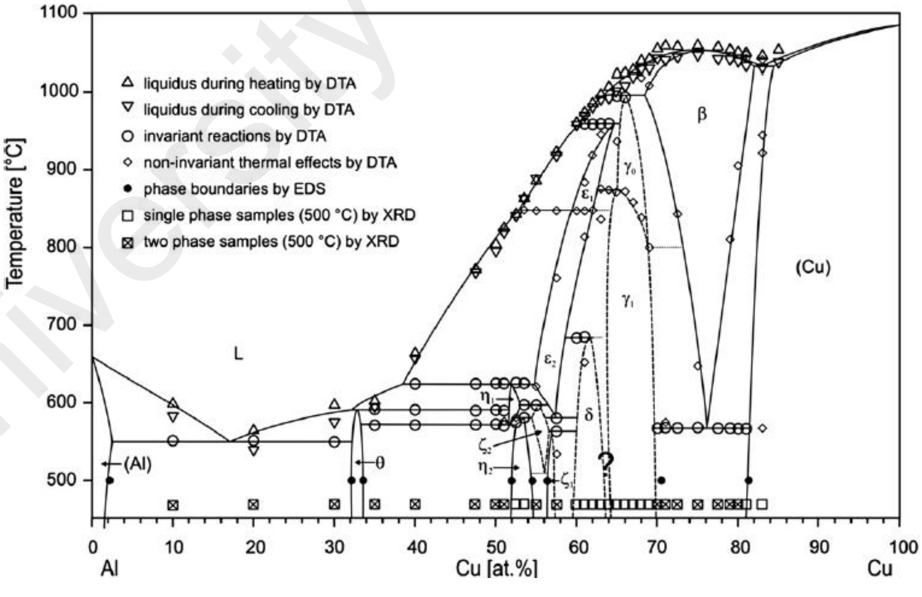

Figure 2.31: The Al-Cu phase diagram determined in the present work with experimental data points.

Table 2.15: Structural information on the compounds in the system Al-Cu

Phase	Composition Range	Peason Symbol	Space Group	Structure Type	Lattice Parameter (Å)
(Al)	0-2.48	*cF*4	*Fm*-3*m*	Cu	a = 4.049750(15)
Ɵ	31.9-33.0	*tI*12	*I*4/*mcm*	Al_2Cu	a = 6.063(3) c = 4.872(3)
η_1	49.8-52.4	*oP*16 or *oC*16 o*32	*Pban* or *Cmmm*	unknown	a = 4.087 b = 12.00 c = 8.635
η_2	49.8-52.3	*mC*20	*C*2/*m*	AlCu	a = 12.066 b = 4.105 c = 6.913 $\beta = 55.04^o$
ξ_1	55.2-59.8	*hP*42 *oF*88	*P*6/*mmm* *Fmm*2	Al_3Cu_4	- a = 8.1267(3) b = 14.4985(5) c = 9.9928(3)
ξ_2	55.2-56.3	*oI*24-3.5	*Imm*2	Al_3Cu_{4-d}	a = 4.0972(1) b = 7.0313(2) c = 9.9793(3)
ε_1	59.4-62.1	Cubic?	unknown		
ε_2	55.0-6.11	*hP*4	*P*63/*mmc*	NiAs	a = 4.146(1) c = 5.063(3)
δ	59.3-6.19	*hR*52	*R*3*m*	$Al_4Cu_{9\ (r)}$	a = 8.7066(1) a = 89.74(1)–[a]
γ_0	59.8-69		*I*-43*m*	Cu_5Zn_8	–[b]
γ_1	52.5-59	*cP*52	*P*-43*m*	Al_4Cu_9	a = 8.7068(3)
β_o	67.6-70.2	unknown	unknown		
β	70.6-82.0	*cI*2	*Im*-3*m*	W	a = 2.9504(2)
α_2	76.5-78			long-period super structure based on Al_3Ti and Cu_3Au	
(Cu)	80.3100	*cF*4	*Fm*-3*m*	Cu	a ? 3.61491

* Bravais lattice is not known; ? Cubic symmetry is questionable.
a Rhombohedral lattice parameters are given in non-standard setting for better comparison with cubic g0.
b No lattice parameters given.

Menshikova, Brodova, Yablonskih, and Astafyev (2016) studied the influence of the cooling rate (2 °C /s and 100 °C /s) and melt heating temperature (from 700 °C to 1200°C) on the phase composition, structure and micro-hardness of the groundmass matrix of Al-rich alloys containing 2,5,7 and 10 at.% of Cu. A higher cooling rate provided a higher mirco-hardness of the Al-Cu alloy groundmass, the is due to higher cooling rate produces a solid solution of Al(Cu) which is more supersaturated and decrease the α-Al lattice parameter. Ata (2017) sintered Al-Cu bimetallic plate at different temperature (300°C, 500°C and 600°C). The intermetallic compound (IMC) of Al_2Cu, Al_4Cu_9, and AlCu are formed at sintering temperature of 300°C, 500°C and 600°C respectively. Fracture strength, electrical resistivity and micro-hardness of 3 samples were identified: the sample which was sintered at 500 °C having a higher fracture strength and lower electrical resistivity than other samples. This is mainly due to an optimal sintering temperature promotes a better diffusion and bonding process.

Table 2.16: Tabulated Summary of 3 different samples of Al-Cu (Ata, 2017)

Sintering Temperature (°C)	Formation of IMC	Fracture Strength (MPa)	Electrical Resistivity (μΩ.mm)	Vicker's micro-hardness (VHN)
300	Al_2Cu	61	130	325
500	Al_4Cu_9	110	50	550
600	AlCu	61	345	620

Wzorek et al. (2017) formed Al-Cu composite by extrusion at three different temperatures: 300°C, 350°C, and 400°C. A slight increase of electrical conductivity is observed with the increase of extrusion temperature. However, higher mechanical strength could be achieved when Al-Cu composite is extruded at a lower temperature of 300°C. Madhududan, Sarcar[1], and Rao (2010) investigated the corrosion behavior of Al-Cu particulate composite, the composite metal with 5%, 10% and 15wt% of Cu were prepared via stir cast technique: Cu as a metallic reinforcement to enhance the corrosion resistance of Al plate. However, composite with higher concentration of Cu reinforcements exhibit worse corrosion resistance than others composite with lower concentration of Cu reinforcement. This is mainly because of agglomeration of Al and Cu results in Al-Cu rich alloy formation, which in turn enhances localized corrosion.

In order to enhance the characteristics of Al-Cu system, Jain, Rana, and Jain (2016) reinforced Al-Cu metal matrix with boron carbide (B_4C) particle by powder metallurgy process, sintering at 580°C and analyze their physical and mechanical properties (Table 2.17). In a nutshell, the hardness and tensile strength of Al-Cu metal matrix is directly proportional to the increase in wt% of B_4C; this is because Carbide itself is a hard particle, when more B_4C is added into Al-Cu matrix which provides more strength to the matrix. also used another Carbide particle, TiC to reinforce a nano-structured Al-Cu powder alloy. By comparing two milling process, namely ball milling and mechanical milling. TiC particles acted as a milling media and reduce the crystalline size of the Al-α phase during ball milling stage, which didn't observed in mechanical milling stage. This un-reactivity of metal with ceramic phase could be due to the fact that the ball milling was performed under low energy conditions.

Table 2.17: Tabulated results of Al-4wt%Cu with different wt% of B_4C

B_4C weight percentage (%)	**Porosity (%)**	**Hardness (BHN)**	**Tensile Strength (MPa)**
0	0.75	35	200
2	0.80	36	209
4	0.90	38	213
6	1.05	39	219
8	1.50	40	224
10	1.75	43	229
12	1.92	49	223

2.6.3 Selection of organic additives for nanopaste

The use of organic additive is important to formulate a nanopaste. The main constituent of organic additives in a nanopaste is the binders and dispersants (or surfactant). Binders are commonly a polymer that contains long chain carbon molecules; they bind and hold nanoparticles in place in nanopaste system. Additionally, it also helps to prevent the crack as disintegration of the material during sintering. Dispersants or surfactants are used for preventing the agglomeration of nanoparticles, which may affect the average particle size of nanopaste. Reported binder-dispersant/surfactant systems in literature are list in Table 2.18.

Table 2.18: Reported binders and surfactants/dispersants for nanopaste systems

Binders	Surfactant/Dispersant	References
Resin Binder	Menhaden fish oil	(John G Bai, Calata, & Lu, 2007; John Guofeng Bai et al., 2007; John G Bai et al., 2006)
Lignoceric acid	Poly(acrylic acid)	(John G Bai et al., 2007; John Guofeng Bai et al., 2007; John G Bai et al., 2006)
Polyvinyl alcohol	Alkylamine	(Wakuda, Kim, & Suganuma, 2008)
	BYK163	(Wakuda et al., 2008)
	Dysperbyk 163	(Wakuda et al., 2008)

2.7 Determination of Operating Temperature

An operating temperature (T_o) is the temperature at which an electronic device operate. T_o is determined by the melting point (T_m) of die-attaches material. For high temperature SiC applications, the selection of materials for die-attach uses must primarily possess high melting temperature. Homologue temperature (T_h) is the ratio of T_o and T_m which is given in Eq. (2.2). This ratio is being set between the range of 0.67 and 0.85, sometimes a midpoint of 0.76 is also used as T_o (Buttay et al., 2011; Masson et al., 2011).

$$T_h = \frac{T_o}{T_m} \tag{2.2}$$

Table 2.19 lists the operating temperature for various Si and SiC devices. For existing Si technology, the reported highest operating temperature is 400°C Si digital logic device,still considerably high. Other than that, the operating temperature for Si devices is ranging between 150 to 300°C, which the existing die-attach materials are capable to cope with the Si based device. Nevertheless, for SiC technology, e.g. SiC DRAM has an operating temperature of 600°C. Thus, the die-attach material used should be able to withstand such high temperature.

Table 2.19: Different Electronic Devices and Their Respective Operating Temperature (Manikam & Cheong, 2011)

Devices by Application	Current Operating Temperature (°C)	Projected Operating Temperature (°C)
Silicon microwave	150	200
Silicon digital logic	300	400
Silicon small signal	250	300
Silicon power	200	N/A
SiC power	300	400
SiC digital logic	100	700
SiC small signal	400	N/A
SiC power N-C MODSFET	600	N/A
SiC DRAM	600	N/A
Nitrides (n-type)	N/A	700
Nitrides microwave	N/A	700

2.8 Design of Experiment (DOE)

The design of experiment (DOE) is a scientific approach to determine the relationship between factors and the output in a process. In DOE approach, an experiment is designed by considering the effects of several factors independently, concurrently or combination of these factors. This information is crucial to control process input and optimizing the output. DOE approaches can be further classified into one factor designs, response surface methods (RSM), reliability DOEs and factorial design. In general, factorial design are the one that commonly used in DOE, whereby each factor have a different number of levels, those factors can be qualitative, quantitative or both. In a full factorial design, each factors and levels are linked with all possible combinations. In research, full factorial design is able to determine the effect of each considered factor on targeted response variable. There are three major components in a full factorial design, i.e. factors, levels and response. In the context of DOE, the independent variable is called factors, and the dependent variable is called response. Experiments are run at different factor values, called levels (Anderson & McLean, 2018).

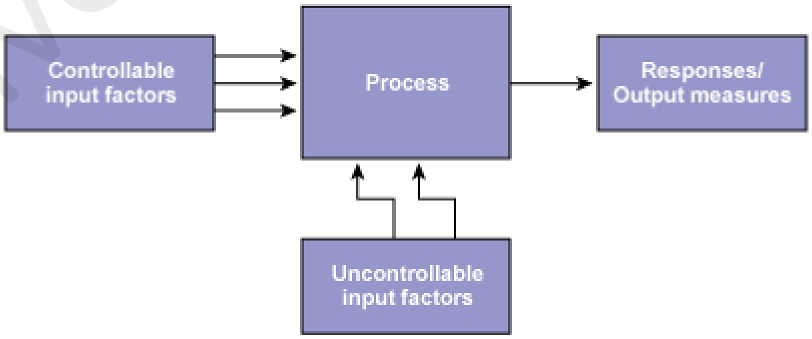

Figure 2.32: Process Factors and Responses

CHAPTER 3

RESEARCH METHODOLOGY

3.1 Introduction

This chapter covers the research methodology and characterization techniques used in this experiment. Subsequently, the materials and experimental procedure are explained in detail. The outline of research methodology is depicted in Figure 3.1: the Al-Cu nanopaste is firstly formulated by appropriate amount of binders, surfactants and thinners. Next, the Al-Cu nanopaste sintering profile is designed to study the influence of different air conditions toward the die attach quality of Al-Cu nanopaste. After that, the Al-Cu nanopaste is characterized via different techniques which are explained by following subsections in this chapter. This study covers 3 major scopes: (i) To design an effective sintering profile by optimizing the sintering temperature ramp rate and dwell time, (ii) To optimize the ratio of Al-Cu nanopaste to organic additives (wt%), the weight percentage of nanoparticles is varied from 4 to 7% (iii) To optimize the ratio of Al to Cu (wt%) associated with the optimized ratio in scope 1, the weight percentage of Al is are 10%,20% 30% and 40% corresponding to the weight percentage of Cu.

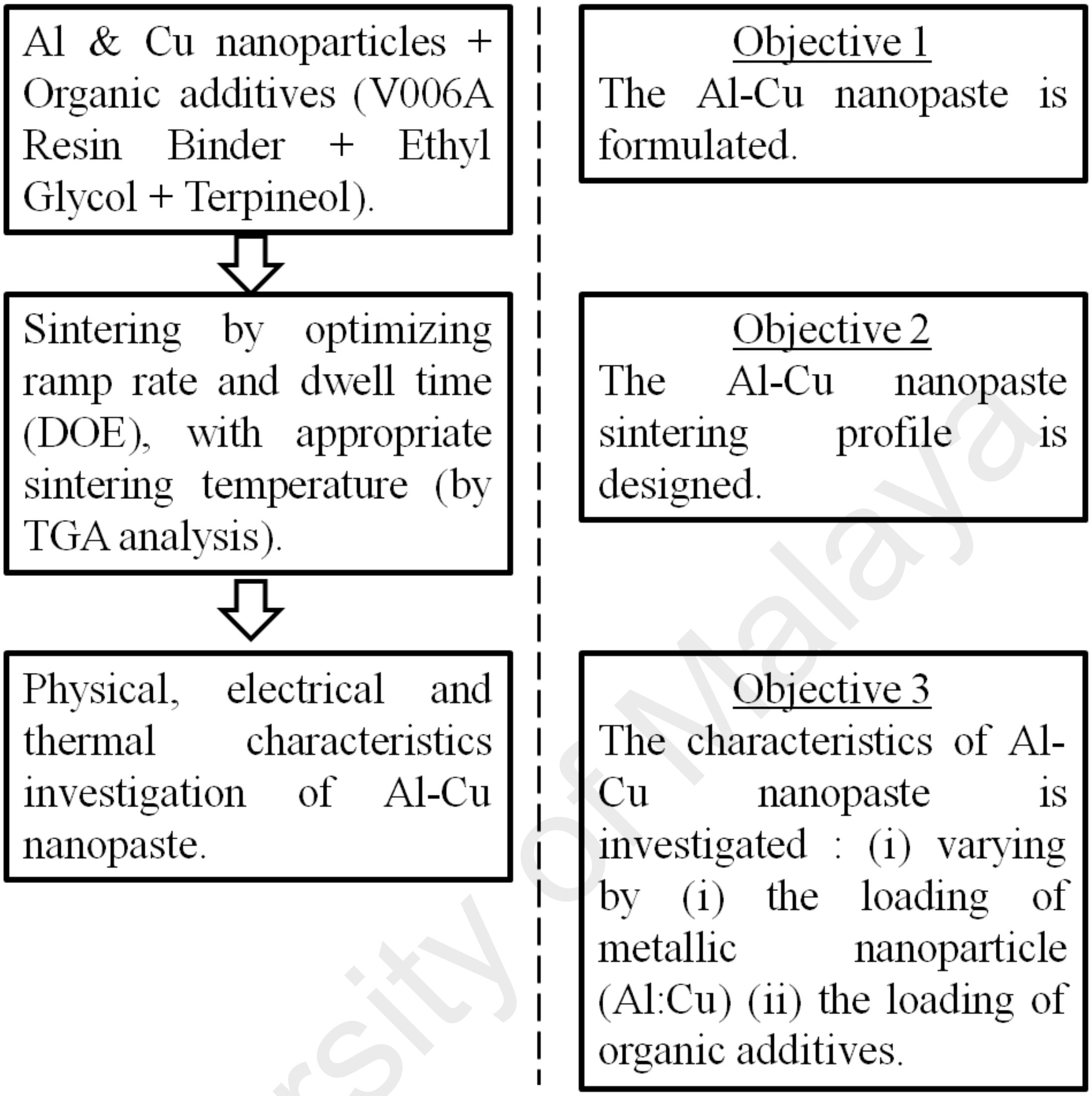

Figure 3.1: An Overview of Research Methodology

3.2 Materials

3.2.1 Materials for the Al-Cu nanopaste formulation

The Al-Cu nanopaste was formulated by using the following components in Table 3.1 which are categorized by material, supplier and specification:

Table 3.1: Material used in Al-Cu nanopaste formulation, supplier and specification

No	Material	Specification	Supplier
1	Al nanoparticles (powder)	60-80nm	Nano Science
2	Cu nanoparticles (powder)	60-80nm	Nano Science
3	Ehtylene Glycol, (EG)	Assay: 99.5%	SigmaAldrich
4	Terpineol	Assay: 96%	SigmaAldrich
5	Ethanol	Assay: 98%	SigmaAldrich
6	Resin binder, V006A	Viscosity: 6%	Heraeus Inc.(USA)

3.2.2 Al-Cu nanopaste formulation

The Al-Cu nanopaste was formulated by mixing the organic constituent (ethanol, V006 resin binder, terpineol and EG) and the metallic nanoparticles according to Table 3.2. The formulation procedure is depicted in Figure 3.2. The Al and Cu nanoparticles are ultrasonically dispersed in EG using an ultrasonic cleaner, ethanol as a solvent is added into the mixture. Next, the V006A resin binder which was dissolved in terpineol was mixed with it and ultrasonically dispersed for 8-10 minutes in an 3-4^{o}C ice bath to prevent the agglomeration of nanoparticles. The final paste was evaporated using a hotplate inside a fume hood at 70^{o}C for 1 hour to remove ethanol for Al-Cu nanopaste, and also to achieve necessary viscosity after the organic additives were dispersed.

In this research, the formulation of Al-Cu die-attach nanopaste can be divided into two parts according to objective 2: (i) The weight percent of organic additives were varied at 21%, 22%, 23% and 24%, the weight loading of EG and terpineol were fixed and 0.5g and 0.3g respectively. However, the weight percent of binder was varied at 4%, 5%, 6% and 7%. The weight of nanoparticle loading was kept at 5.00g, whereby the weight percentage of Al nanoparticle is 20% (shown in Table 3.2). (ii) The weight percentage of

Al was varied at 10%, 20%, 30% and 40%, with was respective to the weight percentage of Cu (90%,80%,70% and 60%), the total weight of nanoparticles was kept at 5.00g. The weight of organic additives was based on the optimize results on part (i).

Table 3.2: Al-Cu die attach nanopaste formulation with different binder loading

Binder (g)	EG (g)	Terpineol (g)	Nanoparticles (g) (20%Al, 80%Cu)	Weight of binder to nanoparticle, %	Weight of organic additives to nanoparticle, %
0.20	0.50	0.30	5.00	4.0	21.0
0.25	0.50	0.30	5.00	5.0	22.0
0.30	0.50	0.30	5.00	6.0	23.0
0.35	0.50	0.30	5.00	7.0	24.0

Table 3.3: Al-Cu die attach nanopaste formulation with different Al loading

Sample	Al-Cu loading (%)	Al wt% to nanoparticle	Cu wt% to nanoparticle
1	$Al_{0.5}$-$Cu_{4.5}$	10.00	90.00
2	$Al_{1.0}$-$Cu_{4.0}$	20.00	80.00
3	$Al_{1.5}$-$Cu_{3.5}$	30.00	70.00
4	$Al_{2.0}$-$Cu_{3.0}$	40.00	60.00

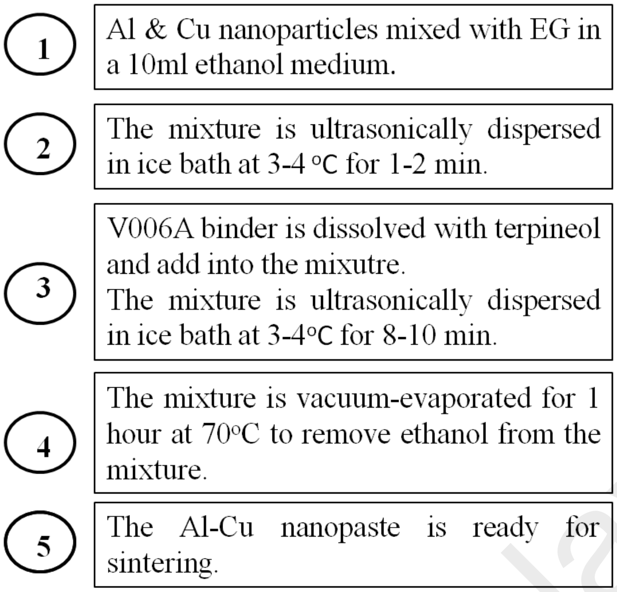

1. Al & Cu nanoparticles mixed with EG in a 10ml ethanol medium.
2. The mixture is ultrasonically dispersed in ice bath at 3-4 °C for 1-2 min.
3. V006A binder is dissolved with terpineol and add into the mixutre. The mixture is ultrasonically dispersed in ice bath at 3-4°C for 8-10 min.
4. The mixture is vacuum-evaporated for 1 hour at 70°C to remove ethanol from the mixture.
5. The Al-Cu nanopaste is ready for sintering.

Figure 3.2: Al-Cu die attach nanopaste formulation process flow

3.3 Experimental procedures

3.3.1 Stencil printing of Al-Cu nanopaste

A stencil with 1.0cm^2 aperture, thickness of 50-75μm was used for screen-printing the Al-Cu die attach area onto the silicone (Si) substrates. Figure 3.3 illustrates the screen-print technique; a squeegee was used to scratch off the excessive Al-Cu nanopaste.

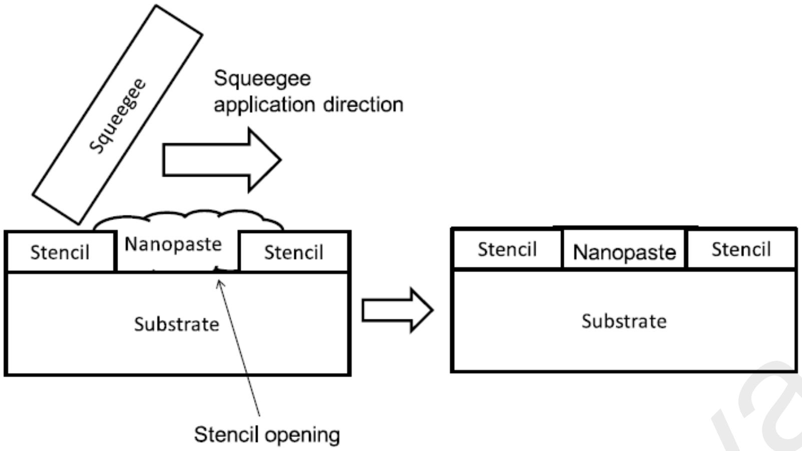

Figure 3.3: Method of stencil printing Al-Cu nanopaste onto Si substrates

3.3.2 Al-Cu nanopaste sintering

The Al-Cu die attach nanopaste was sintered by using a Carbolite horizontal tube furnace. The Al-Cu nanopaste was sintered at 380 ±10 ^{o}C with a dwell time of 30 minutes and ramp rate of 10 ^{o}C/min (results from TGA analysis and DOE which will be discussed in Chapter 4). The designed sintering temperature was chosen based on TGA results which indicated that all organic additives burnt off at 380^{o}C. High temperature should be avoided because oxidation of die attach material's surface would take place which indicates the degradation of both thermal and electrical properties.

3.4 Characterization technique

3.4.1 Physical characterization

3.4.1.1 Scanning electron microscopy (SEM) and energy dispersive X-ray (EDX)

A scanning electron microscopy (FE-SEM) (Zeiss Leo Supra 50 VP) attached with an energy dispersive X-ray (EDX) unit was employed to study the morphology of the post-sintered Al-Cu die attach nanopaste and determine the elemental composition of the samples.

3.4.1.2 X-ray diffraction (XRD)

X-ray diffraction (XRD) was carried out using Cu-$K_{\alpha 1}$ radiation having a wave length value of 1.5406 Å on a D500 Siemens diffractometer to help identify phase of the post-sintered Al-Cu die attach nanopaste. The measurement were scanned from $2\theta = 10^o$ - 90^o, using a step time of 71.60s and step size of 0.034^o.

3.4.2 Thermal characterization

3.4.2.1 Thermogravimetric analysis (TGA)

Thermogravimetric analysis (TGA) measurements were conducted from 30 ^oC to 1000 ^oC at a ramp rate 10 ^oC/min in air using a Perkin Elmer Pyris Diamond system. It was used to monitor organics burn off from the Al-Cu die attach nanopaste.

3.4.3 Electrical characterization

The Current-Voltage (*I-V*) measurements were performed using a computer controlled Keithley 4200 semiconductor characterization system (SCS) system. The prepared nanopaste was first stencil printed onto a Si substrate having before sintering using the designed profile. The *I-V* measurements were conducted using two probes, which were placed at the edges of the measurement area. A total of 100 measurement points were taken for each sample to obtain the mean value, with a total of 3 samples used for every condition. Figure 3.4 depicts the sample and probe setup.

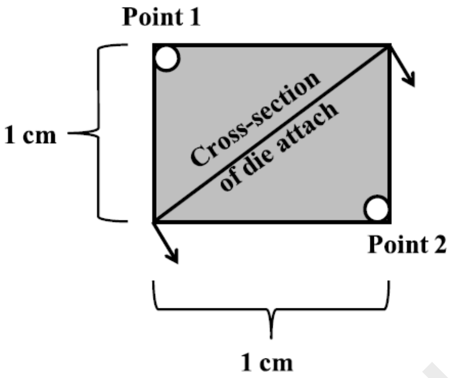

Figure 3.4: I-V measurement setup for Al-Cu die-attach nanopaste

The *I-V* measurement was to calculate the resistance, R, which is represented by Equation 3.5 in which I and V are current and voltage respectively:

$$R = \frac{V}{I} \tag{3.1}$$

The resistivity, ρ, was calculated from Equation 3.6, whereby L is length of the stencil printed area and A represents the cross section of the stencil printed area.

$$R = \frac{\rho L}{A} \tag{3.2}$$

Consequently, the electrical conductivity (σ) of the Al-Cu die attach material can be calculated by Equation 3.7:

$$\sigma = \frac{1}{\rho} \tag{3.3}$$

3.4.4 Design of experiment (DOE)

In this research, a full factorial DOE was used to determine the effect of ramp rate and dwell time on the electrical performance of post-sintered nanopaste. The content of Al and Cu were fixed at 20% and 80% respectively for all runs. In this full factorial DOE, ramp rate and dwell time are the factors for each runs, the ramp rate were varied at 5,7 and 10 ^{o}C/min and the dwell time were varied at 10,20,30,40 and 50 min. The full factorial DOE were set as at least 2 factor having more than 2 levels. The finalized DOE was an 3x5 design having a total of 15 experimental runs shown in Table 3.4.

Table 3.4: A 5x3 General Full Factorial Design with 15 Experimental Runs

Pattern	Ramp rate (^{o}C/min)	Dwell time (min)
11	5	10
21	7	10
13	5	30
32	10	20
25	7	50
23	7	30
22	7	20
14	5	40
34	10	40
15	5	50
12	5	20
24	7	40
35	10	50
31	10	10
33	10	30

CHAPTER 4

RESULT AND DISCUSSION

4.1 Introduction

In this chapter, a comprehensive discussion of the experimental results of the Al-Cu die-attach material development will be presented. The results and discussion are divided into 3 parts: (i) Design of sintering profile for the Al-Cu die attach nanopaste material, (ii) Investigation of physical, electrical and structural characteristics of Al-Cu die attach nanopaste having varying organic additives weight percentage content (17.36-19.36%), (iii) Investigation of physical, electrical and structural characteristics of Al-Cu die attach nanopaste having varying Al weight percentage content (10-40%).

4.2 Design of sintering profile and formulation of Al-Cu nanopaste

4.2.1 Al-Cu nanoparticle analysis

Al and Cu nanoparticle were commercially acquired and analyzed by XRD analysis. For Al nanoparticle, the diffraction peaks were observed at 29.2^{o}, plane (210) and at 43.1^{o}, plane (101), corresponded to ICDD 01-073-2661. Whereas for Cu nanoparticle, the diffraction peaks were observed at $29.2\ ^{o}$ plane (002), 61.9^{o} plane (220) and 74.1^{o} plane (221), corresponded to ICDD 01-070-3038.

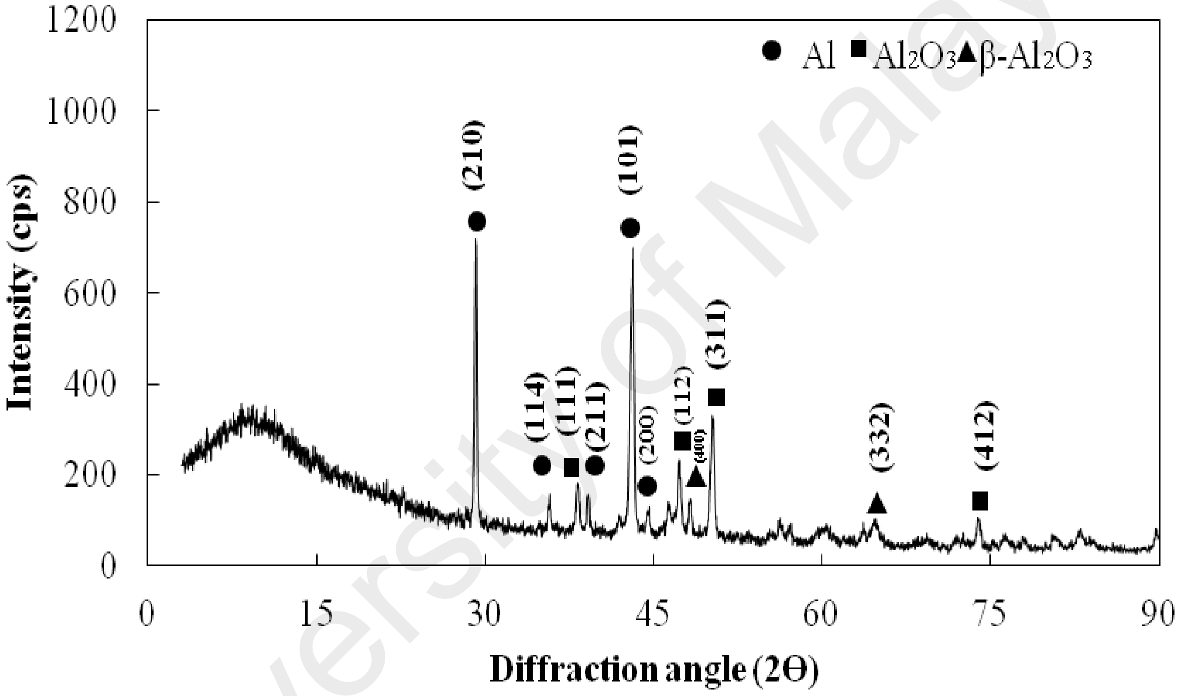

Figure 4.1: XRD diffractogram for Al Nanoparticle, Al at peak 29.2°,plane (210) and peak 43.1°, plane (101)

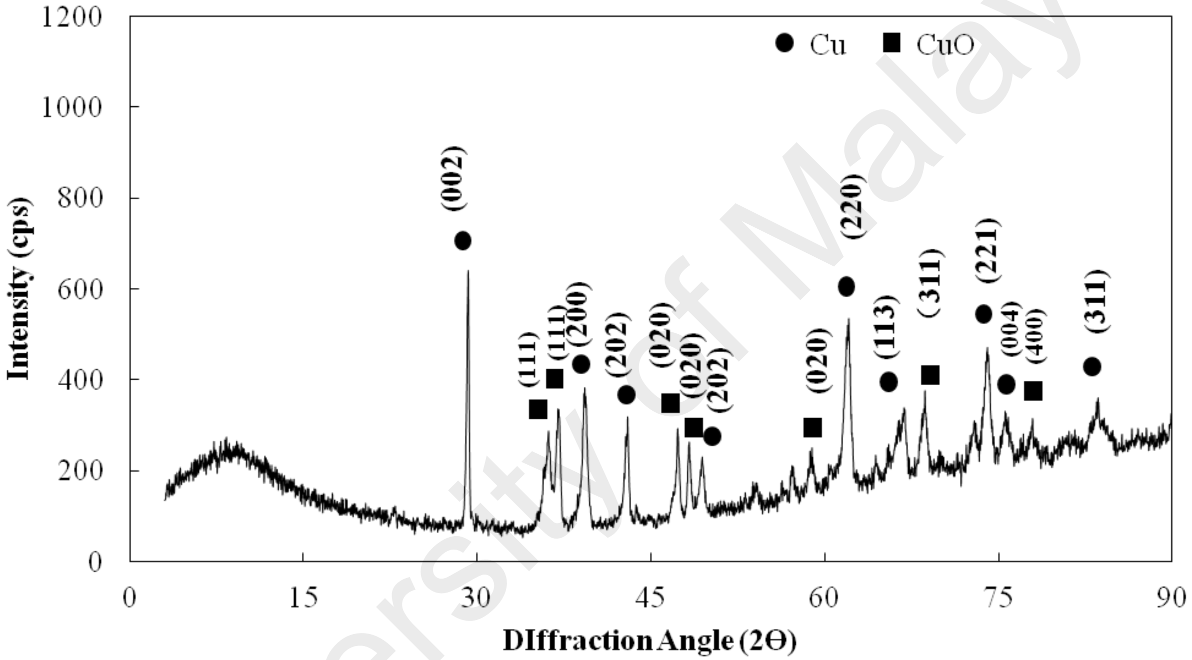

Figure 4.2: XRD diffractogram for Cu Nanoparticle, Cu at peak 29.2 ^{o} plane (002), 61.9^o plane (220) and 74.1^o plane (221)

4.2.2 TGA analysis

In this work, the sintering temperature was designed based on 2 considerations: (i) Sintering temperature not closer to the melting point to protect mechanical properties of nanoparticles. In most cases, the homologous temperature (T_h) (ratio of melting point (T_m) over the operating temperature (T_o)) is typically set between 0.67 and 0.85 in accordance to Equation 4.1. In this work, Al nanoparticle (660^{o}C) has the lower melting point than Cu (1085 ^{o}C). Therefore, 660 ^{o}C is set as T_m and 0.67 is used as $T_{h.}$ As a result of this, the designed sintering temperature cannot exceed 442.2 ^{o}C.

$$T_h = T_o/T_m \tag{4.1}$$

(ii) The sintering temperature promotes the burn-off of organic additives, TGA analysis was carried out to determine the weight loss curve of all organic additives, also to find out their respective evaporation point at which these organic additives disintegrate. Figure 4.3 depicts the TGA plot of all organic additives, EG and terpineol are firstly burst off below 250 ^{o}C, V006A is burnt off at a higher temperature of 380 ^{o}C. These results are important for designing the sintering profile for Al-Cu die-attach nanopaste.

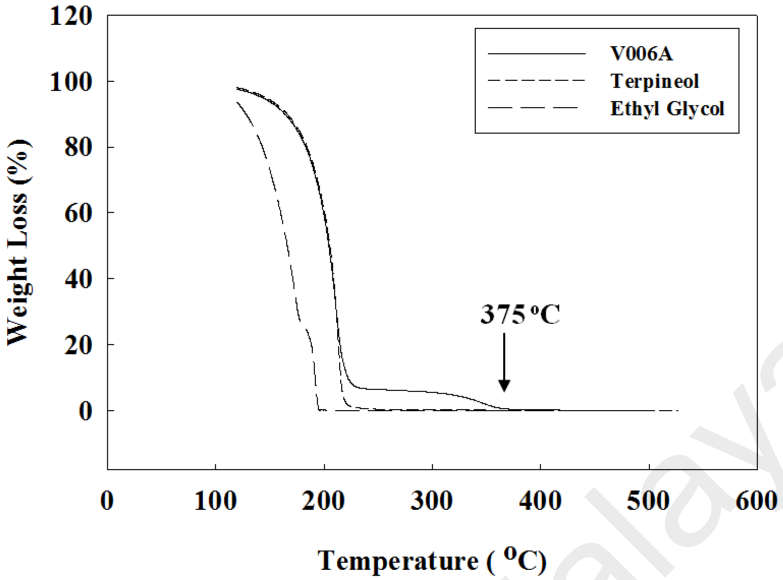

Figure 4.3: TGA analysis of organic additives in Al-Cu die-attach nanopaste

4.3 Sintering Profile of Al-Cu nanopaste

This section presented the way to design a sintering profile which can achieve organic additives burn-off and the coalescence of Al and Cu nanoparticles. A DOE technique was performed to help in optimizing the sintering profile for Al-Cu nanopaste. Ramp rate and dwell time were the tested factor for this DOE. The selection of sintering condition was also presented in this section.

4.3.1 Design of Experiment (DOE) for Sintering Profile Optimization

The TGA result in Figure 4.3 shows all organic additives are burnt-off at 380^{o}C. Nanoparticle is firstly coated with organic layers. Once the temperature rises, the organic layers burn off and the nanoparticles are allowed to fuse in solid-state. Figure 4.4 illustrate the sequence of particle transformation.

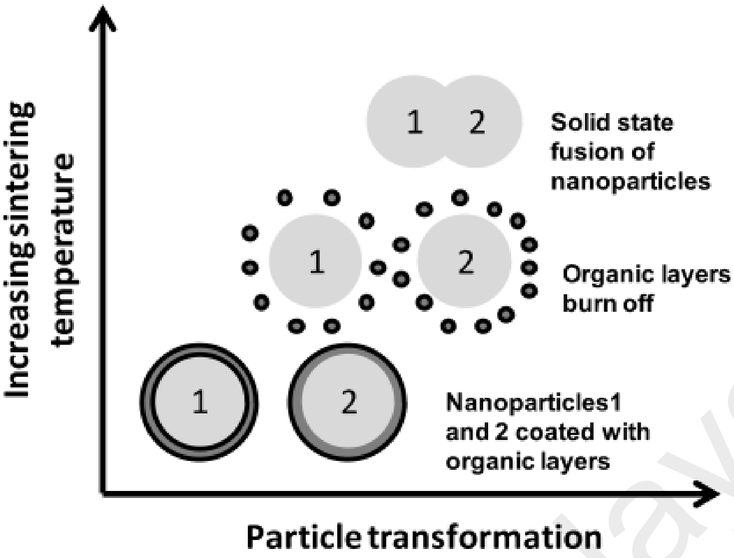

Figure 4.4: Sequence of nanoparticle transformation during sintering

In a sintering process, ramp rate and dwell time are crucial factors to be considered. A full factorial DOE was used to achieve the optimization of sintering profile. In order to ensure the complete burn-off of organic additive, the sintering temperature was fixed at 380^{o}C. The ramp rate were varied at 5,7 and 10 ^{o}C/min and the dwell time were varied at 10,20,30,40 and 50 min. In this full factorial DOE, there had at least 2 factors having more than 2 levels. This full factorial DOE is a 3x5 design that having 15 experimental runs shown in Table 4.1, Each sintering result will be tested by I-V measurement to determine the electrical resistivity for each runs. JMP software from SAS institute. Inc. was employed to perform this full factorial DOE.

Table 4.1: Full Factorial 5x3 DOE for sintering profile optimization

Pattern	Ramp rate (^oC/min)	Dwell time (min)	Result (µΩ.cm)
11	5	10	47.96
21	7	10	46.63
13	5	30	37.65
32	10	20	37.87
25	7	50	48.66
23	7	30	39.19
22	7	20	44.35
14	5	40	49.08
34	10	40	38.94
15	5	50	53.86
12	5	20	45.58
24	7	40	45.94
35	10	50	45.17
31	10	10	42.44
33	10	30	40.59
R^2		0.8095	
P-value		Dwell time: 0.0208 Ramp rate: 0.0240	
Desirability		0.6298	

The result of the summary of fits is shown in Table 4.1. The value of R^2 of 0.8095 was obtained which is close to 1. This implies that the summary of fits between input factors is statistically acceptable. P value for dwell time and ramp rate were 0.0208 and 0.0240, respectively, which is less than the significant level (α) of 0.05 used in this analysis, which means that the relationship of ramp rate and dwell time is significant during the sintering process. In a nutshell, ramp rate off 10^{o}C/min and dwell time of 30 min were recommended by JMP to achieve the highest desirability, which is 0.6298.

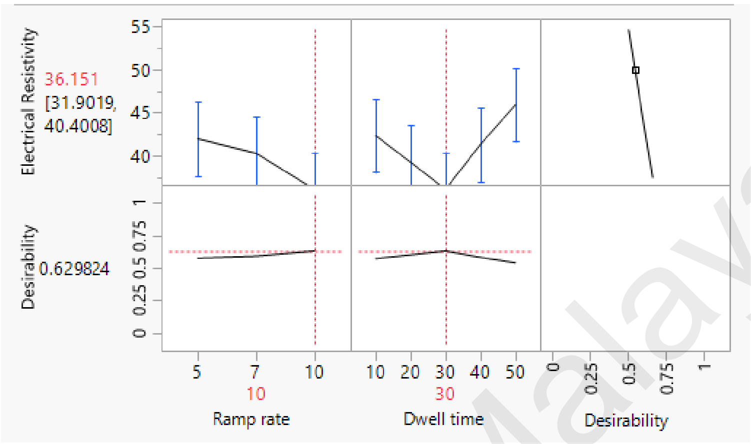

Figure 4.5: Optimized Factors from Full Factorial 5x3 DOE

4.3 Investigation of the Al-Cu nanopaste' physical, electrical and structural characteristics with varying organic additives content

4.3.1 XRD analysis

Figure 4.6 shows the XRD pattern of the Al-Cu die-attach nanopaste at various V006A content (4%, 5%, 6% and 7%). The peaks in Fig.4 were confirmed in accordance of International Centre for Diffraction Database (ICDD). Two significant peaks were observed at 28.0 ^{o} and 39.0^{o}; these peaks were identified as CuAl$_2$ at plane (110) and (001) respectively, corresponded to ICDD 01-074-7053.As sintering effect on Al-Cu nanopaste promotes the burn-off of organic contents in these sample and the solid-state diffusion between the elements of Al and Cu: the CuAl$_2$ peak at plane (001) is getting stronger when the V006A content is lower. Evidently, the surface properties of Cu nanoparticles differ from their bulk counterpart. Higher surface energy of Cu nanoparticles is readily oxidized even in their virgin state without the heat application. In this work, sintering is the heating process that generates more oxidation effects on Cu nanoparticles. Therefore, the rate of fusion between metallic nanoparticles becomes a crucial factor in order to avoid the formation of oxides. For example, it can be easily noticed that $CuAl_2$ peak at (111) plane gets weaker as nanoparticle content gets higher. This is because higher content of organic additives can delay the solid-state fusion between Al and Cu nanoparticles in these samples.

To obtain nanocrystalline size of Al-Cu nanopastes from XRD graph, the average nanocrystalline size given by Debye–Scherrer equation is:

$$D = \frac{K\lambda}{\beta cos\, \Theta} \tag{4.2}$$

Where D is the crystalline size, K is the shape factor which is a constant (0.9), λ is the wavelength of C_u $K_{\alpha 1}$ (0.1541 nm), β is the peak width with half maximum intensity and θ is the peak position. The crystallite size is shown in Figure 4.7. Sample with 5% V006A has the smallest crystallite size among all samples, this can be attributed to the crystallographic rearrangement of Al and Cu atoms during sintering .

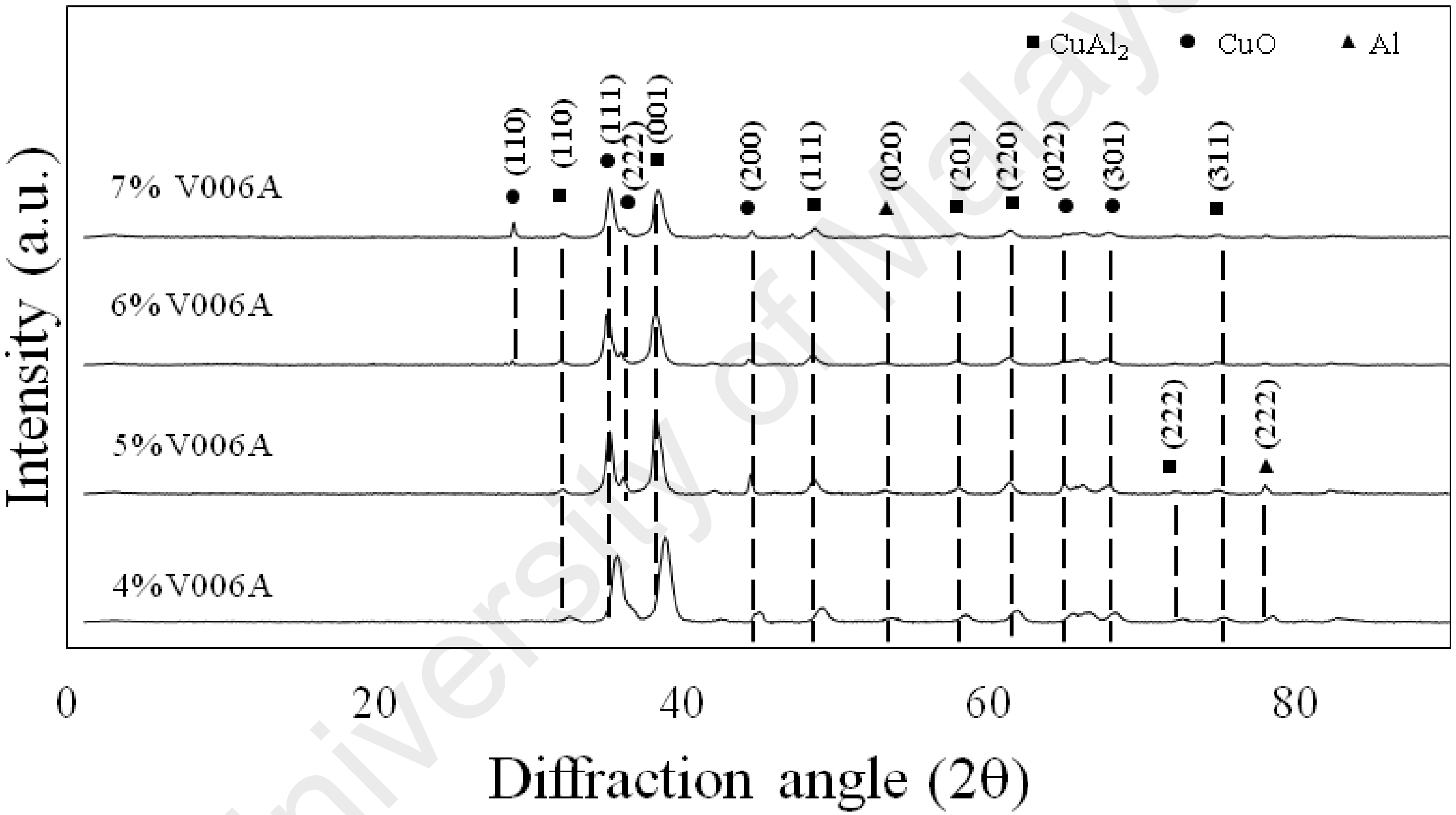

Figure 4.6: XRD diffractogram of Al-Cu nanopaste at various V006A content

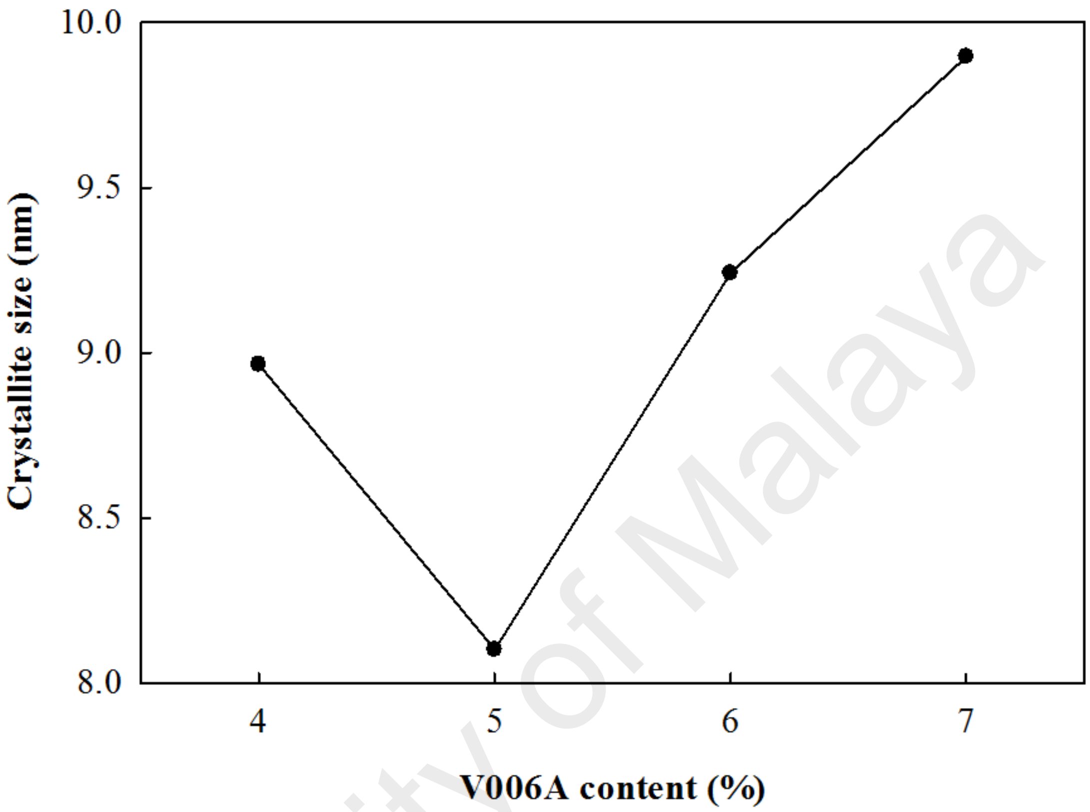

Figure 4.7: Crystallites size of Al-Cu nanopaste at different V006A loadings

4.3.2 SEM analysis

The surface morphology of Al-Cu die-attach nanopaste with different organic loadings were investigated by SEM equipment. Figure 4.8 depicts the microstructure coarsening of the paste with different resin binder weight content. For all samples, necking and coalescence among nanoparticles were observed. Evidently, Al and Cu nanoparticles can be fused at solid state under aforementioned sintering condition. For samples with 6% and 7% V006A, some comparable and larger pores were formed as shown in Figure 4.8 a and b. This can be attributed to the burn-off of organic content and left the space become pores. Likewise, agglomeration of nanoparticles can be easily observed in 4% and 5% V006A as compared to the other 2 samples. These two observations support the idea that larger pores inhibit agglomeration due to fewer interfaces between the nanoparticles. This result coincides with the observation of Manikam, Razak, and Cheong (2013a) in which the organic additives prevents the nanoparticles on the paste system from agglomerating. Thus, the Resin dinder loading plays an important role in the coarsening of the nanoparticle in the paste system. In addition, R. German (2014) suggested that during sintering process, microstructure coarsening is unavoidable. This is due to the fact that the micro-structural features of grains and pores are largely not uniform where one is larger the other would result to energy differences. Smaller micro-structural features connote higher energy per unit volume thus smaller pores coalesce easily forming into a larger pores. Grain size and pore size are key micro-structural features to understand the sintered material.

The oxidation condition was demonstrated by EDX analysis as shown in Fig.7: the spectrum of 5 spots on sample was recorded. Sample with 5% V006A had the lowest percentage of oxygen (O) element at 15.356%. The detected O element is due to the formation of oxide with Al-Cu nanopaste during the sintering process, which generates more oxidation effects on Cu nanoparticles.

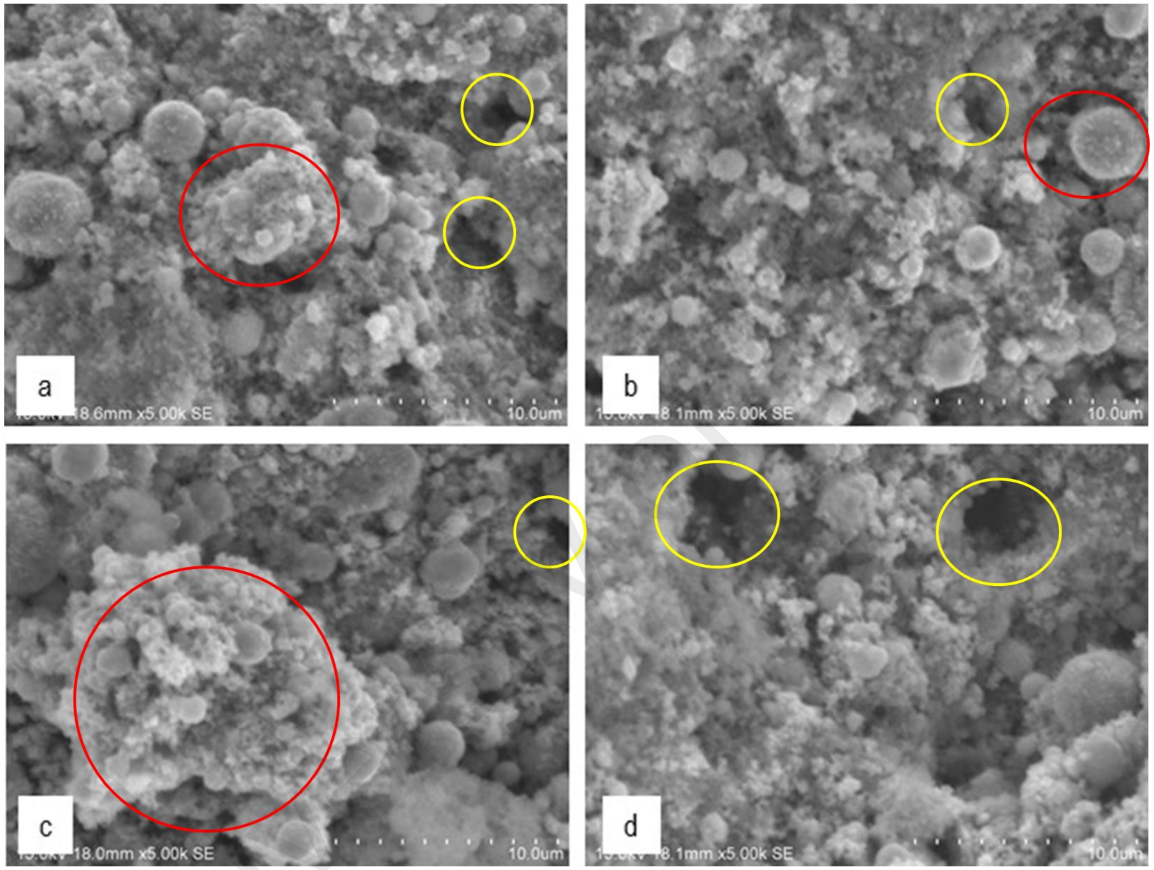

Figure 4.8: SEM images of post sintered Al-Cu die-attach nanopaste with at various V006A content: (a) 4%, (b) 5%, (c) 6% and (d) 7%. Red labels show the agglomeration of nanoparticles, Yellow labels show the pores formation in Al-Cu die-attach nanopaste.

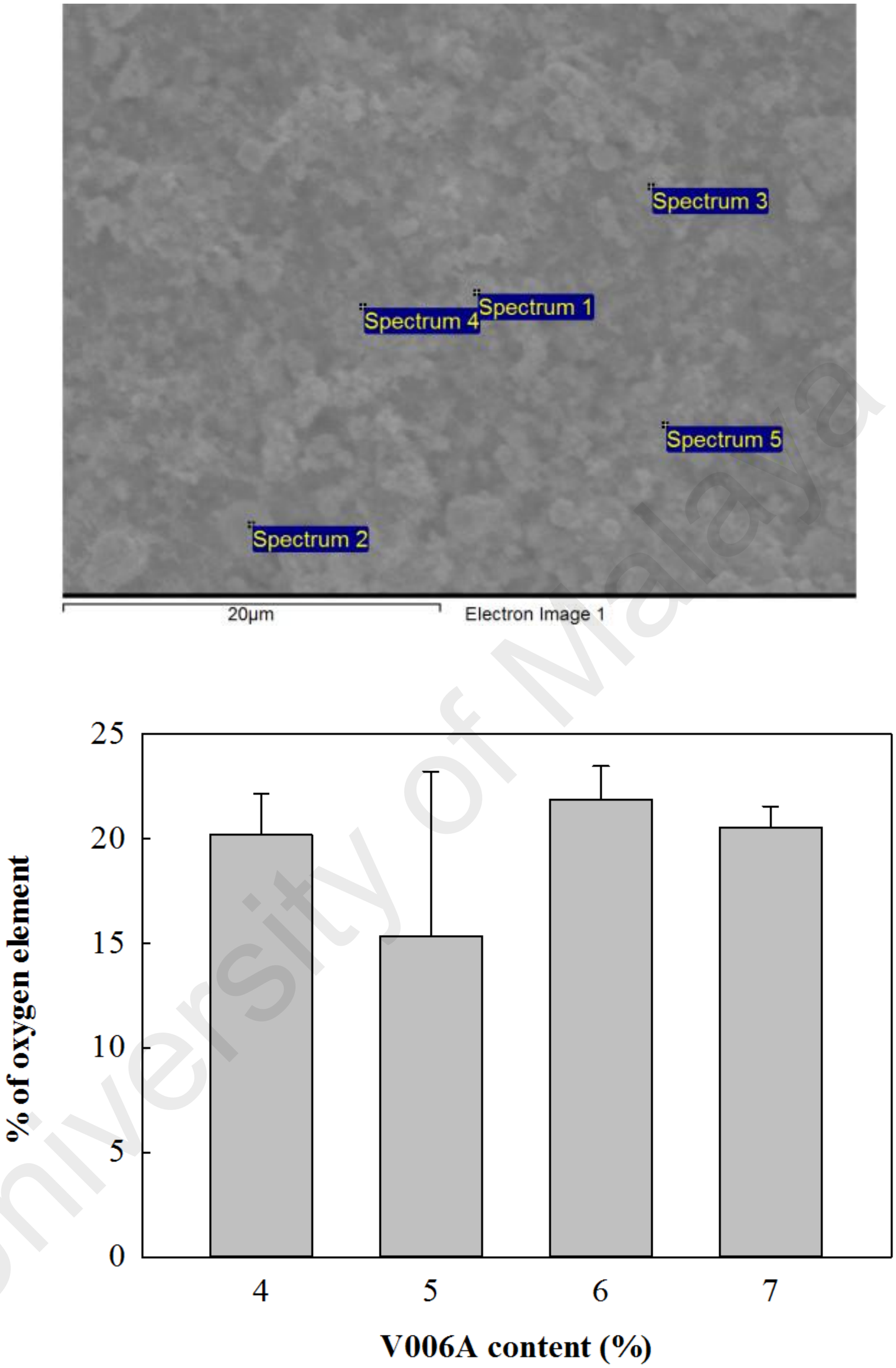

Figure 4.9: EDX analysis of post-sintered Al-Cu nanopaste at different V006A content

4.3.3 I-V measurement

The electrical resistivity of the Al-Cu nanopaste with different V006A content is depicted in Figure 4.10. A slight drop of electrical resistivity can be firstly observed from 4% to 5% V006A. An increase trend is then can be seen from 5% V006A onward. The Al-Cu nanopaste with 5% V006A had the lowest electrical resistivity among all Al-Cu nanopaste, at 21μΩ.cm. In SEM analysis, it can be observed some comparable pores in samples with 6% and 7% V006A content: porous materials generally exhibit higher electrical resistivity. Wherein, the organics burn-off creates open spaces and micropores within sintered Al-Cu nanopaste during sintering. Also, the different nano-sized Al and Cu were shown to restrict the mechanism of densification. In addition, the build-up of CuO which has high dielectric properties had indirectly affected the electrical conductivity of sample. The EDX analysis in Figure 4.9 shows the % of O element is the lowest for sample with 5% V006A (15.36%), compare to the other samples.

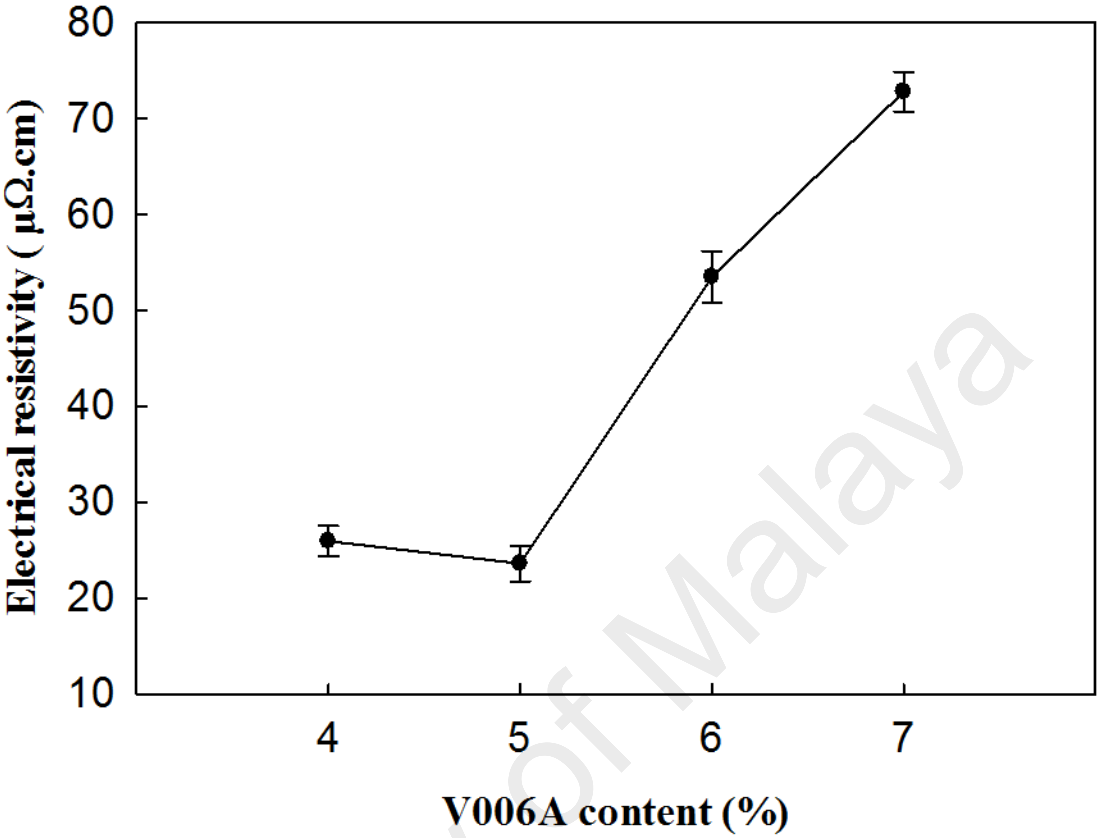

Figure 4.10: Electrical resistivity of post-sintered Al-Cu die-attach nanopastes at various V006A content

4.4 Investigation of the Al-Cu nanopaste' physical, electrical and structural characteristics with varying organic additives content

4.4.1 XRD analysis

Figure 4.11 shows the XRD pattern of the Al-Cu die-attach nanopaste at various Al loading (10-40%). The peaks in Fig.4 were confirmed in accordance of International Centre for Diffraction Database (ICDD). The significant peak for sample with 10% and 20% Al loading was observed at 35.3^o and 39.1^o, these peaks were identified as CuO and $CuAl_2$ at plane (110) and plane (111) respectively, corresponded to ICDD 01-080-1916 and 01-074-7053. Other peaks such as Alumina, Cuprite (Cu2 + 1O) can also be observed, corresponded to ICDD 01-080-2612 and 00-005-0667 respectively. For sample with 30wt% and 40wt% Al loading, 3 significant peaks namely Cuprite (37.8^o), $CuAl_2$ (44.5^o) and Al (39.2^o) at plane (111), plane (200) and plane (111) respectively, corresponded to ICDD 00-005-0667, 01-074-7053 and 01-073-2661.

Al and Cu nanoparticles can be fused at solid-state during low temperature sintering process which can be proved by the XRD analysis. However, the buildup of oxidation layer at Al and Cu nanoparticles (Alumina and CuO) during the sintering process can degrade the properties of Al-Cu die-attach nanopaste. In some case, the incomplete coalescence of nanoparticles was observed, which indicated the inhomogeneous mixing of these nanoparticles, or the agglomeration of nanoparticles occurs during the processing of nanopaste.

4.4.2 SEM analysis

Figure 4.12 compares the microstructure for the Al-Cu nanopaste samples with various Al loading after sintering at 380^{o}C. The lower organic additives content assisted the grain growth and the coalescence of Al and Cu nanoparticles, which can be observed in Figure 4.12. In conclusion, orgnanic additives in the formulation of nanopaste are important as it controls the densification of the material during sintering. The formation of pores is due to the burn-off of organic additives during sintering stage, it is understood that an organic-metallic system will undergo 3 essential stages during sintering, first step is de-binding of the organic additives, second step is the coalescence of particles, and finally a slight dilation in which re-crystallization is anticipated.

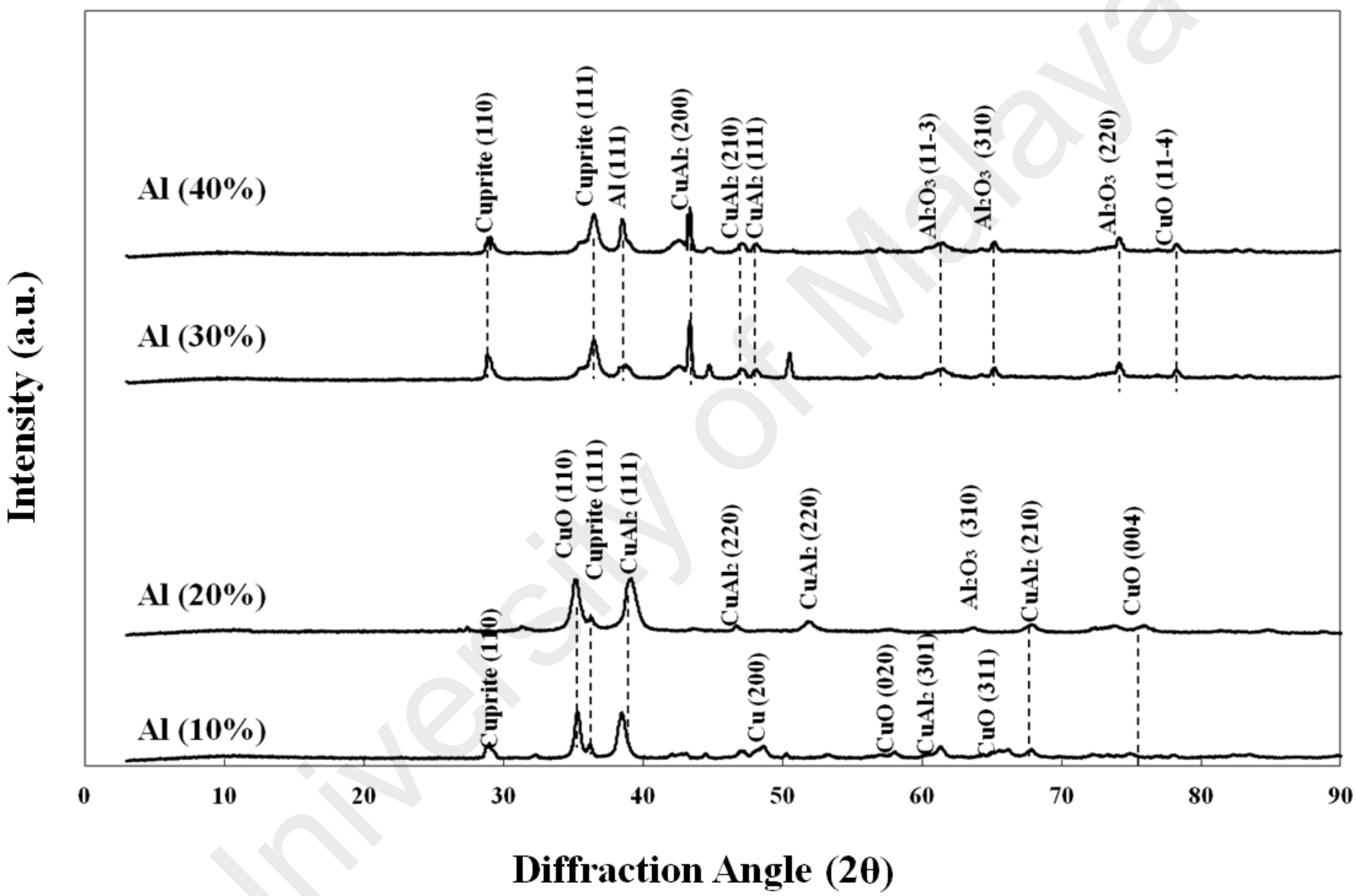

Figure 4.11: XRD diffractogram of Al-Cu nanopaste at different Al loadings

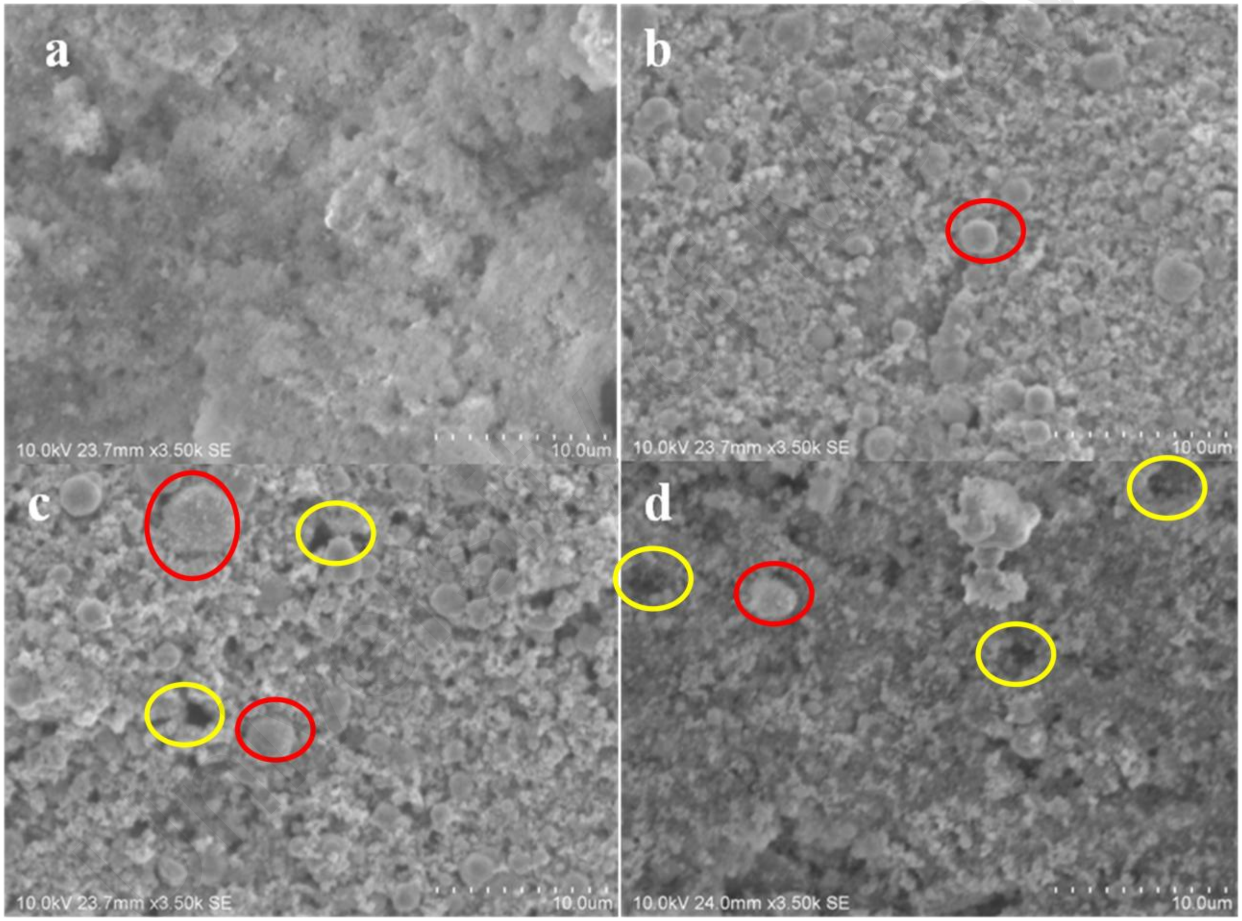

Figure 4.12: Microstructure for Al-Cu nanopaste at various Al weight loading (a) 10wt% (b) 20wt% (c) 30wt% (d) 40wt%, Red labels show the agglomeration of nanoparticles, Yellow labels show the pores formation in Al-Cu die-attach nanopaste.

4.4.3 I-V measurement

Figure 4.13 shows the electrical resistivity of sintered Al-Cu nanopaste decreased when the weight percentage content of Al decreased. A sharp rise of electrical resistivity can be observed between samples having 40-100%. The $Al_{0.5}$-$Cu_{4.5}$ die-attach nanopaste had the lowest electrical resistivity, at 16μΩ.cm. Pure Al nanopaste has an electrical resistivity of 9238μΩ.cm. In addition, the pure Cu nanopaste demonstrates the lowest electrical resistivity, at 16 μΩ.cm. The increase of electrical resistivity for Al-Cu nanopaste with the increase of Al weight percentage content can be contributed to the ease of Al itself of being oxidized. Nanoparticles are normally possesses high surface energy and tend to form an oxidation layer on their particle's surface, which can degrade the electrical performance indirectly. This can be proved in XRD analysis, where the Alumina (Al_2O_3) was detected at sample with higher Al weight percentage loading (30%-40%). Al_2O_3 has higher dielectric properties, is formed during the oxidation process.

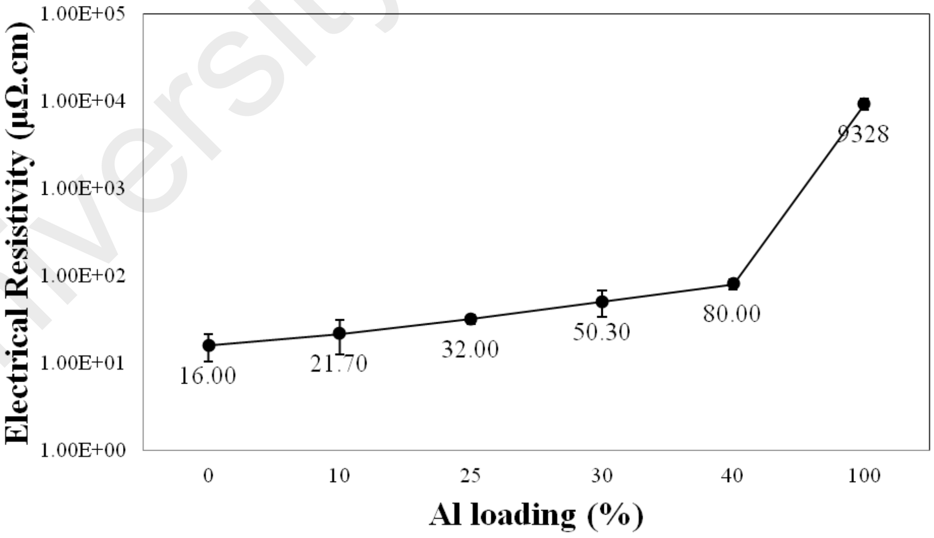

Figure 4.13: Electrical resistivity of post-sintered Al-Cu die-attach nanopastes at various Al loading (10-40wt%)

4.5 Summary

In this chapter, the sintering profile was designed based on TGA analysis and DOE results. DOE results provide the best desirability of 62.98%, at ramp rate 10^{o}C/min and a dwell time of 30 min. TGA analysis showcased the burn-off of organic additives at 380 ^{o}C, which is crucial for designing an effective sintering profile that can promote the coalescence of Al and Cu nanoparticle. Subsequently, the investigation of physical, electrical and structural characteristic of Al-Cu die-attach nanopaste (i) at various organic additives weight percentage content (4-7%), (ii) at various Al weight percentage content (10-40%). The compound $CuAl_2$ was detected in Al-Cu die attach nanopaste's diffractogram. SEM analysis revealed the solid-state fusion of nanoparticle for post-sintered Al-Cu die-attach nanopaste. Also, pores formation within die-attach nanopaste can be spotted due to the volatility of organic additives. 5% V006A exhibits the lowest electrical resistivity at 21.0 μΩ.cm, and the sample with 10% of Al loading exhibits the lowest electrical resistivity at 21.70 μΩ.cm, which is acceptable for high temperature applications.

CHAPTER 5

CONCLUSION AND RECOMMENDATIONS

5.1 Conclusion

The Al-Cu die-attach nanopaste was synthesized using organic additives which can be burnt off at 380^{o}C in air. The sintering temperature (380^{o}C) aided the solid-station fusion of Al and Cu nanoparticles. The dwell time was 30 minutes and and ramp rate was 10 ^{o}C/min respectively. The compound $CuAl_2$ was detected at the post-sintered Al-Cu die-attach nanopaste in XRD diffractogram. The effects of organic additives toward Al-Cu die-attach nanopaste were significant, as the burn-off of organic additives left void within die-attach material, the 5% V006A demonstrates the best result of electrical resistivity at 21.0.μΩ.cm.

It was observed that the increase of Al weight percent content, the electrical properties reduced gradually. The lowest electrical resistivity value was obtained at 21.70μΩ.cm.This value was much lower than the most die-attach material (conductive adhesives, solder alloy and conductive glasses). Overall, Al-Cu die-attach nanopaste exhibits acceptable properties which is suitable for high temperature applications. The microstructure of Al-Cu nanopaste depicted the formation of pores and the aggregation of nanoparticles, which can relate to its electrical properties: $Al_{0.5}$-$Cu_{4.5}$ die-attach nanopaste demonstrate least pore formation, which result in lowest electrical resistivity.

5.2 Recommendations

1) Reducing the processing temperature can avoid the oxidation of Al and Cu nanoparticle during the sintering process. E.g. the application of pressure, employs

low burn off temperature organic additives which can help to reduce the sintering temperature.

2) Optimizing the sintering gas condition by controlling the ratio of N_2:O_2. O_2 is crucial in assisting the burn off of C molecules from the organic additives. The role of N_2 is to minimize the oxidation of Al and Cu nanoparticles, which would further degrade their properties.

3) Additional techniques e.g. microwave irradiation can be replaced to reduce the lengthy sintering process, which might result in crack's formation in die-attach material. Also, microwave irradiation sintering can improve the grain growth and densification.

REFERENCES

AbdElhafez, A., & Forsyth, A. (2009). *A review of more-electric aircraft.* Paper presented at the 13th International Conference on Aerospace Science & Aviation Technology (ASAT-13), Paper No. ASAT-13-EP-01.

Abtew, M., & Selvaduray, G. (2000). Lead-free solders in microelectronics. *Materials Science and Engineering: R: Reports, 27*(5-6), 95-141.

Ahmed, S., Basit, M., Suhling, J. C., & Lall, P. (2016). *Effects of aging on SAC-Bi solder materials.* Paper presented at the Thermal and Thermomechanical Phenomena in Electronic Systems (ITherm), 2016 15th IEEE Intersociety Conference on.

Anderson, V. L., & McLean, R. A. (2018). *Design of experiments: a realistic approach*: Routledge.

Ata, M. H. (2017). Properties of Al/Cu Bimetallic Plate Prepared by P/M Technique: Sintering Temperature Effect.

Bai, J. G., Calata, J. N., & Lu, G.-Q. (2007). Processing and characterization of nanosilver pastes for die-attaching SiC devices. *IEEE Transactions on electronics packaging manufacturing, 30*(4), 241-245.

Bai, J. G., Yin, J., Zhang, Z., Lu, G.-Q., & van Wyk, J. D. (2007). High-temperature operation of SiC power devices by low-temperature sintered silver die-attachment. *IEEE transactions on advanced packaging, 30*(3), 506-510.

Bai, J. G., Zhang, Z. Z., Calata, J. N., & Lu, G.-Q. (2006). Low-temperature sintered nanoscale silver as a novel semiconductor device-metallized substrate interconnect material. *IEEE Transactions on Components and Packaging Technologies, 29*(3), 589-593.

Baird, T., Fields, T., Drummond, R., Mathison, D., Langseth, B., Martin, A., & Silipigno, L. (1993). High-pressure, high-temperature well logging, perforating and testing. *Oilfield Review, 5*(2/3), 15-32.

Biswas, A., Bayer, I. S., Biris, A. S., Wang, T., Dervishi, E., & Faupel, F. (2012). Advances in top–down and bottom–up surface nanofabrication: Techniques, applications & future prospects. *Advances in colloid and interface science, 170*(1-2), 2-27.

Buttay, C., Planson, D., Allard, B., Bergogne, D., Bevilacqua, P., Joubert, C., . . . Tournier, D. (2011). State of the art of high temperature power electronics. *Materials Science and Engineering: B, 176*(4), 283-288.

Callanan, B. (2011). Application considerations for silicon carbide MOSFETs. *Cree Inc. Application Note*.

Casady, J., & Johnson, R. W. (1996). Status of silicon carbide (SiC) as a wide-bandgap semiconductor for high-temperature applications: A review. *Solid-State Electronics, 39*(10), 1409-1422.

Cheng, S., Huang, C.-M., & Pecht, M. (2017). A review of lead-free solders for electronics applications. *Microelectronics Reliability, 75*, 77-95.

Choi, H. (2017). Overview of silicon carbide power devices. *Fairchild semiconductor*.

Chuang, R. W., & Lee, C. C. (2002). Silver-indium joints produced at low temperature for high temperature devices. *IEEE Transactions on Components and Packaging Technologies, 25*(3), 453-458.

Colson, P., Henrist, C., & Cloots, R. (2013). Nanosphere lithography: a powerful method for the controlled manufacturing of nanomaterials. *Journal of Nanomaterials, 2013*, 21.

Coolidge, W. D. (1913). Production of refractory conductors: Google Patents.

Coppola, L., Huff, D., Wang, F., Burgos, R., & Boroyevich, D. (2007). *Survey on high-temperature packaging materials for SiC-based power electronics modules.* Paper presented at the Power Electronics Specialists Conference, 2007. PESC 2007. IEEE.

Datian, C., Zhifa, W., Huabo, W., & Jinwen, L. (2008). Preparation and property of novel-type Au-19.25 Ag-12.80 Ge solder alloy. *Rare Metal Materials and Engineering, 37*(4), 690-693.

Dorso, L., Bigot-Corbel, E., Abadie, J., Diab, M., Gouard, S., Bruchertseifer, F., . . . Davodeau, F. (2016). Long-term toxicity of 213Bi-labelled BSA in mice. *PloS one, 11*(3), e0151330.

Dreike, P., Fleetwood, D., King, D., Sprauer, D., & Zipperian, T. (1994). An overview of high-temperature electronic device technologies and potential applications. *IEEE Transactions on Components, Packaging, and Manufacturing Technology: Part A, 17*(4), 594-609.

Dušek, M., Szendiuch, I., Bulva, J., & Zelinka, M. Wettability–SnPb and Lead-free.

El-Daly, A., El-Hosainy, H., Elmosalami, T., & Desoky, W. (2015). Microstructural modifications and properties of low-Ag-content Sn–Ag–Cu solder joints induced by Zn alloying. *Journal of Alloys and Compounds, 653*, 402-410.

Fedlheim, D. L., & Foss, C. A. (2001). *Metal nanoparticles: synthesis, characterization, and applications*: CRC press.

Fleming, W. J. (2008). New automotive sensors—A review. *IEEE Sensors Journal, 8*(11), 1900-1921.

Frazier, A. B., Warrington, R. O., & Friedrich, C. (1995). The miniaturization technologies: Past, present, and future. *IEEE Transactions on Industrial Electronics, 42*(5), 423-430.

German, R. (2014). *Sintering: from empirical observations to scientific principles*: Butterworth-Heinemann.

German, R. M. (1996). Sintering theory and practice. *Solar-Terrestrial Physics*, 568.

Glass, J., Messier, R., & Fujimori, N. (1990). Diamond, Silicon Carbide and Related Wide Bandgap Semiconductors: Pittsburgh, PA (USA); Materials Research Society.

Goh, K.H., Lee, H.J., Lau, S.K., Teh, P.C., S. Ramesh, Tan, C.Y., Wong, Y.H. (2017). Investigation of the effect of anodization time and annealing temperature on the physical properties of ZrO2 thin film on a Si substrate. *Materi. Research Express* vol 4, no. 8, 086414.

Guarnieri, M., Di Noto, V., & Moro, F. (2010). A dynamic circuit model of a small direct methanol fuel cell for portable electronic devices. *IEEE Transactions on Industrial Electronics, 57*(6), 1865-1873.

Hartnett, A., & Buerki, S. (2009). Process and reliability advantages of AuSn eutectic die attach. *Proc. 42nd IMAPS*, 281-287.

Huang, M., & Wang, L. (2005). Effects of Cu, Bi, and In on microstructure and tensile properties of Sn-Ag-X (Cu, Bi, In) solders. *Metallurgical and Materials Transactions A, 36*(6), 1439-1446.

Inada, T., & Wong, C. (1998). *Fundamental study on adhesive strength of electrical conductive adhesives (ECAs).* Paper presented at the Advanced Packaging Materials, 1998. Proceedings. 1998 4th International Symposium on.

Inoue, Y., & Kikuchi, M. (2003). Present and future trends of stainless steel for automotive exhaust system. *High-temperature, 950*, 750.

Ivey, D. (1998). Microstructural characterization of Au/Sn solder for packaging in optoelectronic applications. *Micron, 29*(4), 281-287.

Jain, S., Rana, R., & Jain, P. (2016). Study of microstructure and mechanical properties of Al-Cu metal matrix reinforced with B4C particles Composite. *International Research Journal of Engineering and Technology, 3*(1), 499-504.

Jiang, D.-s., Wang, Y.-p., & Hsiao, C. (2006). *Effect of minor doping elements on lead free solder joint quality*. Paper presented at the Electronics Packaging Technology Conference, 2006. EPTC'06. 8th.

Kang, S.-J. L. (2004). *Sintering: densification, grain growth and microstructure*: Elsevier.

Kiencke, U., & Nielsen, L. (2000). Automotive control systems: for engine, driveline, and vehicle: IOP Publishing.

Kim, S., Kim, K.-S., Kim, S.-S., & Suganuma, K. (2009). Interfacial reaction and die attach properties of Zn-Sn high-temperature solders. *Journal of electronic materials, 38*(2), 266-272.

Kirschman, R. K. (1999). *High temperature electronics*: IEEE Press.

Kisiel, R., & Szczepański, Z. (2009). Die-attachment solutions for SiC power devices. *Microelectronics Reliability, 49*(6), 627-629.

Krishnan, S., Haseeb, A., & Johan, M. R. (2012). Preparation and low-temperature sintering of Cu nanoparticles for high-power devices. *IEEE Transactions on Components, Packaging and Manufacturing Technology, 2*(4), 587-592.

Kwak, H., & Hubing, T. (2007). An overview of advanced electronic packaging technology. *Clemson University Vehicular Electronics Lab*.

Lalena, J. N., Dean, N. F., & Weiser, M. W. (2002). Experimental investigation of Ge-doped Bi-11Ag as a new Pb-free solder alloy for power die attachment. *Journal of electronic materials, 31*(11), 1244-1249.

Lee, C. C., Wang, C. Y., & Matijasevic, G. (1993). Au-In bonding below the eutectic temperature. *IEEE Transactions on Components, Hybrids, and Manufacturing Technology, 16*(3), 311-316.

Lee, H.-H., Chou, K.-S., & Shih, Z.-W. (2005). Effect of nano-sized silver particles on the resistivity of polymeric conductive adhesives. *International Journal of Adhesion and Adhesives, 25*(5), 437-441.

Lee, J.-E., Kim, K.-S., Suganuma, K., Inoue, M., & Izuta, G. (2007). Thermal properties and phase stability of Zn-Sn and Zn-In alloys as high temperature lead-free solder. *Materials transactions, 48*(3), 584-593.

Lee, J.-E., Kim, K.-S., Suganuma, K., Takenaka, J., & Hagio, K. (2005). Interfacial properties of Zn–Sn alloys as high temperature lead-free solder on Cu substrate. *Materials transactions, 46*(11), 2413-2418.

Li, Y., & Wong, C. (2006). Recent advances of conductive adhesives as a lead-free alternative in electronic packaging: Materials, processing, reliability and applications. *Materials Science and Engineering: R: Reports, 51*(1-3), 1-35.

Liong, S., Wong, C., & Burgoyne, W. (2005). Adhesion improvement of thermoplastic isotropically conductive adhesive. *IEEE Transactions on Components and Packaging Technologies, 28*(2), 327-336.

Liu, X., Ohnuma, I., Kainuma, R., & Ishida, K. (1998). Phase equilibria in the Cu-rich portion of the Cu–Al binary system. *Journal of Alloys and Compounds, 264*(1-2), 201-208.

Liu, Y., Sun, F., & Liu, X. (2010). *Improving Sn-0.3 Ag-0.7 Cu low-Ag lead-free solder performance by adding Bi element.* Paper presented at the Strategic Technology (IFOST), 2010 International Forum on.

Lu, D., Tong, Q. K., & Wong, C. (1999a). Mechanisms underlying the unstable contact resistance of conductive adhesives. *IEEE Transactions on electronics packaging manufacturing, 22*(3), 228-232.

Lu, D., Tong, Q. K., & Wong, C. P. (1999b). *Conductivity mechanisms of isotropic conductive adhesives (ICAs).* Paper presented at the Advanced Packaging Materials: Processes, Properties and Interfaces, 1999. Proceedings. International Symposium on.

Lu, D., & Wong, C. (1999). High performance conductive adhesives. *IEEE Transactions on electronics packaging manufacturing, 22*(4), 324-330.

Lu, D., & Wong, C. (2000). Development of conductive adhesives for solder replacement. *IEEE Transactions on Components and Packaging Technologies, 23*(4), 620-626.

Macarthy, S. (1995). Paper presented at the Proceedings of the surface mount international, San Jose.

Madhududan, S., Sarcar¹, M., & Rao, N. B. a. K. (2010). Corrosion studies of Al-Cu Particulate composites produced through liquid metallurgy route.

Manikam, V. R., & Cheong, K. Y. (2011). Die attach materials for high temperature applications: A review. *IEEE Transactions on Components, Packaging and Manufacturing Technology, 1*(4), 457-478.

Manikam, V. R., Cheong, K. Y., & Razak, K. A. (2011). Chemical reduction methods for synthesizing Ag and Al nanoparticles and their respective nanoalloys. *Materials Science and Engineering: B, 176*(3), 187-203.

Manikam, V. R., Razak, K. A., & Cheong, K. Y. (2012a). *Sintering of Ag 80-Al 20 nanoalloy for high temperature die attach applications on silicon carbide-based power devices: The effects of ramp rate and dwell time.* Paper presented at the 2012 35th IEEE/CPMT International Electronics Manufacturing Technology Conference (IEMT).

Manikam, V. R., Razak, K. A., & Cheong, K. Y. (2012b). Sintering of silver–aluminum nanopaste with varying aluminum weight percent for use as a high-temperature die-attach material. *IEEE Transactions on Components, Packaging and Manufacturing Technology, 2*(12), 1940-1948.

Manikam, V. R., Razak, K. A., & Cheong, K. Y. (2013a). A novel silver–aluminium high-temperature die attach nanopaste system: the effects of organic additives content on post-sintered attributes. *Journal of Materials Science: Materials in Electronics, 24*(8), 2678-2688.

Manikam, V. R., Razak, K. A., & Cheong, K. Y. (2013b). Physical and electrical attributes of sintered Ag 80–Al 20 high temperature die attach material with different organic additives content. *Journal of Materials Science: Materials in Electronics, 24*(2), 720-733.

Manikam, V. R., Razak, K. A., & Cheong, K. Y. (2013c). Reliability of sintered Ag80–Al20 die attach nanopaste for high temperature applications on SiC power devices. *Microelectronics Reliability, 53*(3), 473-480.

Masson, A., Buttay, C., Morel, H., Raynaud, C., Hascoët, S., & Grémillard, L. (2011). *High-temperature die-attaches for SiC power devices.* Paper presented at the Power Electronics and Applications (EPE 2011), Proceedings of the 2011-14th European Conference on.

Matienzo, L., Egitto, F., & Logan, P. (2003). The use of silane coupling agents in the design of electrically stable interfaces of 6061 T6 aluminum alloy surfaces and epoxy-based electrically conductive adhesives. *Journal of materials science, 38*(24), 4831-4842.

McLean, D. (1962). *Mechanical properties of metals* (Vol. 129): Wiley New York.

Menshikova, S. G., Brodova, I. G., Yablonskih, T. I., & Astafyev, V. V. (2016). Study of the structure and properties of Al-Cu alloys (up to 10 at.% Cu) produced at different cooling rates. *MAYFEB Journal of Materials Science, 1*.

Mir, I., & Kumar, D. (2008). Recent advances in isotropic conductive adhesives for electronics packaging applications. *International Journal of Adhesion and Adhesives, 28*(7), 362-371.

Murray, J. L. (1985). The aluminium-copper system. *International metals reviews, 30*(1), 211-234.

Naayagi, R. (2013). *A review of more electric aircraft technology.* Paper presented at the Energy Efficient Technologies for Sustainability (ICEETS), 2013 International Conference on.

Naidich, Y. V., Zhuravlev, V., & Krasovskaya, N. (1998). The wettability of silicon carbide by Au–Si alloys. *Materials Science and Engineering: A, 245*(2), 293-299.

Natter, H., Hempelmann, R. (1996) Nanocrystalline copper by pulsed electrodeposition: the effects of organic additives, bath temperature, and pH. *J. Phy.Chem.*, vol. 100, no. 50 pp. 19525-19532.

Nguyen, M. N. (1990). Low stress silver-glass die attach materials. *IEEE Transactions on Components, Hybrids, and Manufacturing Technology, 13*(3), 478-483.

Ni, W., Huang, Y., Wang, X., Zhang, J., & Wu, K. (2014). Associations of neonatal lead, cadmium, chromium and nickel co-exposure with DNA oxidative damage in an electronic waste recycling town. *Science of the Total Environment, 472*, 354-362.

Parmentier, B., Vermesan, O., & Beneteau, L. (2003). Design of high temperature electronics for well logging applications.

Pokluda, O., Bellehumeur, C. T., & Vlachopoulos, J. (1997). Modification of Frenkel's model for sintering. *AIChE journal, 43*(12), 3253-3256.

Riani, P., Arrighi, L., Marazza, R., Mazzone, D., Zanicchi, G., & Ferro, R. (2004). Ternary rare-earth aluminum systems with copper: a review and a contribution to their assessment. *Journal of Phase Equilibria and Diffusion, 25*(1), 22-52.

Sarlioglu, B., & Morris, C. T. (2015). More electric aircraft: Review, challenges, and opportunities for commercial transport aircraft. *IEEE Transactions on Transportation Electrification, 1*(1), 54-64.

She, X., Huang, A. Q., Lucia, O., & Ozpineci, B. (2017). Review of silicon carbide power devices and their applications. *IEEE Transactions on Industrial Electronics, 64*(10), 8193-8205.

Smith, D. R., & Fickett, F. (1995). Low-temperature properties of silver. *Journal of Research of the National Institute of Standards and Technology, 100*(2), 119.

Song, J.-M., Chuang, H.-Y., & Wen, T.-X. (2007). Thermal and tensile properties of Bi-Ag alloys. *Metallurgical and Materials Transactions A, 38*(6), 1371-1375.

Song, J.-M., Chuang, H.-Y., & Wu, Z.-M. (2006). Interfacial reactions between Bi-Ag high-temperature solders and metallic substrates. *Journal of electronic materials, 35*(5), 1041-1049.

Song, J.-M., Chuang, H.-Y., & Wu, Z.-M. (2007). Substrate dissolution and shear properties of the joints between Bi-Ag alloys and Cu substrates for high-temperature soldering applications. *Journal of electronic materials, 36*(11), 1516-1523.

Tan, F., Qiao, X., Chen, J., & Wang, H. (2006). Effects of coupling agents on the properties of epoxy-based electrically conductive adhesives. *International Journal of Adhesion and Adhesives, 26*(6), 406-413.

Tan, K. S., & Cheong, K. Y. (2013). *Effect of sintering temperature on silver-copper nanopaste as high temperature die attach material.* Paper presented at the Advanced Materials Research.

Tan, K. S., & Cheong, K. Y. (2014a). Mechanical properties of sintered Ag–Cu die-attach nanopaste for application on SiC device. *Materials & Design, 64*, 166-176.

Tan, K. S., & Cheong, K. Y. (2014b). Physical and electrical characteristics of silver-copper nanopaste as alternative die-attach. *IEEE Transactions on Components, Packaging and Manufacturing Technology, 4*(1), 8-15.

Tan, K. S., Wong, Y. H., & Cheong, K. Y. (2015). Thermal characteristic of sintered Ag–Cu nanopaste for high-temperature die-attach application. *International Journal of Thermal Sciences, 87*, 169-177.

Tong, Q., Vona, S., Kuder, R., & Shenfield, D. (1998). *The recent advances in surface mount conductive adhesives.* Paper presented at the Adhesive Joining and Coating Technology in Electronics Manufacturing, 1998. Proceedings of 3rd international Conference on.

Traeger, R., & Lysne, P. (1988). High temperature electronics application in well logging. *IEEE Transactions on Nuclear Science, 35*(1), 852-854.

Turner, R., Fuierer, P. A., Newnham, R., & Shrout, T. (1994). Materials for high temperature acoustic and vibration sensors: A review. *Applied acoustics, 41*(4), 299-324.

Von Zahn, U., Kumar, S., Niemann, H., & Prinn, R. (1983). 13. COMPOSITION OF THE VENUS ATMOSPHERE. *Venus*, 299.

Vons, S., Tong, Q. K., Kuder, R., & Shenfield, D. (1998). *Surface mount conductive adhesives with superior impact resistance.* Paper presented at the Advanced Packaging Materials, 1998. Proceedings. 1998 4th International Symposium on.

Wakuda, D., Kim, K.-S., & Suganuma, K. (2008). Room temperature sintering of Ag nanoparticles by drying solvent. *Scripta Materialia*, *59*(6), 649-652.

Watson, J., & Castro, G. (2012). High-temperature electronics pose design and reliability challenges. *Analog Dialogue, 46*(2), 3-9.

Watson, J., & Castro, G. (2015). A review of high-temperature electronics technology and applications. *Journal of Materials Science: Materials in Electronics, 26*(12), 9226-9235.

White, H., & Shremp, R. (1939). Beryllium oxide: I. *Journal of the American Ceramic Society, 22*(1‐12), 185-189.

Wzorek, Ł., Wędrychowicz, M., Wiewióra, M., Noga, P., Skrzekut, T., Wzorek, A., & Łyp-Wrońska, K. (2017). Possibility of Al-Cu composite manufacturing from fine metal fractions by recycling process. *Metallurgy and Foundry Engineering, 43*(2).

Xu, S., & Dillard, D. A. (2003). Determining the impact resistance of electrically conductive adhesives using a falling wedge test. *IEEE Transactions on Components and Packaging Technologies, 26*(3), 554-562.

Xu, X., Gurav, A. S., Lessner, P. M., & Randall, C. A. (2011). Robust BME class-I MLCCs for harsh-environment applications. *IEEE Transactions on Industrial Electronics, 58*(7), 2636-2643.

Ye, L., Lai, Z., Liu, J., & Tholen, A. (1999). Effect of Ag particle size on electrical conductivity of isotropically conductive adhesives. *IEEE Transactions on electronics packaging manufacturing, 22*(4), 299-302.

Zwolinski, M., Hickman, J., Rubin, H., Zaks, Y., McCarthy, S., Hanlon, T., Lan, S. (1996). Electrically conductive adhesives for surface mount solder replacement. *IEEE Transactions on Components, Packaging, and Manufacturing Technology: Part C, 19*(4), 241-250.

LIST OF PUBLICATIONS

1. Siah, M.Z., Yborde, D.C., Sukiman, N.L., S.Ramesh & Wong, Y.H. (2019). Effects of Resin Binder on Characteristics of Sintered Aluminum-Copper Nanopaste as High Temperature Die Attach Material. *IEEE Transactions on Components, Packaging and Manufacturing Technology*.